# On-shelf nutrient trapping enhances the fertility of the southern Benguela upwelling system

**Raquel Flynn**

Thesis presented for the degree of Master of Science

in the Department of Oceanography

University of Cape Town

December 2018




**Supervisor:** Dr Sarah Fawcett

**Co-supervisor:** Assoc. Prof Julie Granger

**Plagiarism Declaration**

I know the meaning of plagiarism and declare that all the work in the dissertation, save for t
which is properly acknowledged, is my own.

Signed by candidate

……

Raquel Flynn

……

Date

## Abstract

The southern Benguela upwelling system (SBUS), located off the southwest coast of Africa, supports high rates of primary productivity that sustain important commercial fisheries. The exceptional fertility of this system is reportedly fuelled not only by upwelled nutrients, but also by nutrients regenerated on the broad and shallow continental shelf. We present the first nitrate nitrogen (N) and oxygen (O) isotope data ($\delta^{15}N$ and $\delta^{18}O$, respectively) from the SBUS, generated for samples collected along four hydrographic lines in February (summer) and May (early winter) of 2017. During summer upwelling, a decrease in nitrate $\delta^{18}O$ on the shelf reveals that on average, 30% of the subsurface nutrients derive from *in situ* remineralization of sinking phytoplankton biomass. In the more quiescence winter, an average of 35% of the on-shelf nitrate is regenerated, with the signal propagating further westward along the mid-shelf region such that the total regenerated nitrate burden is greater during this season. In both seasons, a shoreward increase in subsurface nitrate $\delta^{15}N$ and decrease in N* (i.e., total dissolved nitrogen – 16 x phosphate + 2.9) suggests N loss to benthic denitrification coincident with the on-shelf remineralization, which implies that an even higher quantity of nitrate is regenerated than we calculate. Our data show that remineralized nutrients get trapped on the SBUS shelf in summer and early winter, enhancing the nutrient pool that can be upwelled to support surface productivity and decreasing bottom water oxygen concentrations. The proposed mechanism for this "nutrient trapping" involves upwelled nutrients being removed from surface waters and converted into organic biomass that is sequestered and remineralized on the shelf while the now nutrient-deplete surface waters are advected offshore by Ekman transport. This process is aided by a number of equatorward-flowing fronts that impede the lateral exchange of waters in the upper 200 m of the water column, increasing their residence time on the shelf. The extent to which remineralized nutrients are trapped on the SBUS shelf has implications for bottom water hypoxia. Trapped nutrients will be supplied to the surface during upwelling, supporting high rates of primary productivity and a large sinking biomass flux. The subsequent on-shelf remineralization of this organic matter has the potential to further decrease already-low bottom water oxygen concentrations.

**Acknowledgements**

To my supervisor, Sarah Fawcett, thank you for the incredible experiences and opportunities that you have afforded me. Sarah has taught me to think critically and has been invaluable throughout my Masters, providing me with constant mentorship and support.

I am grateful to Julie Granger for allowing me to spend time in her lab. I have learnt a lot, and her sabbatical could not have been at a better time. The hours spent delving into my data and the thought-provoking discussions were essential for the ideas presented in this thesis.

Thank you to the crew and scientists of the *FRV* Algoa. Without their help with sampling, especially at the early hours of the morning, the science would not have been possible.

The support from the Fawcett-Altieri lab has been phenomenal throughout my degree. The invoking stimulating discussions provided me with the opportunity to further engage with my topic allowing me to develop my ideas. It has been incredible working with people working on so many different projects and has allowed me to grow as a scientist.

To Jason Dionysopoulos, thank you for being so understanding and always being there to listen to new thoughts on my data. For the late nights in the lab helping me parafilm samples, and coming up with new ways to correct my data. Your constant support and understanding will never be forgotten.

Finally, to my family, especially my parents, thank you for always supporting me and being as excited about my research and experiences as I am. Mom and dad, you have provided me with the opportunity to continue studying and I am eternally grateful for that.

## Contents

# 1. Introduction and Literature Review

## 1.1 The marine nitrogen cycle and the biological carbon pump

Nitrogen is an important nutrient for the growth of phytoplankton in the euphotic zone (the upper sunlit layer) of the ocean. During photosynthesis, phytoplankton use light, carbon dioxide ($CO_2$; a greenhouse gas), and macro- (mainly nitrogen and phosphorous) and micronutrients (e.g., iron) in order to build their biomass. On average across the global ocean, approximately 10% of the atmospheric $CO_2$ that is fixed by phytoplankton is exported to the deep ocean through the sinking of particulate organic carbon (POC) that is subsequently remineralised back to dissolved inorganic carbon (DIC) in the ocean interior or stored in the sediments (Laws et al. 2000; Henson et al. 2011; Sigman and Hain 2012; Figure 1.1). This process of phytoplankton fixing $CO_2$ and sequestering it in the deep ocean through their sinking biomass is termed the ocean's "biological carbon pump" (Volk and Hoffert 1985; Falkowski et al. 1998).

Bio-available nitrogen exists in various forms in the ocean. The most abundant species is nitrate ($NO_3^-$), with ammonium ($NH_4^+$) and nitrite ($NO_2^-$) constituting the other major inorganic forms. The main external sources of nitrogen to the ocean are biological $N_2$ fixation, atmospheric deposition and riverine inputs, while the removal of nitrogen is largely due to the processes of denitrification and anammox (Figure 1.1). These inputs and outputs directly control the total oceanic nitrogen budget, while nitrogen assimilation by phytoplankton, particulate organic nitrogen (PON) export, ammonification (the heterotrophic breakdown of PON to ammonium) and nitrification (the oxidation of ammonium to nitrite and nitrate by nitrifying bacteria and archaea) affect the distribution and form of the nitrogen species present in the ocean but do not alter the total inventory (Figure 1.1).

The main "regenerated" form of nitrogen to phytoplankton is ammonium (Dugdale and Goering 1967), potentially augmented by dissolved organic nitrogen (DON) compounds such as urea (Bronk 2002). These forms of nitrogen are termed regenerated because they are recycled in the euphotic zone through heterotrophic metabolism. Nitrate, on the other hand, is mainly generated in the aphotic zone below the sunlit upper layer by nitrifying bacteria and archaea. This nitrate is then supplied to the euphotic zone by physical processes such as Ekman

upwelling or wind-driven mixing, providing phytoplankton with a "new" nitrogen source. Primary production fuelled by ammonium is termed "regenerated production" while that fuelled by upwelled nitrate is termed "new production" (Dugdale and Goering 1967). Over appropriate space and time scales, the rate of new production must be balanced by a downward flux of PON (and stoichiometrically-associated POC) out of the euphotic zone. We can thus use nitrate-based phytoplankton growth as a proxy for carbon export potential (Eppley and Peterson 1979), provided that a number of assumptions are not violated (Dugdale and Goering 1967; Bronk et al. 1994; Yool et al. 2007). For example, if PON is remineralised and nitrified in the euphotic zone, carbon export may be overestimated. This is because euphotic zone nitrification yields regenerated rather than new nitrate, and its consumption by phytoplankton contributes to regenerated rather than new production (Dugdale and Goering 1967; Eppley and Peterson 1979; Dore and Karl 1996; Raimbault et al. 1999; Diaz and Raimbault 2000; Yool et al. 2007). Nonetheless, if fluxes such as regenerated nitrate production can be constrained, the coupling between new production and carbon dioxide drawdown allows us to use measurements of the nitrogen cycle to inform our understanding of the ocean's carbon cycle.

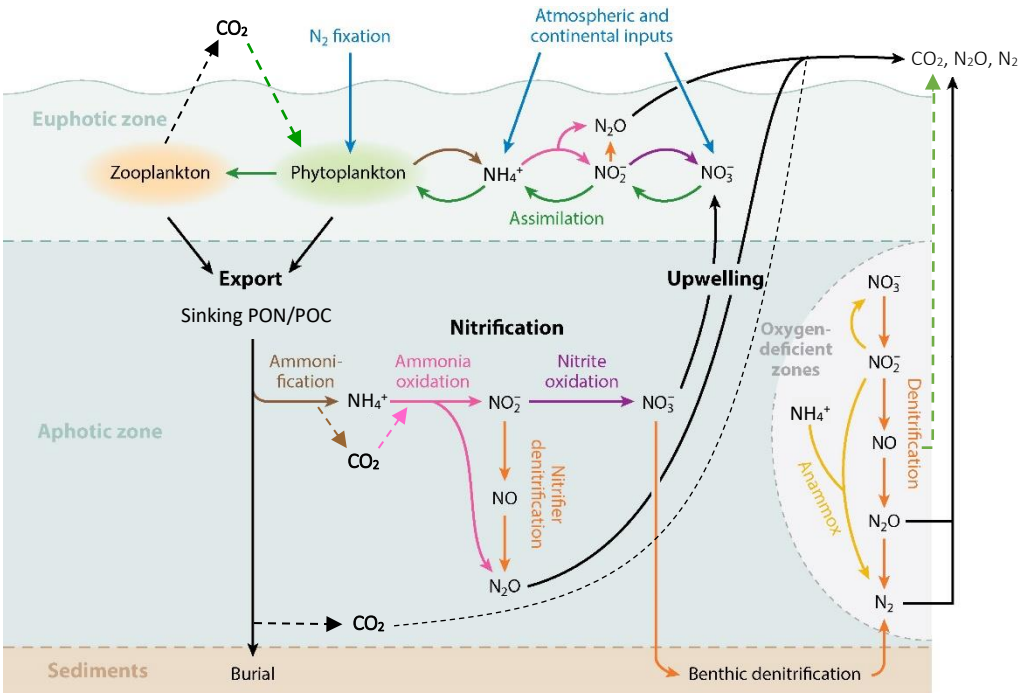


**Figure 1.1** Representation of the marine nitrogen cycle, with the major inputs in blue ($N_2$ fixation and atmospheric nitrogen deposition) and the major outputs in yellow and orange (anammox and denitrification). Biological processes are shown in colour while physical

processes are shown in black. The dominant biological process occurring in the euphotic zone is phytoplankton assimilation of nitrate ($NO_3^-$), nitrite ($NO_2^-$) and ammonium ($NH_4^+$), while the dominant biological process in the aphotic zone is remineralisation (ammonification) and nitrification of particulate organic nitrogen (PON) to ammonium, nitrite and nitrate. A brief overview of relevant co-occurring marine carbon cycle processes are also represented (dashed lines). Atmospheric carbon dioxide ($CO_2$) dissolved in surface waters is "fixed" by phytoplankton during photosynthesis to produce biomass, supported by nitrate assimilation. Carbon dioxide is produced during heterotrophic activities such as the aerobic and anaerobic remineralisation of organic biomass, and consumed by chemoautotrophic bacteria during nitrification. The sinking of particulate organic nitrogen and carbon biomass (PON/POC) sequesters carbon dioxide in the deep ocean where it is stored for hundreds to thousands of years. Carbon dioxide may be brought to the surface again, along with nutrients and other dissolved gases, during an upwelling event [Adapted from Casciotti 2016].

### 1.1.1 Quantifying the nitrogen cycle using nitrate isotopes

***The theory of nitrogen isotopes***

The isotopes of a given element have the same number of protons and electrons but varying numbers of neutrons, which causes them to have different atomic masses. For instance, nitrogen has two stable isotopes, $^{14}N$ and $^{15}N$. $^{14}N$ is the most abundant form and constitutes 99.63% of all nitrogen on Earth, with $^{15}N$ constituting 0.37%. The different masses of the nitrogen isotopes renders them a useful tool for tracking chemical and biological processes as the lighter isotope, $^{14}N$, is often preferentially reacted over its heavier counterpart, $^{15}N$ (Mariotti et al. 1981). These reactions cause changes in the ratio of $^{15}N/^{14}N$, quantified in delta notation (in permil (‰) vs. $N_2$ in air) as:

$$\delta^{15}N = ([(^{15}N/^{14}N)_{sample}/(^{15}N/^{14}N)_{standard}]-1) \times 1000 \quad (1.1)$$

Processes that alter the distribution of stable isotopes can be unidirectional, yielding kinetic isotope fractionation, or act in both directions, leading to equilibrium isotope fractionation (Sharp 2007). Biological reactions such as nitrogen assimilation are typically unidirectional (Mariotti et al. 1981). During nitrate assimilation, phytoplankton preferentially consume $^{14}N$-bearing nitrate ($^{14}N$-containing bonds are more easily broken), such that at any given point in

time, their PON biomass will be lower in $\delta^{15}N$ than the nitrate being consumed. As consumption proceeds, the reactant nitrate pool becomes enriched in $^{15}N$, as does the PON produced, therefore increasing the $\delta^{15}N$ of both pools. The extent of this isotope fractionation is described by the isotope effect (ε), which is approximated as:

$$\varepsilon\ (‰) = (1 - {}^{15}k/{}^{14}k) \times 1000 \quad (1.2)$$

where $^{14}k$ and $^{15}k$ are the rate coefficients of the light and heavy isotopes of nitrogen, respectively (Mariotti et al. 1981).

Kinetic isotopic fractionation can be described by two simple end-member models, the Rayleigh and the steady state models.

***The Rayleigh model***

The Rayleigh model approximates a closed system (i.e., no inputs or outputs) wherein the initial supply of a reactant undergoes a unidirectional reaction with a constant ε (Figure 1.2; Mariotti et al. 1981; Sigman et al. 1999b; Sigman et al. 2009b). As the reaction evolves, the concentration of the reactant pool, in this case, the nitrate concentration, decreases and its $\delta^{15}N$ ($\delta^{15}N_{reactant}$) rises due to isotope fractionation (Figure 1.2 solid black line). The $\delta^{15}N_{reactant}$ under Rayleigh conditions is defined as:

$$\delta^{15}N_{reactant} = \delta^{15}N_{initial} - \varepsilon\ (\ln(f)) \quad (1.3)$$

where $\delta^{15}N_{initial}$ is the $\delta^{15}N$ of the nitrate at the start of the reaction, ε is the isotope effect of nitrate assimilation and *f* is the fraction of nitrate remaining (i.e., $[NO_3^-]/[NO_3^-]_{initial}$).

As the reactant nitrate is converted into PON, the product of the reaction, its $\delta^{15}N$ rises. The $\delta^{15}N$ of the PON that is instantaneously produced at any point during the reaction, $\delta^{15}N_{instantaneous}$ (Figure 1.2 dashed black line), has a $\delta^{15}N$ defined as:

$$\delta^{15}N_{instantaneous} = \delta^{15}N_{reactant} - \varepsilon \quad (1.4)$$

The $\delta^{15}N_{instantaneous}$ is therefore lower than the $\delta^{15}N_{reactant}$ by the amount of the isotope effect (Figure 1.2 black arrow; Mariotti et al. 1981). The $\delta^{15}N$ of the integrated product pool

($\delta^{15}N_{integrated}$; Figure 1.2 dotted dashed black line) increases more gradually as it is defined as the total accumulated product of the reaction. The $\delta^{15}N_{integrated}$ is defined as:

$$\delta^{15}N_{integrated} = \delta^{15}N_{initial} + \varepsilon \left( \frac{f}{1-f} \right) \ln(f) \quad (1.5)$$

At the end-point of the reaction (i.e., when $[NO_3^-] = 0$), the $\delta^{15}N_{integrated}$ will be equal to $\delta^{15}N_{initial}$ (Figure 1.2) because, when $f = 0$, the entire reactant pool ($^{14}N$ and $^{15}N$) has been converted into product.

When a mixing event occurs during nitrate assimilation, violating the Rayleigh model's closed system criterion, the resultant water parcel will have a $\delta^{15}N$ and nitrate concentration in between that of the newly supplied and partially consumed nitrate pools (i.e., between the Rayleigh end-members; Figure 1.3; Sigman et al. 1999a). The extent to which the mixing line differs from the Rayleigh model depends on the amount of substrate that had been consumed at the time of mixing. The greater the extent of the nitrate utilisation prior to mixing, the more the product of the mixing event will deviate in its nitrate concentration and $\delta^{15}N$ from the relationship predicted by the Rayleigh model (Figure 1.3; Sigman et al. 1999a). In most ocean regions, the degree of nitrate utilisation in surface waters is high (Redfield 1958), such that violation of the Rayleigh model due to local mixing events is always a concern.

***The steady-state model***

The steady-state model approximates an open system (i.e., nitrogen is continuously supplied in order to balance its output by consumption and export, such that the gross supply of reactant equals the sum of the product and the residual reactant nitrogen that is exported) (Sigman et al. 1999a; Hayes 2002). Similar to the Rayleigh model, as the steady-state reaction evolves and the nitrate concentration decreases, its $\delta^{15}N$ increases, as does the $\delta^{15}N_{product}$ (Figure 1.2 grey lines). At the end-point of the reaction (i.e., when $[NO_3^-] = 0$), the $\delta^{15}N_{product}$ is equal to the $\delta^{15}N_{initial}$ (Figure 1.2; Equation 1.7). In order to quantify the $\delta^{15}N$ of the above-mentioned pools for a given $\varepsilon$ and $f$, we use the formulae below (Sigman et al. 1999a):

$$\delta^{15}N_{reactant} = \delta^{15}N_{initial} - \varepsilon (1 - f) \quad (1.6)$$

$$\delta^{15}N_{product} = \delta^{15}N_{initial} - \varepsilon (f) \quad (1.7)$$

Figure 1.2 shows that at low degrees of nitrate utilisation, approximately ≤30%, the Rayleigh and steady-state models evolve similarly; therefore, in regions of the ocean where ≤30% of the nitrate supplied is utilised (e.g., the Antarctic Zone of the Southern Ocean), either model can be applied (Sigman et al. 1999a). This is not the case in most ocean regions, however, where surface nutrients concentrations are low (i.e., the degree of nitrate consumption is high).

The equations given above for the Rayleigh and steady-state models are simplified, approximate forms of the full expressions. Moreover, neither model is truly representative of reactions taking place in the ocean, which is highly dynamic and where complications such as mixing are the norm. Nonetheless, these models provide a framework in which nitrogen isotope measurements can be interpreted in order to describe and understand chemical and biological processes in the ocean.

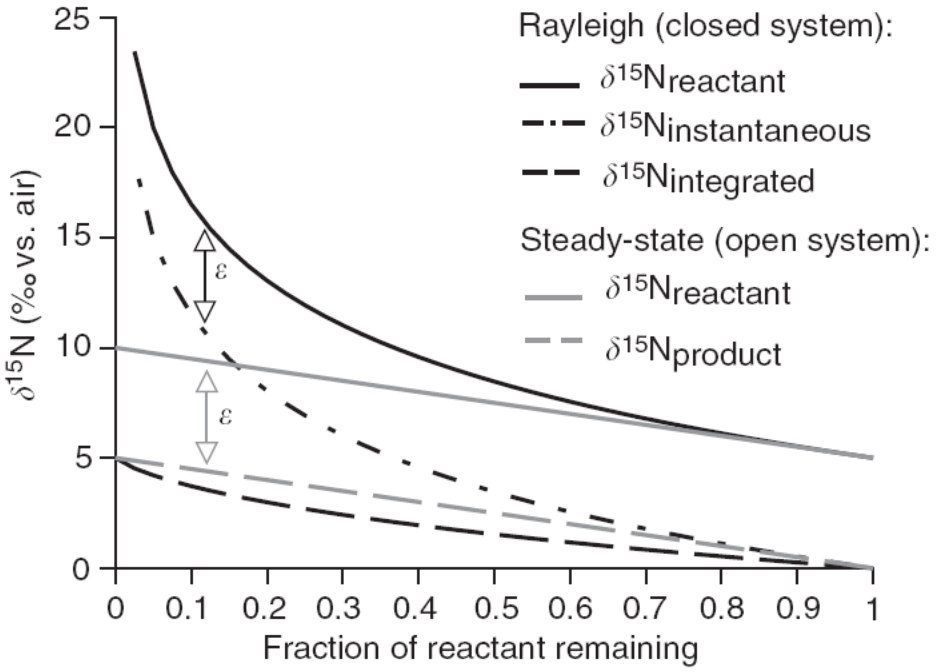


**Figure 1.2** The Rayleigh (black lines) and steady-state (grey lines) models of kinetic isotope fractionation showing the changes in the $\delta^{15}N$ of the reactant (solid lines) and product pools (dashed lines) as the reactant is consumed. The fraction of reactant remaining (*f)* is quantified as $[NO_3^-]/[NO_3^-]_{total}$. Both models assume a constant ε of 5‰. See text for details about the models represented here [Figure from Sigman et al. 2009b].

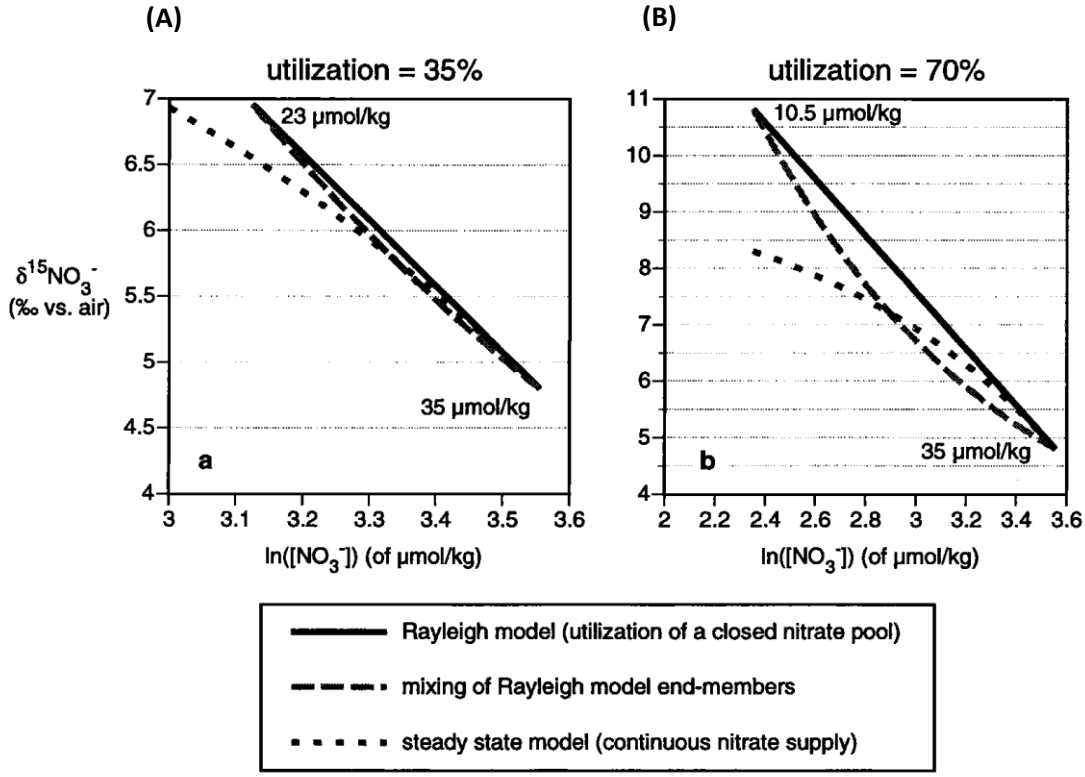


**Figure 1.3** Theoretical evolution of the $\delta^{15}N$ of nitrate as a function of nitrate concentration (shown here as its natural logarithm) for different models of nitrate supply and consumption: the Rayleigh model (solid line), the steady-state model (dotted line), and the mixing of Rayleigh model end-members (dashed line). The $\delta^{15}N/[NO_3^-]$ relationship is shown assuming a) 35% utilisation of the initial nitrate pool and b) 70% utilisation of the initial nitrate pool. Initial conditions used in the model include source water with a nitrate concentration of 35 µmol $kg^{-1}$ and a $\delta^{15}N$ of 4.8‰, and a constant nitrate assimilation ε of 5‰ [Figure from Sigman et al. 1999a].

***The nitrogen and oxygen isotopes of nitrate***

Nitrate is comprised of two elements, nitrogen (N) and oxygen (O), each with their own stable isotopes. Oxygen has three stable isotopes $^{16}O$, $^{17}O$ and $^{18}O$, with $^{16}O$ constituting approximately 98.8% of all oxygen on Earth and the other two isotopes constituting 0.03% and 0.2%, respectively (Baertschi 1976; Casciotti et al. 2002, 2016). As for the nitrogen isotopes, physical, chemical, and biological processes change the ratio of oxygen isotopes in the environment. The oxygen isotope ratio, $^{18}O/^{16}O$, is quantified in delta notation (in permil (‰) vs. VSMOW) as:

$$\delta^{18}O = ([(^{18}O/^{16}O)_{sample}/(^{18}O/^{16}O)_{standard}]-1) \times 1000) \quad (1.8)$$

Until the development of the "denitrifier method" (Sigman et al. 2001; Casciotti et al. 2002), simultaneous measurement of the nitrogen and oxygen isotopes of nitrate in seawater was not possible. This method uses naturally occurring denitrifying bacteria that lack the nitrous oxide ($N_2O$) reductase enzyme, the terminal enzyme in the denitrification reaction that reduces nitrous oxide to di-nitrogen gas ($N_2$), to reduce dissolved nitrate to $N_2O$ by the following pathway:

$$2NO_3^-{}_{(aq)} \rightarrow 2NO_2^-{}_{(aq)} \rightarrow 2NO_{(g)} \rightarrow N_2O_{(g)} \quad (1.9)$$

The quantitative reduction of nitrate by *Pseudomonas chlororaphis* and *Pseudomona chlororaphis* spp. *aureofaciens* (hereafter, *P. aureofaciens*) produces $N_2O$ with a $\delta^{15}N$ that is the same as and a $\delta^{18}O$ that is related to that of the initial nitrate. The nitrogen and oxygen isotopes of the $N_2O$ can then be measured using isotope ratio mass spectrometry (IRMS) (Sigman et al. 2001; Casciotti et al. 2002; McIlvin and Casciotti 2007; Weigand et al. 2016).

Prior to the development of the denitrifier method, the $\delta^{15}N$ of nitrate was measured using "passive ammonia diffusion" (Sigman et al. 1997). This method involves converting nitrate to ammonia using Devarda's alloy and diffusing the ammonia onto a glass fibre disk that is then analysed using combustion IRMS. At best, this method allows for the measurement of the $\delta^{15}N$ of seawater samples with $[NO_3^-]$ >2 µM (Sigman et al. 1997). It is also associated with a significant blank, requires a large sample volume, is very time time-consuming, and does not yield oxygen isotope data. The denitrifier method has therefore revolutionized the study of nitrate isotopes as it allows for the analysis of both nitrogen and oxygen isotopes at nitrate concentrations low as 0.3-0.5 µM (e.g., Fawcett et al. 2015), requires small quantities of sample (~10 nmoles), and is compatible with high sample throughput (~11-15 minutes per sample) (Sigman et al. 2001; Casciotti et al. 2002; McIlvin and Casciotti 2007; Weigand et al. 2016).

Measurements of the dual isotopes of nitrate (i.e., $\delta^{15}N$ and $\delta^{18}O$) are more powerful than using nitrate $\delta^{15}N$ alone. This is largely due to the observation that some biological processes cause the N and O isotopes to change in unison (i.e., along a 1:1 line in $\delta^{15}N$ vs. $\delta^{18}O$ space) while

other processes act to decouple the isotopes (i.e., causing a deviation from the 1:1 line in $\delta^{15}N$ vs. $\delta^{18}O$ space; Figure 1.4A) (Granger et al. 2004; Sigman et al. 2005; Granger et al. 2008; Sigman et al. 2009; Granger et al. 2010; Rafter et al. 2013). For example, nitrate assimilation increases the $\delta^{15}N$ and $\delta^{18}O$ of the residual nitrate pool equally. Thus, nitrate samples will fall along a 1:1 line in $\delta^{15}N$ vs. $\delta^{18}O$ space if the nitrate pool is acted on by nitrate assimilation only (Figure 1.4). The rate at which $^{14}N$ is utilised over $^{15}N$ during nitrate assimilation is therefore similar to that of $^{16}O$ over $^{18}O$, which means that $^{18}\varepsilon/^{15}\varepsilon \sim 1$ (Granger et al. 2004; Granger et al. 2010; Karsh et al. 2012). Denitrification (the step-wise reduction of nitrate to $N_2$ gas by denitrifying bacteria) has also been observed to yield an equal rise in nitrate $\delta^{15}N$ and $\delta^{18}O$ (Granger 2006; Granger et al. 2008; Sigman et al. 2009; Figure 1.4). This similarity in $^{18}\varepsilon/^{15}\varepsilon$ for nitrate assimilation and denitrification is thought to derive from the same enzyme being used for both processes (Granger et al. 2008; Karsh et al. 2012; Treibergs and Granger 2016).

The biological processes that consume nitrate in the ocean have similar effects on the $\delta^{15}N$ and $\delta^{18}O$ of the nitrate pool. This is not the case for the processes that produce nitrate, however. The remineralisation and nitrification of PON causes a decoupling of the $\delta^{15}N$ and $\delta^{18}O$ of nitrate, which leads to a deviation from the 1:1 assimilation/denitrification line in $\delta^{15}N$ vs. $\delta^{18}O$ space. This is because the $\delta^{15}N$ of newly nitrified nitrate is set by the $\delta^{15}N$ of the ammonium being nitrified and, by extension, the PON pool from which it is remineralised. By contrast, the $\delta^{18}O$ of newly nitrified nitrate is set by the $\delta^{18}O$ of seawater (Sigman et al. 2005; Sigman et al. 2009a; Sigman et al. 2009c) because 5/6 of the oxygen atoms added during nitrification derive from seawater (Casciotti et al. 2002; Sigman et al. 2009a). The $\delta^{18}O$ of newly nitrified nitrate has been shown to equal the $\delta^{18}O$ of seawater (~0‰; Bigg and Rohling 2000) plus an $\varepsilon \sim 1.15$‰, producing nitrate with a $\delta^{18}O$ of ~1.15‰ (Sigman et al. 2009).

Because PON sets the $\delta^{15}N$ of newly nitrified nitrate, there are a number of nitrogen cycle processes that, when followed by nitrification, can drive nitrate $\delta^{15}N$ and $\delta^{18}O$ to deviate from a 1:1 relationship. These include: 1) $N_2$ fixation, 2) partial nitrate consumption, and 3) complete nitrate consumption (Sigman et al. 2005; Rafter et al. 2013).

PON deriving from $N_2$ fixation is low in $\delta^{15}N$ as, by definition, $N_2$ in air has a $\delta^{15}N$ of 0‰. There is a small $\varepsilon$ associated with the dissolution of atmospheric $N_2$ in seawater and its subsequent fixation, which yields PON that is supported by $N_2$ fixation with a $\delta^{15}N$ of -2‰ to 0‰ (Minagawa and Wada 1986; Carpenter et al. 1997). When this PON is remineralised and

nitrified, it produces nitrate with an equally low $\delta^{15}N$ (-2‰ to 0‰) and, as described above, a $\delta^{18}O \geq 1.15‰$. Thus, $N_2$ fixation followed by nitrification causes a deviation above the 1:1 line in nitrate $\delta^{15}N$ vs. $\delta^{18}O$ space (Figure 1.4A and E; Sigman et al. 2005; Rafter et al. 2013).

PON formed from the partial consumption of nitrate will have a $\delta^{15}N$ that is lower than that of the nitrate supply due to isotopic fractionation (Equations 1.4 and 1.5). Upon remineralisation and nitrification, this PON will produce nitrate with a $\delta^{15}N$ that is lower than the nitrate supply and the partially consumed nitrate pool, with the latter having increased in $\delta^{15}N$ due to consumption. The $\delta^{15}N$ of the combined nitrate pool (i.e., the partially consumed plus newly nitrified nitrate) remains unaltered, however, and assuming no gain or loss of nitrogen, will equal that of the nitrate supply (Sigman et al. 1999a). By contrast, the $\delta^{18}O$ of the nitrate added during nitrification is high compared to that removed during consumption (≥1.15‰ vs. -3‰, assuming a deep ocean nitrate $\delta^{18}O$ of 2‰ and an assimilation O isotope effect of 5‰) (Sigman et al. 2005; Granger et al. 2010; Buchwald and Casciotti 2012). The partial consumption of nitrate by phytoplankton coupled with nitrification therefore acts to raise the $\delta^{18}O$ of the combined nitrate pool while its $\delta^{15}N$ remains unchanged (Sigman et al. 2009; Rafter et al. 2013; Fawcett et al. 2015), thus driving nitrate above the 1:1 line in $\delta^{15}N$ vs. $\delta^{18}O$ space (Figure 1.4A and C).

The remineralisation and nitrification of PON produced from complete nitrate consumption leads to a decrease in nitrate $\delta^{18}O$ relative to its $\delta^{15}N$. This is because when the PON is nitrified, it produces nitrate with a $\delta^{15}N$ equal to that of the nitrate supply that was consumed. By contrast, the $\delta^{18}O$ is lowered relative to the source nitrate as the nitrification value is lower than the $\delta^{18}O$ that was removed (typically ≥2‰) (Sigman et al. 2009a). The net result of complete nitrate consumption coupled with nitrification is thus a deviation below the 1:1 line in nitrate $\delta^{15}N$ vs. $\delta^{18}O$ space (Figure 1.4A and D; Sigman et al. 2009c)

In some marine environments such as coastal systems where sedimentary processes are relevant to the upper water column, the dual isotopes can reflect additional overlapping processes. For example, on shallow continental shelves, coupled nitrification-denitrification in the sediments has been shown to raise the $\delta^{15}N$ and lower the $\delta^{18}O$ of the overlying nitrate (Granger et al. 2011). The $^{15}N$ enrichment is due to the loss of low-$\delta^{15}N$ nitrogen as $N_2$ gas, which occurs as follows. Organic matter in the sediments is remineralized to ammonium that

is similar in $\delta^{15}N$ to the PON from which it derives and that is subsequently released into bottom waters overlying the sediments. The partial nitrification of this ammonium, which occurs with a large ε (≥14‰; Casciotti et al. 2003), enriches the residual ammonium pool in $\delta^{15}N$ and produces newly nitrified nitrate that is low in $\delta^{15}N$. The low-$\delta^{15}N$ nitrate, in turn, becomes the substrate for sedimentary denitrification (Christensen et al. 1987; Seitzinger 1988; Devol 1991; Devol and Christensen 1993; Jahnke and Jahnke 2000), which produces isotopically light $N_2$ that represents a loss from the fixed nitrogen inventory (Brandes and Devol 1997). The net effect is thus to raise the nitrate $\delta^{15}N$ above that of the PON that was remineralised. The $\delta^{18}O$ of nitrate, on the other hand, is lowered during nitrification such that the net result of coupled nitrification-sedimentary denitrification is a deviation below the 1:1 line in $\delta^{15}N$ vs. $\delta^{18}O$ space (Granger et al. 2011).

To further investigate and track the (de)coupling of nitrate $\delta^{15}N$ and $\delta^{18}O$ in the ocean, the tracer Δ(15-18) was defined (Sigman et al. 2005; Rafter et al. 2013):

$$\Delta(15\text{-}18) = \delta^{15}N - \delta^{18}O \quad (1.10)$$

Using the source nitrate $\delta^{15}N$ and $\delta^{18}O$ to a particular region, its Δ(15-18) can be calculated. The evolution of Δ(15-18) from the source water value, either with depth or laterally, allows us to disentangle the various nitrogen cycle processes influencing the biogeochemistry of the water column.

Nitrate assimilation and denitrification act to raise the $\delta^{15}N$ and $\delta^{18}O$ of the nitrate pool in concert such that its Δ(15-18) remains unchanged even as the residual nitrate pool becomes enriched in both isotopes (Figure 1.4B; Granger et al. 2004; Sigman et al. 2005; Granger et al. 2008; Rafter et al. 2013). A Δ(15-18) decline suggests that either $N_2$ fixation or partial nitrate assimilation has previously occurred (Figure 1.4A, B and F; Sigman et al. 2000; Sigman et al. 2009a; Rafter et al. 2013). We can distinguish between these two processes by also looking at the nitrate $\delta^{15}N$ and $\delta^{18}O$ data. The decrease in Δ(15-18) due to $N_2$ fixation is driven largely by a decrease in the $\delta^{15}N$ of the combined nitrate pool. This, as mentioned above, is due to the remineralisation of low-$\delta^{15}N$ PON that yields newly nitrified nitrate with a similarly low $\delta^{15}N$ (Sigman et al. 2000; Sigman et al. 2005; Rafter et al. 2013). On the other hand, the decline in Δ(15-18) due to partial nitrate assimilation is driven by a decrease in the $\delta^{18}O$ of the combined nitrate pool while its $\delta^{15}N$ remains largely unaltered (Sigman et al. 2009a; Rafter et al. 2013;

Fawcett et al. 2015). Finally, a rise in Δ(15-18) can be driven by either a decrease in nitrate $\delta^{18}O$ or an increase in nitrate $\delta^{15}N$. Newly nitrified nitrate produced from the remineralization of PON deriving from complete consumption of surface nitrate has a $\delta^{15}N$ that resembles the source nitrate and a $\delta^{18}O$ similar to seawater (i.e., lower than the $\delta^{18}O$ of the nitrate that was consumed). This nitrate, when added to the subsurface nitrate pool, will lower its $\delta^{18}O$ and increase its Δ(15-18) (Sigman et al. 2009a, c; Rafter et al. 2013). Coupled nitrification-denitrification in the sediment will also increase nitrate Δ(15-18) in the bottom waters overlying the sediments, but in this case by increasing nitrate $\delta^{15}N$ and decreasing its $\delta^{18}O$ (Granger et al. 2011).

The effects of many of the biological processes discussed above are clearly visible in Figure 1.4F, which is shown as an example. Here, the Δ(15-18) of Circumpolar Deep Water nitrate is 3‰ (i.e., $\delta^{15}N$ = 5‰ and $\delta^{18}O$ = 2‰). The modification of this nitrate due to organic particle remineralization and nitrification can be tracked through the changes in its Δ(15-18) as it circulates from the deep Pacific, through the surface waters of the Southern Ocean, and into the intermediate depth Pacific (Rafter et al. 2013).

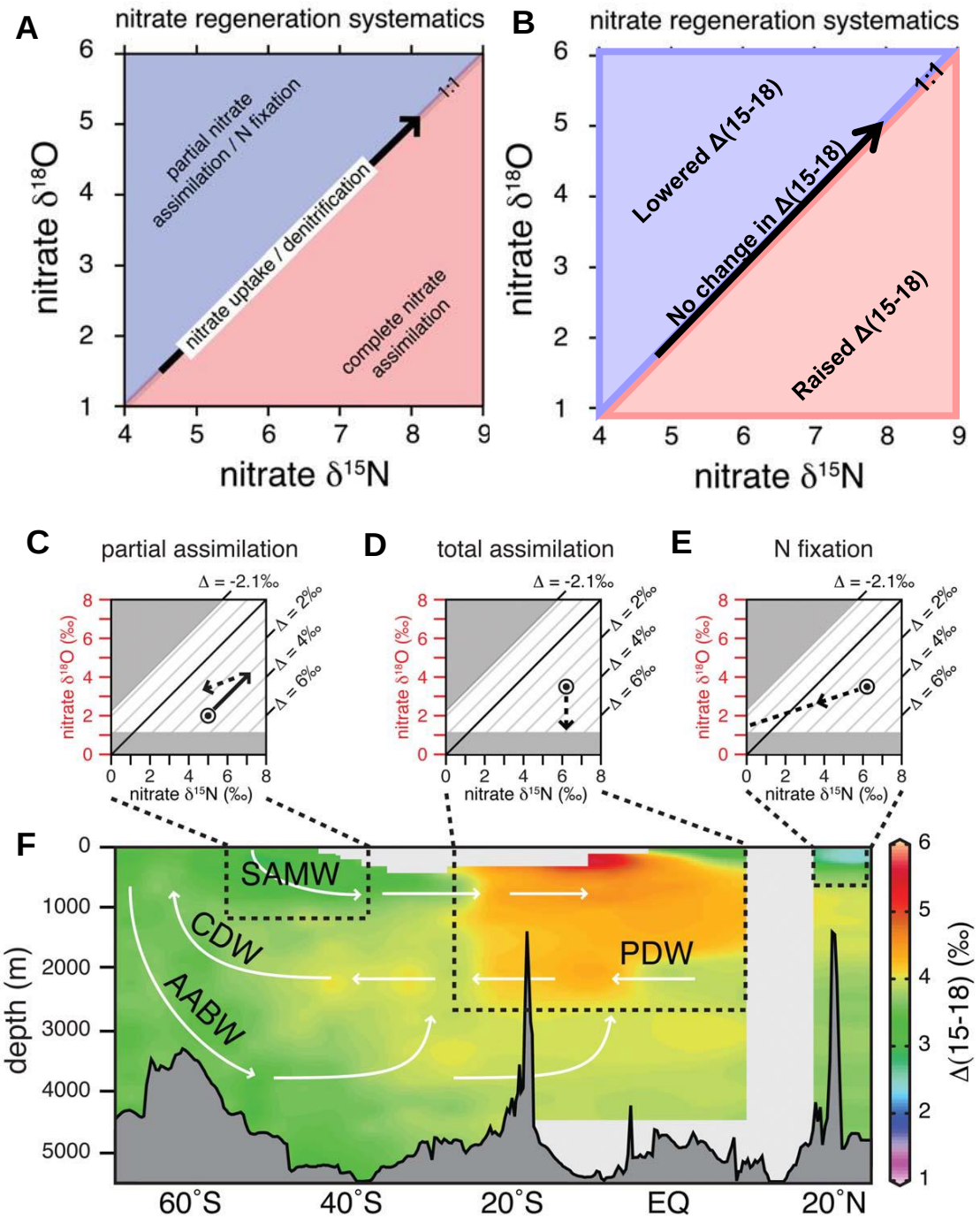


**Figure 1.4** Simple models for the modification of the dual nitrate isotopes by various biological processes occurring in the ocean. (A) Nitrate $\delta^{15}N$ and $\delta^{18}O$ evolve in a ratio of 1:1 during nitrate assimilation and denitrification. Low-$\delta^{15}N$ nitrate is introduced through the nitrification of particles produced by $N_2$ fixation or partial nitrate assimilation, driving a positive deviation from the 1:1 line, while low-$\delta^{18}O$ nitrate is introduced through the nitrification of particles produced by complete nitrate assimilation, introducing a negative deviation from 1:1. (B) The

change in Δ(15-18) due to the various biological processes represented in panel A. (C) Partial nitrate assimilation leads to an initial rise in the $\delta^{15}N$ and $\delta^{18}O$ of the residual nitrate pool (solid arrow) followed by a decrease in $\delta^{15}N$ relative to $\delta^{18}O$ due to organic matter remineralisation (dotted arrow). Mixing of the residual and remineralised nitrate produces a combined nitrate pool that is high in $\delta^{18}O$ relative to its $\delta^{15}N$. (D) Where surface nitrate is completely consumed, remineralisation of particles produces regenerated nitrate with a $\delta^{15}N$ that is equivalent to the source nitrate that was consumed while the $\delta^{18}O$ of regenerated nitrate is set by the (low) $\delta^{18}O$ of seawater. (E) $N_2$ fixation produces particles that are low in $\delta^{15}N$. The nitrate resulting from the nitrification of these particles is similarly low in $\delta^{15}N$ with a $\delta^{18}O$ set by seawater, together driving a change in the isotopic composition of the combined nitrate pool in the direction of the dashed arrow. (F) The evolution of nitrate Δ(15-18) in the Pacific Ocean from a deep ocean value of ~3‰ due to the various biological processes represented in panels C-E [Figure adapted from Rafter et al. 2013].

## 1.2 The southern Benguela upwelling system

Eastern boundary currents are some of the most productive ecosystems in the global ocean (Ryther 1969; Pauly and Christensen 1995). These regions occupy roughly 1% of ocean area while accounting for 20% of the world's fish catches (Pauly and Christensen 1995). The Benguela Current is the eastern boundary current of the South Atlantic gyre and extends from Angola to the Agulhas bank (Figure 1.5; Peterson and Stramme 1991; Wedepohl et al. 2000). The Benguela upwelling system is unique in that it is bounded on either end by warm waters. The northern boundary is defined by the Angola-Benguela Front where the cool, equatorward flowing Benguela Current meets the warm, poleward flowing Angola Current. The southern boundary is defined by the position of the Agulhas Current retroflection (Shannon and Nelson 1996; Veitch et al. 2009).

### 1.2.1 Physical dynamics of the Benguela upwelling system

The Benguela Current flows towards the equator along the eastern boundary of the South Atlantic gyre and is 200-300 km wide (Defant 1936). As the current flows northwards, it meanders along the coast. Upon reaching the Angola-Benguela Front at 20°S, the current is

forced to change direction and begins flowing in a westerly direction (Stander et al. 1969; Shannon et al. 1973; Harris and Shannon 1979; Nelson and Hutchings 1983). The mean annual transport of the Benguela Current has been estimated to be approximately 15 Sv, with the current typically flowing equatorward at speeds between 10-30 cm $s^{-1}$ (Shannon 1985).

The Benguela upwelling system (BUS) includes seven sites ("cells") where wind-driven upwelling is most prominent. The most energetic site is the Lüderitz upwelling cell at 27ºS. Due to the intensity of this upwelling cell, it acts as a barrier that separates the northern BUS (NBUS) from the southern BUS (SBUS; Figure 1.5; Shannon 1985; Shannon and Nelson 1996; Hutchings et al. 2009b), hindering the transport of water masses, organisms, particles and nutrients. between the two subsystems (Shannon and Pillar 1986; Duncombe Rae 2005; Lett et al. 2007; Gibbons and Hutchings 1996). Three of the seven upwelling sites are located in the SBUS. Upwelling at these sites is influenced by a combination of the shelf width and coastal topography near Hondeklip Bay (Namaqualand cell), Cape Columbine (Columbine cell) and the west coast of the Cape Peninsula (Cape Point cell; Figure 1.5) (Nelson et al. 1983).

Upwelling in the BUS is highly variable and seasonal, with the exception of at the Lüderitz cell where upwelling is perennial (Hutchings et al. 2009b). As in other wind-driven upwelling systems, when upwelling occurs in the BUS it is driven by equatorward winds that lead to the offshore Ekman transport of surface waters. This allows cool, nutrient-rich deeper waters to be upwelled to the surface to fuel primary productivity (Nelson and Hutchings 1983). The equatorward winds are associated with the position of the South Atlantic anticyclone (SAA; Shannon 1985). During summer, the increased heating of land induces low pressure systems that enhance the zonal gradient between the SAA and southern Africa, intensifying the southerly wind stress (Figure 1.6A and B; Nelson and Hutchings 1983). During winter, the SAA shifts northwards with the movement of the Intertropical Convergence Zone (ITCZ). This shift causes the NBUS to be dominated by southerly winds while the SBUS, south of St Helena Bay, is subjected to atmospheric frontal activity, particularly cold front systems, that induce westerly wind stresses (Figure 1.6C and D; Shillington 1998, Hardman-Mountford 2003). In the northern region of the SBUS, north of St Helena Bay, south easterly winds continue to dominate in winter, albeit not to the same extent as in the summer. This is due to a wintertime relaxation in the pressure gradient between the continent and ocean as a consequence of less continental heating (Figure 1.7B; Nelson and Hutchings 1983). The change in wind direction and strength leads to a dampening of upwelling in the SBUS during the winter. The SBUS

therefore experiences upwelling predominantly during the spring and summer (Hutchings et al. 2009a).

The seasonality in SBUS upwelling is evident in the sea surface temperature gradients observed in the different seasons. During summer, the temperature gradient between the inshore and offshore waters is large, with inshore temperatures as low as 9°C and offshore temperatures reaching 22°C (Shannon 1966; Lamont et al. 2015). In the winter, the inshore-offshore temperature gradient is not as stark due to the decrease in upwelling favourable winds and offshore cooling. Andrews and Hutchings (1980) postulated that in winter, downwelling was induced in the SBUS by the prevailing northerly winds, leading to offshore surface waters being advected inshore. More recent studies have shown that during periods of quiescence (i.e., when upwelling favourable winds cease), the mean surface transport remains offshore with onshore advection rarely observed (i.e., the SBUS appears to never experience downwelling; Barange and Pillar 1992; Carr and Kearns 2003; Veitch et al. 2009). During periods of quiescence, the isopycnals outcrop at the inshore surface due to the nearshore bathymetry that forces on-shelf bottom waters to the surface. The isopycnal outcropping observed during quiescence is termed "quiescent upwelling" (Shannon 1985) and is the reason that the inshore SBUS waters do not warm up much in winter.

In the SBUS, the Benguela Current is characterized by two flow paths traveling equatorward: the Benguela Coastal Current (BCC; Figure 1.5) and the Benguela Oceanic Current (BOC; Figure 1.5) (Veitch et al. 2010). The oceanic flow, i.e., the BOC and the portion of the current that is situated within the Agulhas eddy corridor, is induced by the Oceanic Front (OF) that separates the cool, inshore upwelling region from the warmer offshore waters of the South Atlantic subtropical gyre (Garzoli and Gordon 1996). The coastal flow, i.e., the BCC and the portion of the current present over the continental shelf, is steered by the shelf edge and induced by coastal upwelling (Veitch et al. 2010). North of Cape Columbine, where the continental shelf broadens, the Cape Jet (CJ), which originates on the western Agulhas bank (Bang and Andrews 1974; Shelton and Hutchings 1982; Boyd et al. 1992; Largier et al. 1992; Boyd and Shillington 1994; Boyd and Nelson 1998), branches into two flows that form the Columbine Front (CF) and the Shelf Break Front (SBF; Figure 1.5) (Shannon 1985; Shannon and Nelson 1996; Veitch et al. 2010). The CF is induced by coastal, wind-driven upwelling and the SBF to its west is formed by cool waters that are upwelled due to the rapid shallowing of the

continental shelf (Shannon 1985). The bifurcation of the CJ is not a year-round feature. The CF and SBF have been observed to merge during periods of intense and quiescent upwelling, in both cases as a result of the erosion of the surface water temperature gradient between the fronts. This occurs when upwelling is so intense that the rapid supply of cold, deep waters removes the temperature gradient, and during quiescent upwelling periods, particularly in autumn and winter, when surface cooling from the atmosphere and decreased offshore advection of surface waters causes the temperature gradient to disappear (Figure 1.8; Nelson and Hutchings 1983; Shannon and Nelson 1996; Shannon 1985).

The fronts that are present in the SBUS can be identified on the basis of their temperature and position on the shelf. Lamont et al. (2015) found that there are seasonal changes in the fronts along a hydrographic line extending offshore from St Helena Bay, termed the St Helena Bay monitoring line. In late summer, all three fronts are present unless upwelling is extremely intense (see above). The CF, which is induced by coastal upwelling, occurs along the 200 m isobath and is identified by the 15ºC isotherm (Shannon 1985; Lamont et al. 2015). The SBF, which is induced by upwelling at the shelf break, is present along the shelf break (defined as the 300 m isobath) and identifiable by the 17ºC isotherm (Veitch et al. 2009; Veitch et al. 2010; Lamont et al. 2015). The OF is present in late summer only and is defined by the 18ºC isotherm, clearly separating Modified Upwelled Water from the warmer offshore Oceanic Surface Water (Lamont et al. 2015). In winter, the SBF and CF are observed to merge, as described above and this merged front is identified by the 14ºC isotherm. In sum, the fronts present in the SBUS vary seasonally along with changes in the upwelling dynamics, with implications for the residence time of surface (and possible subsurface) waters and the offshore advection of plankton and nutrients.

The CJ is an important physical feature for South African fish stocks. Commercially important fish species such as anchovy spawn on the Agulhas bank and rely on the northward flowing jet to transport their eggs and larvae into St Helena Bay, the largest bay in the SBUS. The retention of the eggs and larvae in St Helena Bay provides the larvae access to sufficient resources to increase their recruitment (Shelton and Hutchings 1982; Parada et al. 2003). Due to the topography surrounding Cape Columbine and Cape Point, wind velocity is observed to decrease within St Helena Bay and Table Bay, north of Cape Columbine and Cape Point, respectively, which induces a cyclonic wind-stress curl. This results in the retention of upwelled waters in St Helena Bay and Table Bay (Kamstra 1985; Jury 1985) providing suitable

conditions for mass phytoplankton blooms, which in turn enhances the recruitment of commercially-important fish stocks (Andrews and Hutchings 1980; Shannon et al. 1984; Shannon 1985; Shannon 2003).

The fronts of the SBUS also act as physical barriers to the offshore advection of surface waters (Barange et al. 1992). For example, Andrews and Hutchings (1980) deduced that when surface waters advecting offshore reach a front, they are subducted below it (Figure 1.8), evidenced by maximum chlorophyll concentrations occurring along the base of the thermocline (Andrews and Hutchings 1980). During both quiescent and intense upwelling, the merging of the CF and SBF allows inshore waters to be advected as far as the SBUS midshore (out to the shelf break), increasing the residence time of inshore surface waters and allowing phytoplankton to more completely consume the nutrients available in these waters (Barange and Pillar 1992).

The SBUS is clearly a highly variable hydrographic region. In contrast to the fairly significant body of knowledge that exists regarding the physics of the SBUS, relatively little is known of its biogeochemistry. Seasonal variability is expected given the strong seasonality of the upwelling, and the character of this seasonality is likely to have implications for the biology of this commercially important region.

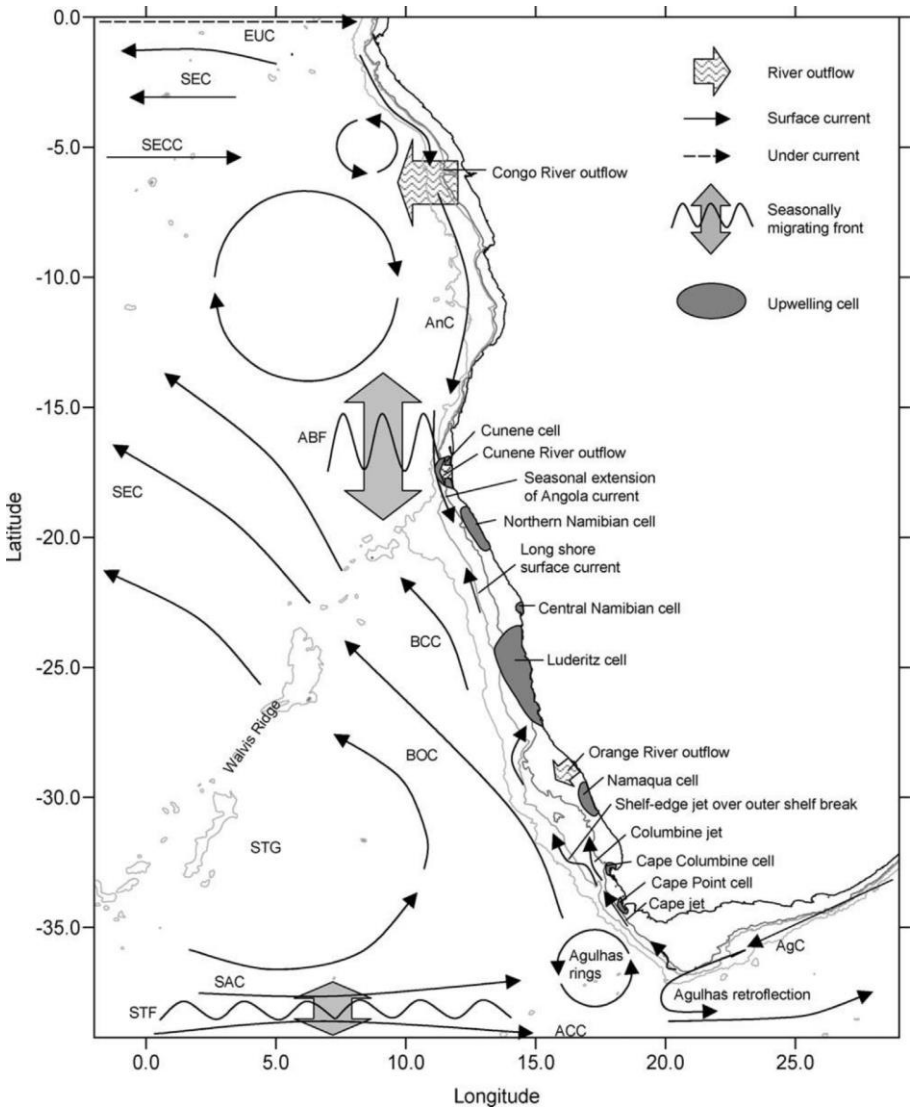


**Figure 1.5** A map showing the Benguela upwelling system and relevant features of the southeast Atlantic Ocean including the surface currents (solid lines and arrows), the upwelling cells (grey circles), and the north and south frontal zones that border the Benguela upwelling system (the Angola-Benguela Front (ABF) and Subtropical Front (STF), respectively). The focus of this thesis is the region to the south of the Orange River outflow. Other relevant acronyms include AnC (Angola Current), SEC (South Equatorial Current), BCC (Benguela Coastal Current), BOC (Benguela Oceanic Current), STG (subtropical gyre), SAC (South Atlantic Current), AgC (Agulhas Current) [Figure from Hardman-Mountford et al. 2003].

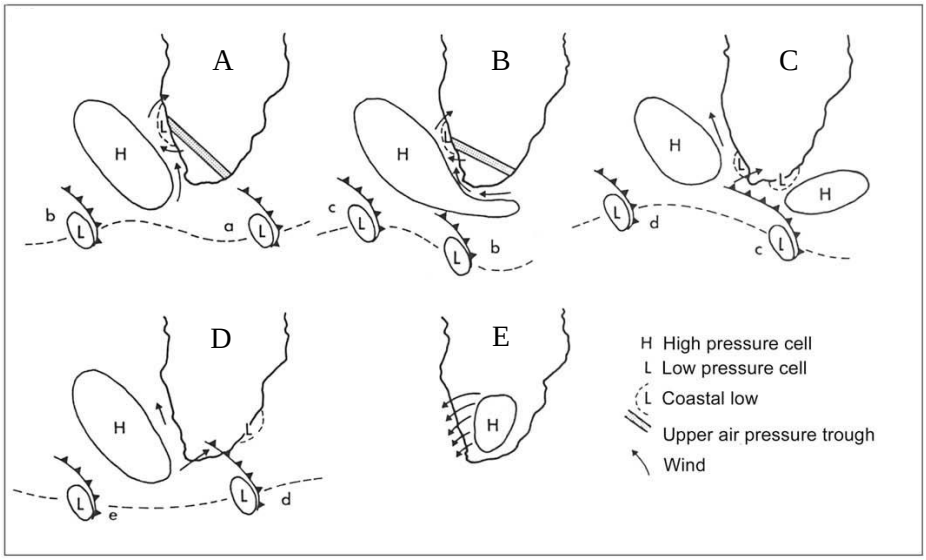


**Figure 1.6** The position of the South Atlantic anticyclone (represented here as the large high pressure cell, H) and low pressure cells (L) over the South Atlantic and their influence on the local wind dynamics in the SBUS under different conditions. A) South Atlantic anticyclone established, coastal low at Lüderitz, southerly winds in the SBUS; B) South Atlantic anticyclone extends eastwards, coastal low at Lüderitz moves south, gale force winds in the SBUS; C) South Atlantic anticyclone weakens allowing the front to ridge, inducing westerly winds in the SBUS; D) South Atlantic anticyclone strengthens, southerly winds in the SBUS; E) Berg wind conditions: warm, dry offshore winds originating from the interior of South Africa [Figure from Nelson and Hutchings 1983].

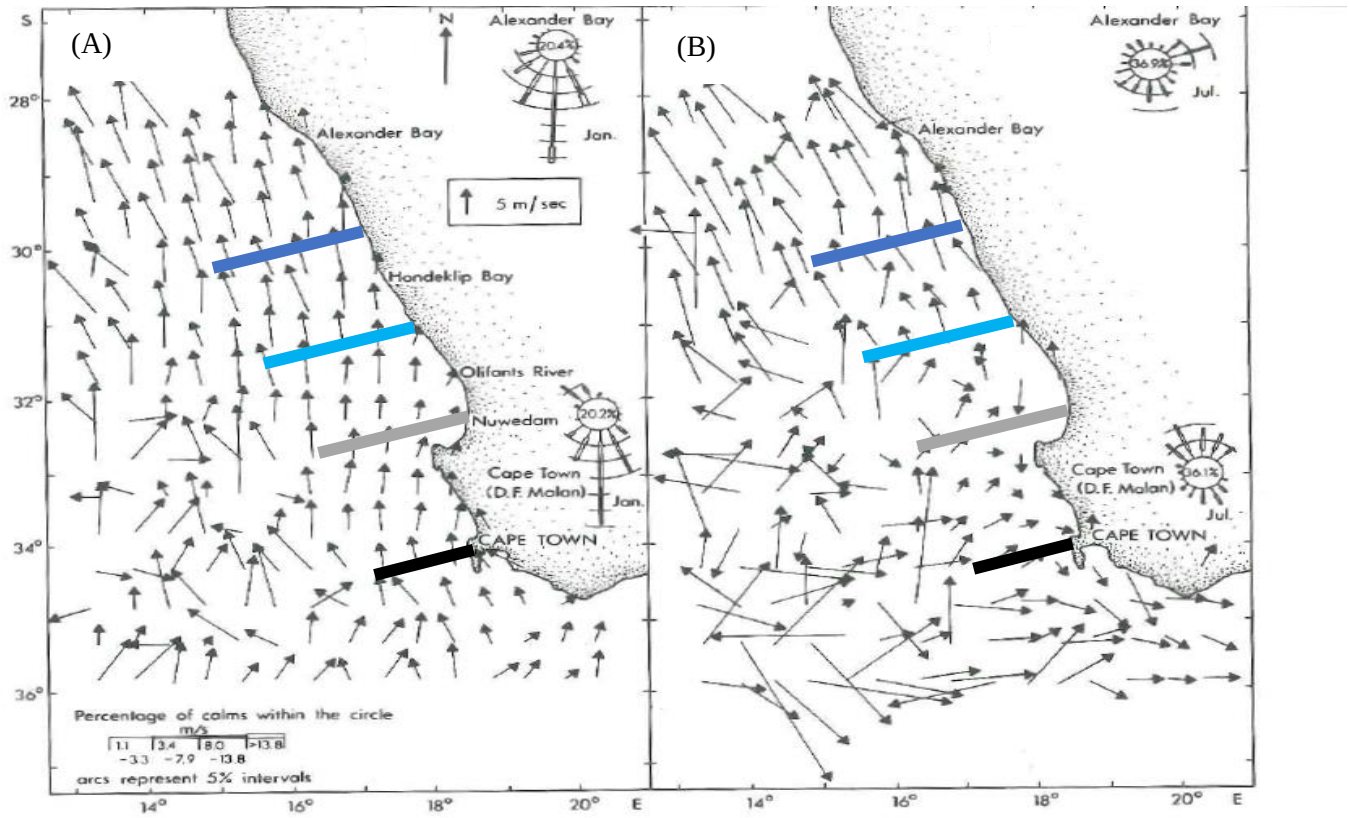


**Figure 1.7** A schematic of the mean wind speed vectors in A) summer and B) winter with the position of the Integrated Ecosystem Programme monitoring lines (see chapter 2) overlaid. These included, from north to south, the Kleinsee monitoring line (dark blue), Namaqualand monitoring line (light blue), St Helena Bay monitoring line (grey), and Scarborough monitoring line (black) [Figure adapted from Shannon 1985].

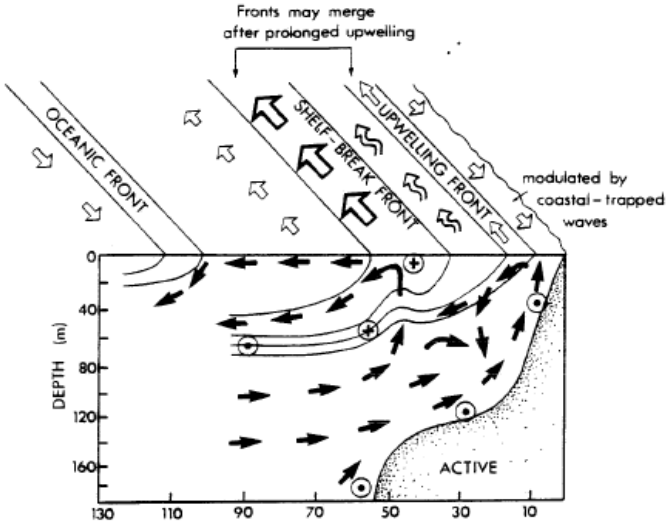


**Figure 1.8** A 3-dimensional representation of the cross-shelf circulation in the Benguela upwelling system. The positions of the various fronts are indicated by lines and text, and the

net direction of Ekman transport is shown by the solid arrows. The open arrows show the surface transport induced by the various fronts, with subsurface transport indicated by the transport dots (poleward currents) and crosses (equatorward currents) [Figure from Barange and Pillar 1992].

### 1.2.2 Biogeochemistry of the Benguela upwelling system and South Atlantic

The SBUS is an important socio-economic region for South Africa as it sustains a large portion of the country's commercial fisheries (Shannon et al. 2003). The biogeochemistry of the SBUS underpins its productivity and thus the food supply available to important marine resources. St Helena Bay, an important nursery ground for sardine and anchovy, has been the focus of numerous studies of primary productivity, as well as of seasonal changes in upwelling conditions and nutrients (e.g., Chapman et al. 1991; Hutchings et al. 2012; Lamont et al. 2015). However, less is known of the other upwelling cells and how they might influence the biogeochemistry and productivity of the greater SBUS.

#### *On-shelf processes*

The upwelling of nutrient-rich, deep water to the euphotic zone stimulates phytoplankton growth in the SBUS (Legendre 1981; Barber and Smith 1981; Mitchell-Innes and Walker 1991; Brown et al. 1991; Pitcher et al. 1992), as in all wind-driven upwelling systems. Inlets and bays located along the coastline of the SBUS act as upwelling shadows, retaining upwelled waters and allowing for the development of large phytoplankton blooms inshore (Graham et al. 1997). The death and subsequent sinking and remineralisation of the particulate organic matter associated with these large blooms often leads to events of hypoxia (and occasionally, anoxia) on the SBUS shelf (Pitcher and Calder 2000; Levin et al. 2009; Monteiro et al. 2011; Pitcher et al. 2014), the most frequent and intense of which are observed in St Helena Bay (De Decker 1970; Bailey and Chapman 1985; Bailey 1991; Monteiro and van der Plas 2006; Hutchings et al. 2012). Changes in the dissolved oxygen concentration have been suggested as the environmental factor with the largest impact on marine resources in the region (Van der Lingen et al. 2006). For example, west coast rock lobster (*Jasun Ialandii*) have been observed to "walk out" of the ocean when oxygen in inshore SBUS waters declines to hypoxic levels. In one such event in February 2015, 200 tons of west coast rock lobster were stranded onshore causing the fishery to lose an estimated R114,000,000 (~$7,000,000; National Ocims 2018).

The remineralisation of particulate organic matter in bottoms waters on the shelf of the BUS has been documented in the literature since the 1960s (Hart and Currie 1960). This process has been shown to regenerate high concentrations of nutrients (mainly nitrate, phosphate and silicic acid) on the shelf in the NBUS and SBUS, at times leading to a higher nutrient burden on the shelf than the concentrations observed in the upwelling source waters available (Calvert and Price 1970).

The regeneration of nutrients on the shelf of the BUS by heterotrophic bacteria leads to low oxygen concentrations in subsurface waters (Calvert and Price 1970). In regions of the NBUS where active upwelling does not occur, low to zero oxygen concentrations have been observed to be accompanied by low nitrate and high nitrite concentrations, interpreted as evidence of water column denitrification (Calvert and Price 1970). However, Kuypers et al. (2005) conclude that annamox rather than denitrification is the major pathway for nitrogen loss in the NBUS, and therefore could also be important within the SBUS. Neither denitrification nor anammox have ever been directly observed in the water column of the SBUS, which does not sustain anoxic conditions for extended periods (Pitcher and Weeks 2006; Hutchings et al. 2009). Denitrification has however been identified in the sediments of the SBUS on the basis of porewater nitrate and ammonium concentration and the lower than Redfield N:P ratios in the overlying water column (Bailey 1987; Bailey and Chapman 1991; Tyrell and Lucas 2002), is supported by perennial anoxia and a near-constant supply of fresh organic matter from the overlying surface waters. Despite the implications of denitrification and annamox for regulating primary production, the effects of these processes have never been quantified.

The BUS has been identified as the most productive of the four major upwelling systems based on satellite data and modelling studies (Carr 2001; Carr and Kearns 2003; Rossi et al. 2009; Lachkar and Gruber 2012). The largest compilation study of net primary productivity (NPP) in the SBUS to date (Brown et al. 1991) found that *in situ* rates of NPP were ~50% higher than those estimated by an ecosystem model presented in Field et al. (1991). NPP in the SBUS may be even higher than suggested by satellite data. Studies have suggested that the on-shelf regeneration of nutrients in the SBUS to concentrations exceeding those in the source waters may explain the high observed rates of NPP (Jones 1971; Bailey and Chapman 1985; Bailey 1985; Probyn 1987; Waldron et al. 1992; Hutchings et al. 1995; Tyrell and Lucas 2002). The *in situ* sedimentation and remineralization of PON produced from the high rates of NPP has been shown to deplete bottom oxygen concentrations and further enhance the on-shelf

concentration of regenerated nutrients (Bailey and Chapman 1985; Bailey 1991). However, the mechanism(s) that sustain these high concentrations of nutrients on-shelf, and the extent to which their concentrations and distributions vary seasonally, remain unknown.

***Upwelling source waters***

In addition to the complex nutrient cycling occurring inshore of the Benguela Current, the water masses feeding the SBUS are integral to our understanding of the biogeochemistry of the region. The waters that upwell onto the shelf and into the euphotic zone will shape the marine community and control the extent of organic carbon production and net carbon dioxide removal as they replenish surface waters with nutrients and oxygen (Brown et al. 1991; Kampf and Chapman 2016). Previous studies have shown that the main water masses present in the SBUS are Upper Circumpolar Deep Water (UCDW), Antarctic Intermediate Water (AAIW), Subantarctic Mode Water (SAMW), South Atlantic Subtropical Mode Water (SASTMW), Modified Upwelled Water (MUW) and Oceanic Surface Water (OSW) (Figure 1.9; Donners et al. 2005; Duncombe Rae 2005; Lamont et al. 2015). SAMW is the major source of upwelled water to the shelf and inshore SBUS (Lamont et al. 2015).

UCDW and AAIW are categorised as deep water masses in the SBUS. AAIW overlies UCDW, is present below 400 m off the shelf and does not upwell onto the shelf (Lamont et al. 2015). SAMW is present between 200-400 m off the shelf and is upwelled onto the shelf throughout the year (Figure 1.9; Lamont et al. 2015). SAMW upwells inshore of the CF, throughout the year, and inshore of the SBF during summer (Lamont et al. 2015). SASTMW overlays SAMW off the shelf and does not appear to upwell inshore of the CF (Figure 1.9; Lamont et al. 2015). Modified Upwelled Water (MUW) overlies SAMW and SASTMW and is present in surface waters inshore of the OF, with MUW occupying the thermocline (i.e., the upper 100 m of the water column) with increased vertical extent in winter; while Oceanic Surface Water (OSW) is present in the surface west of the OF (Lamont et al. 2015).

The studies cited above characterized the oxygen concentration, salinity and temperature of the above-mentioned water masses; however, no study has yet characterized their nutrient concentrations and nitrate isotopic composition. Characterizing the seasonal changes in the nutrient concentrations and isotopic composition of SAMW and SASTMW on the shelf allows us to identify and disentangle the various biological processes ongoing in the surface and

subsurface of the on-shelf waters, with implications for understanding the drivers of primary production and oxygen dynamics in the SBUS.

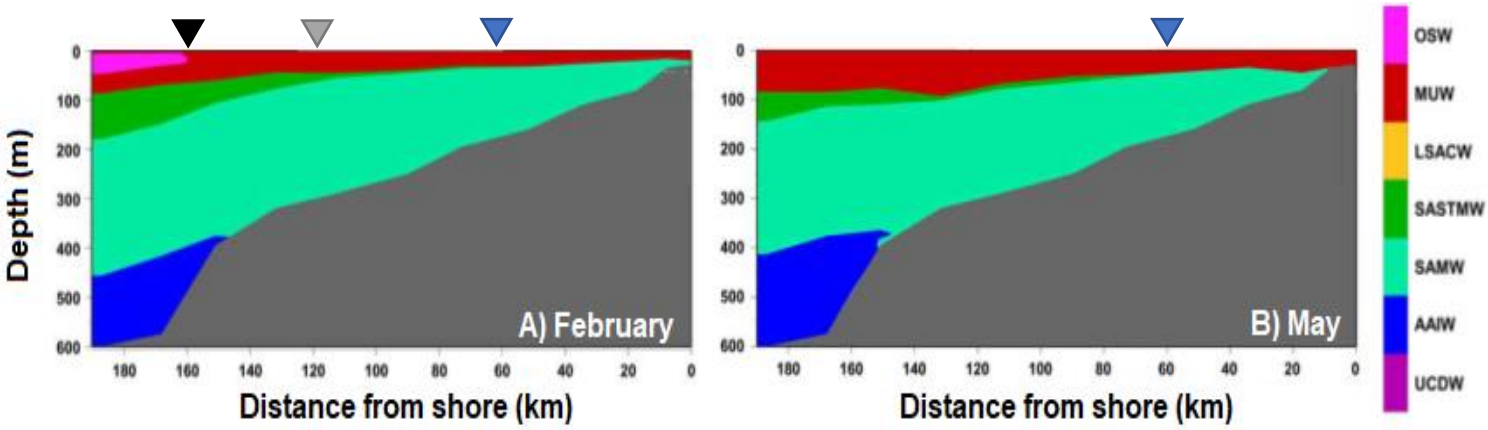


**Figure 1.9** A climatology (2000-2012) of the vertical distribution of water masses along the St Helena Bay monitoring line in A) February and B) May. The inverted triangles indicate the climatology position of the Columbine Front (CF; blue triangle), the Shelf Break Front (SBF; grey triangle), and the Oceanic Front (OF; black triangle). The water masses present in the SBUS are Ocean Surface Water (OSW), Modified Upwelled Water (MUW), South Atlantic Subtropical Mode Water (SASTMW), Subantarctic Mode Water (SAMW), Antarctic Intermediate Water (AAIW) and Upper Circumpolar Deep Water (UCDW) [Figure from Lamont et al. 2015].

### 1.3 Nitrate isotopes in other upwelling systems

Although measurements of the dual nitrate isotopes (i.e., $\delta^{15}N$ and $\delta^{18}O$) had not been conducted in the SBUS prior to the present study, there have been nitrate isotope studies in other upwelling systems. Below, we focus on nitrate isotope data from the NBUS and California upwelling system as the NBUS forms part of the greater BUS while the California upwelling is the best studied of the four major upwelling systems and does not exhibit permanent oxygen-deplete conditions in the water column (Wankel et al. 2007; Bograd et al. 2008).

The NBUS is characterised by very high rates of primary production and low oxygen concentrations that vary on a seasonal timescale (e.g., Monteiro et al. 2008; Louw et al. 2016). Using measurements of nitrate isotopes, Nagel et al. (2013) and Emeis et al. (2017) conclude that in the suboxic waters of the NBUS, heterotrophic denitrification takes place in the water column over the shelf and upper continental slope. The evidence presented to support this is a rise in nitrate $\delta^{15}N$ and $\delta^{18}O$ along a 1:1 line in $\delta^{15}N$ vs. $\delta^{18}O$ space along with a decrease in the nitrate concentration for samples collected in the subsurface (Emeis et al. 2017). In addition, the diatomaceous ooze found on the NBUS shelf has a $\delta^{15}N$ (5-8‰), that is on average higher than that of South Atlantic Central Water, the source water mass to the NBUS surface waters. The authors interpret the elevated $\delta^{15}N$ of the diatomaceous ooze as reflecting the assimilation of nitrate that is higher in $\delta^{15}N$ than the source waters because of isotopic fractionation during local water column denitrification (i.e., after the source water had upwelled onto the shelf) (Emeis et al. 2009; Meisel et al. 2011; Nagel et al. 2016; Emeis et al. 2017).

Another line of evidence for denitrification in the NBUS is that it hosts a nutrient N:P ratio that is lower than Redfield (i.e., lower than 16:1) (Dittmar and Birkicht 2001; Tyrrell and Lucas 2002; Nagel et al. 2013; Emeis et al. 2017). It has been hypothesized that the decrease in the N:P ratio due to denitrification is further enhanced by phosphate efflux from the sediment under low oxygen conditions (Bailey 1987; Kuypers et al. 2005; Nagel et al. 2013). Interestingly, once the low N:P water is upwelled to the surface again, it apparently does not stimulate $N_2$ fixation in the NBUS as might be expected (Deutsch et al. 2007). Indeed, Wasmund et al. (2015) found almost no evidence for $N_2$ fixation in the NBUS and adjacent ocean based on *in situ* rate measurements. A follow-up study attributed this to a lack of seeding populations of $N_2$ fixing phytoplankton and bacteria in the region (Emeis et al. 2017). Nagel et al. (2013) conclude, using nitrate $\delta^{15}N$ data, that no $N_2$ fixation occurs in on-shelf surface waters of the NBUS. The authors also postulate, however, that $N_2$ fixation may occur in the surface waters offshore, although contributing a small proportion of new nitrogen to the fixed nitrogen pool. In another study conducted in the region, the highest measured $N_2$ fixation rate in the NBUS or adjacent South Atlantic gyre was < 8 nmol N $L^{-1}$ $d^{-1}$ (Sohm et al. 2011). This rate, while not insignificant, would contribute a very small quantity of fixed nitrogen relative to other available sources such as nitrate and ammonium. In addition, the average $N_2$ fixation rate for the region was much lower than this (<3 nmol N $L^{-1}$ $d^{-1}$; Sohm et al. 2011).

The California upwelling system, like the SBUS, does not experience permanent low $O_2$ concentrations as observed in some of the other upwelling systems (e.g., Rosenberg et al. 1983). In Monterey Bay in the California upwelling, Wankel et al. (2007) measured the dual isotopes of nitrate over an annual cycle and concluded that the euphotic zone hosts significant rates of partial nitrate assimilation followed by nitrification year-round. The evidence supporting this was an increase in nitrate $\delta^{18}O$ that was consistently higher than the rise in nitrate $\delta^{15}N$ (see section 1.1 above). They authors calculated that 15-27% of the nitrate assimilation occurring in the California upwelling is supported by euphotic zone nitrification and should be considered regenerated rather than new production. Coupled nitrate assimilation-nitrification may also prove important in the SBUS, although as yet direct measurements of nitrification are scarce. Nonetheless, if nitrification is occurring in the SBUS euphotic zone at rates that are significant relative to that of upward nitrate supply, the implications is that existing estimates of new production and carbon export potential may be too high (Yool et al. 2007).

### 1.4 Scope of thesis

In this thesis, the first nitrate N and O isotope data for the SBUS are presented in the context of other biogeochemical and physical variables. The focus of this study was to use the stable isotopes of nitrate, along with nutrient and oxygen concentrations, derived biogeochemical tracers, and physical data to characterize the seasonal nitrogen cycle of the SBUS in order to better understand the productivity and oxygen dynamics of this economically- and ecologically-important region.

First, the methods used for the collection and analysis of samples from the summer and winter of 2017 are described. Second, the results of these analyses are presented within the hydrographic context offered by four monitoring lines that cover the aerial extent of the SBUS and that were occupied in both seasons. Third, an overview is given of the concentrations and cycling of nutrients upwelled in SAMW and SASTMW, which strongly suggests that high quantities of nutrients are regenerated on the mid- and inshore shelf, raising the concentration of nutrients available for upwelling above that of the source waters. The proportion of nutrients regenerated *in situ* is quantified using the oxygen isotope ratios of nitrate. Along with the nitrogen isotope ratios, these data also provide insights into the changes in nitrogen cycling

between the intense upwelling period in summer and the period of quiescence in winter, particularly with respect to the addition and removal of on-shelf nitrate. The spatial evolution of numerous on-shelf biogeochemical tracers is examined in order to test the hypothesis that benthic recycling enhances the productivity of the SBUS. Finally, arguments are presented that the primary mechanism leading to on-shelf nutrient trapping involves the various northward-flowing, seasonally variable fronts that characterise the SBUS. The features aid in the sequestration of sinking organic matter to the on-shelf benthos where it is regenerated. Seasonal shifts in the position of the fronts can explain the observed spatial changes in the on-shelf regenerated nutrient pool, with important implications for the intensity and aerial extent of oxygen-deplete bottom waters in the SBUS.

## 2. Methods

### 2.1 Field methods

Hydrographic stations in the SBUS were occupied in February, May and August 2017 aboard the *FRV* Algoa as part of the Department of Environmental Affairs' Integrated Ecosystem Programme (IEP) surveys. During each cruise, samples were collected at 44 stations along 4 transects located perpendicular to the shoreline between 29°38.38'S and 34°56.08'S (Kleinsee, Namaqualand, St Helena Bay and Scarborough monitoring lines), spanning the continental shelf and slope (Figure 2.1).

Hydrographic measurements were made using a conductivity-temperature-depth profiler (CTD). The temperature and conductivity probes were calibrated by the manufacturer while the CTD oxygen sensor was calibrated against discrete seawater samples analyzed for dissolved oxygen concentration by Winkler titration (Carpenter 1965; Grasshoff et al. 1983).

Discrete water masses were identified based on their temperature and salinity characteristics. Potential temperature, which normalises for the change in temperature with pressure, was plotted against absolute salinity, which cannot be directly measured and is derived from practical salinity. Potential temperature and absolute salinity were used to derive density. The formula for the conversion of temperature to potential temperature is derived from Poisson's equation:

$$\theta = T\,(p_0/p)^k \qquad (2.1)$$

Where $\theta$ is the potential temperature, T is the ambient temperature, $p_0$ is the pressure at the surface, p is the pressure at the depth of interest, and k is 0.286.

In order to convert practical salinity to absolute salinity, the Thermodynamic Equation of Seawater (TEOS-10) is used:

$$S_A = (1.0047 \text{ x practical salinity}) + \delta S_A \quad (2.2)$$

Where $S_A$ is absolute salinity and $\delta S_A$ is a correction for dissolved matter that does not contribute to conductivity.

Density (sigma-theta) was derived from temperature, salinity and pressure based on the equation of state:

$$\sigma_\theta = \rho\ (S_A, \theta, p) - 1000 \quad (2.3)$$

Where $\rho$ is density, calculated as:

$$\rho - \rho_0 = a\ (T - T_0) + b\ (S - S_0) + kp \quad (2.4)$$

Where a = 0.15 kg/m$^3$/°C, b = 0.78 kg/m$^3$/part per thousand and k = 4.5x10$^3$ kg/m$^3$/decibar.

At all stations, mixed layer depth (MLD) was determined from depth profiles of sigma-theta ($\sigma_\theta$). The MLD criterion used was a threshold value of $\Delta\sigma_\theta$ = 0.03 kg. m$^{-3}$ from the value at 10 m depth (de Boyer Montégut et al., 2004).

Seawater samples were collected at discrete depth intervals from the surface to the bottom using a tethered rosette holding twelve 6-L Niskin bottles. From each CTD station, nitrate isotope and nutrient samples were collected throughout the water column in 60 mL HDPE bottles. Each bottle was rinsed three times prior to being filled to just below the neck and immediately frozen at -20°C pending analysis. Prior to shipping and analysis, all nitrate isotope samples were filtered using a 0.2 µm syringe filter.

Water samples for bulk nitrogen isotopic analysis of particulate nitrogen (PON) were collected during two of the three cruises (February and May), predominantly from the ship's underway system (intake at 5 m). Seawater was filtered through a pre-combusted GF-75 glass fibre filter (with a nominal pore size of 0.3 µm) using an inline filter when collected from the underway, and under gentle vacuum for the samples collected in Niskin bottles. After filtration, the final volume of water filtered was noted. The samples were then folded in half using ethanol-cleaned forceps and stored in ashed tinfoil envelopes at -80°C pending analysis.

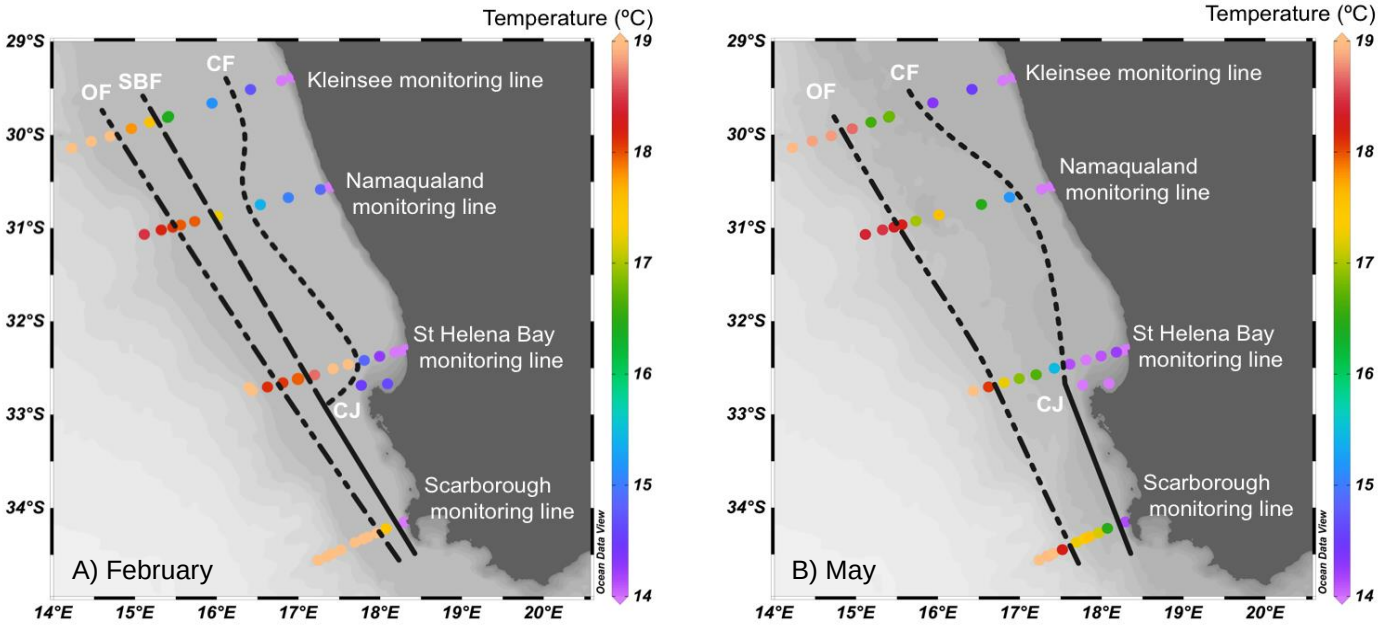


**Figure 2.1** A map of the southern Benguela Upwelling System (SBUS) showing the four IEP monitoring lines. The coloured dots show the *in situ* sea surface temperature at each station during the time of sampling in A) February and B) May 2017. The fronts that occur in the SBUS during these seasons are identified on the figure. These include the Cape Jet (CJ; solid line), the Columbine Front (CF; dotted line), the Shelf Break Front (SBF; dashed line), and the Oceanic Front (OF; dashed-dotted line). The St Helena Bay and Scarborough monitoring lines are located at the Cape Columbine and Cape Peninsula upwelling cells, respectively, with the Kleinsee monitoring line situated north of the Namaqua upwelling cell and Namaqualand monitoring line situated south of this upwelling cell.

## 2.2 Laboratory methods

### 1. Nutrient concentrations

#### a. Analysis of nitrate and silicic acid concentrations

Nitrate and silicic acid concentrations were measured on a Lachat QuickChem Flow Analysis platform following published auto-analysis protocols (Diamond 1994; Grasshoff 1976). Two channels were used for the nutrient analysis, one using the cadmium column method to reduce nitrate to nitrite and the other for the determination of silicic acid. The reduction of nitrate to nitrite by cadmium occurs as follows:

$$NO_3^- + H_2O + EDTA + Cd^0 \rightarrow NO_2^- + 2OH + Cd(EDTA)^{2-} \qquad (2.5)$$

EDTA (ethylenediaminetetracetic acid) is added to bind the $Cd^{2+}$; without the EDTA, $Cd(OH)_2$ would precipitate onto the cadmium column interfering with the flow of the sample through the column (Margeson et al. 1980). Once nitrate is reduced to nitrite, 0.1 mL of 0.2 N sulfanilimide and 0.004 N N-(1-naphtyl) ethylenediamine dihydrochloride mixed reagent is added in-line, resulting in the production of a coloured compound (Bendschneider and Robinson 1952). Sample absorbance at a wavelength of 543 nm is automatically measured and recorded. The measured nitrate concentration includes nitrite, and the nitrate concentration is obtained by subtraction.

Samples with nitrate concentrations of less than 2 µM were calibrated against nitrate standards dissolved in seawater in lieu of Milli-Q to account for any matrix effects. The use of artificial seawater substantially decreased the matrix effect and allowed for a lower detection limit for nitrate.

Silicic acid concentrations were determined using the colourimetric method of Grasshoff (1976). Silicic acid reacts with 0.2 mL of 0.2 N ammonium molybdate under acidic conditions forming a yellow beta molybdosilicic acid. The beta molybdoscilicic acid is then reduced with 0.2 mL of 0.2 N ascorbic acid to form a blue compound. Prior to passing through the

spectrophotometric module, 0.2 mL of 1 N oxalic acid is added to the sample to reduce the interferences caused by ambient phosphate. The absorbance of the solution is then measured at a wavelength of 820 nm and automatically recorded.

For both nitrate and silicic acid, standards were prepared daily, and a standard curve covering the range of expected sample concentrations was inserted at the beginning of each run of approximately 150 samples. Two reference materials of known concentration were run at the beginning of the run to ensure the accuracy of the standard curve (manufactured by the General Environmental Technos Co. Ltd; Lot. CG-0214 with $[NO_3^-]$ = 24 µM and $[Si(OH)_4]$ = 59 µM). Throughout the run, two to three "check standards" of concentrations covering the range of sample concentrations were run after every 10 samples to control for instrument drift; in the event that there was drift, it could be corrected using the "check standards". Duplicate samples were measured for nitrate and silicic acid on different days, and the standard deviation for duplicates was ≤0.5 µM. The Lachat QuickChem Flow Autoanalysis platform configuration used here has a detection limit of 0.1 µM.

### b. Analysis of nitrite concentrations

Nitrite concentrations were determined using the benchtop colorimetric Greiss reaction (Bendschneider and Robinson 1952; Parsons et al. 1984). 0.1 mL of 0.05 N Sulfanilimide in dilute acid and 0.1 mL of 0.004 N N-(1-naphtyl) ethylenediamine dihydrochloride were added to 5 mL of sample. Each sample was vortexed between the addition of each reagent and measured within two hours of reagent addition. Standards covering the range of expected sample concentrations were prepared daily from gravimetric stocks (10 mM) and were treated in the same manner as the samples. All samples were measured in duplicate on different days, and the standard deviation for duplicates was ≤0.1 µM. Absorbance was measured using a Thermo Scientific Geneysis 30 Visible spectrophotometer at a wavelength of 543 nm. The method has a detection limit of 0.05 µM.

### c. Analysis of phosphate concentrations

Phosphate was determined using the Strickland and Parsons colourimetric method (Strickland and Parsons 1968). The method requires 5 mL of sample to be transferred to a borosilicate test tube to which 0.5 mL of a mixed reagent containing 0.3 N ascorbic acid, 0.15 N ammonium molybdate, 8 N sulphuric acid and 0.002 N potassium antimonyl-tartrate solution is then added. Samples are vortexed, and absorbance is read within two hours of mixed reagent addition. Standards covering the range of expected sample concentrations were prepared daily from gravimetric stocks (10 mM) and were treated in the same manner as the samples. All samples were measured in duplicate on different days, and the standard deviation of duplicates was ≤0.1 µM. Samples and standards were measured using a Thermo Scientific Geneysis 30 Visible spectrophotometer at a wavelength of 880 nm. The method has a detection limit of 0.05 µM.

## 2. Analysis of nitrate N and O isotope ratios

Nitrate N and O isotope ratios were measured using the "denitrifier method" (Sigman et al. 2001; Casciotti et al. 2002; McIlvin and Casciotti 2011). Nitrate is added to active denitrifying bacteria that lack a terminal $N_2O$ reductase enzyme and convert aqueous nitrate quantitatively to $N_2O$ gas. The N and O isotope ratios of the $N_2O$ gas are then analysed by isotope ratio mass spectrometry (IRMS).

Prior to isotopic analysis, samples collected from depths shallower than 500 m were divided into two aliquots. 15 mL of the summer samples and 20 mL of the winter samples were transferred to acid-washed 60 mL HDPE bottles. One of the aliquots was treated with sulfamic acid to remove nitrite (Granger and Sigman 2009). 10 µL of 2 N sulfamic acid was added for every 1 mL of sample to yield a pH of ~3. The samples were shaken vigorously and left to react for 10 minutes, then neutralised with 2 N NaOH to yield a pH of ~7.5. The samples were then frozen at -20°C until analysis.

As mentioned in chapter 1, *P. aureofaciens* is one of the bacterial cultures used in the denitrifier

method. 500 mL bottles of autoclaved nitrate-containing growth media were inoculated with 0.3 mL of concentrated *P. aureofaciens* seed culture. These cultures were grown over a 7-10 day period, at which point the complete consumption of nitrate in the media was verified prior to harvesting. In the case where all nitrate was not utilised, the media was disposed of. This is important because incomplete nitrate utilisation is indicative of sub-optimal bacterial growth, which is likely to affect the conversion of sample nitrate to $N_2O$ gas. Healthy cultures were dispensed into 12 x 50 mL centrifuge tubes and centrifuged for 10 minutes at 7600 rpm using a fixed angle rotor. The spent medium was discarded and the pellet of *P. aureofaciens* was resuspended in approximately 25 mL of nitrate-free medium, supplemented with an anti-foaming surfactant, and vortexed. The resuspended cultures were combined in a 125 mL Erlenmeyer flask and gently homogenized. Three mL of the resuspended culture was dispensed into 60 muffled 20 mL borosilicate vials. The vials were capped with a butyl septa and an aluminium crimp seal. Once crimped, a 1.5 inch long, 25-gauge venting needle was inserted into each vial and the vials were purged for 5 hours with either helium or nitrogen gas (10-20 ml/min). The purging gas is introduced through a 26-gauge short needle inserted through the septum so as to bubble the medium. The vials were checked every 15 minutes to ensure that samples were bubbling. If not, the vials were not used as they may have been contaminated with air.

Once the vials had undergone degassing, 20 nmoles of sample or standard nitrate was added to each vial. In the instance where the samples had a nitrate+nitrite concentration of <2 µM, only 10 nmoles of sample or standard nitrate was added to minimize liquid volume in the vials. In order to calibrate the sample isotope ratios after IRMS analysis, certified nitrate isotope ratio reference materials dissolved in nutrient-free seawater were included in all batch analyses. These included IAEA-$NO_3^-$, potassium nitrate with a $\delta^{15}N$ and $\delta^{18}O$ of 4.7 ± 0.2‰ vs. $N_2$ air (Gonfiantini et al. 1995) and 25.6 ± 0.4‰ vs. VSMOW (Böhlke et al. 2003), respectively, and USGS34, potassium nitrate with a $\delta^{15}N$ and $\delta^{18}O$ of -1.8 ± 0.1‰ vs. $N_2$ air and -27.9 ± 0.3‰ vs. VSMOW (Böhlke et al. 2003), respectively. These standards were inserted between every 10 to 15 samples throughout a run. Nitrate standards in individual runs were diluted in nutrient-free seawater to concentrations equivalent to those of the samples to minimize potential matrix effects on the $\delta^{18}O$ of the nitrate measurements (Weigand et al. 2016). An internal standard, collected from the deep Atlantic, was analysed in duplicate in each run in order to evaluate the accuracy of the calibration between runs. Once all the vials contained sample, they were

incubated in the dark for 12 to 24 hours to allow the denitrification reaction to take place. In each run, two vials had no sample added to them and were used to determine any $N_2O$ blank.

After incubation, samples were either frozen pending IRMS analysis, or analysed directly on a continuous flow ThermoFisher Delta V Advantage IRMS interfaced with a GasbenchII, gas chromatography-based device for $N_2O$ extraction, concentration, and purification (Casciotti et al. 2002; McIlvin and Casciotti 2011) and an GC PAL autosampler, and controlled using the programme Isodat. Prior to loading the samples into the autosampler rack, a few drops of 10 N NaOH were added to each sample to kill the bacteria and trap any $CO_2$, which has a mass-to-charge ratio identical to that of $N_2O$.

The isotope ratios of $^{15}N/^{14}N$ ($\delta^{15}N$) and $^{18}O/^{16}O$ ($\delta^{18}O$) measured by the IRMS are reported in delta ($\delta$) notation in units of per mil (‰):

$$\delta X = ((R_{sample} / R_{standard}) - 1) \times 1000 \quad (2.6)$$

Where $R_{sample}$ is the measured $^{15}N/^{14}N$ or $^{18}O/^{16}O$ of the sample and $R_{standard}$ is that of the $N_2O$ reference gas measured simultaneously by the IRMS. The IRMS software therefore reports values of $\delta^{15}N$ and $\delta^{18}O$ relative to the reference gas being used by the instrument. From measurements of the certified nitrate isotope materials IAEA-$NO_3^-$ and USGS34, these instrumental $\delta$ values are converted to $\delta^{15}N$ and $\delta^{18}O$ relative to the universal standards using the following equation:

$$\delta_{X-B} = \delta_{X-A} + \delta_{A-B} + 0.001\delta_{X-A}\delta_{A-B} \quad (2.7)$$

Where $\delta_{X-B}$ is the $\delta$ value of the sample relative to the international standard (i.e., $N_2$ in air for $\delta^{15}N$ and Vienna Standard Mean Ocean Water (VSMOW) for $\delta^{18}O$), $\delta_{X-A}$ is the $\delta$ value of the

sample relative to the reference gas, in this case $N_2O$, and $\delta_{A-B}$ is the δ value of the reference gas relative to the international standard (Sharp 2007).

Values of nitrate $\delta^{15}N$ are thus reported vs. $N_2$ in air and $\delta^{18}O$ are reported vs. VSMOW throughout this thesis, converted using equation 2.7. All samples were measured in triplicate in separate batch analyses. Sample standard deviations are reported in the results section below.

### 3. Bulk PON $\delta^{15}N$

The frozen filters were prepared for isotopic analysis as follows: the filters were dried in an oven for 24 hours at 45°C then fumed in a desiccator in the presence of 12 N HCl for 24 hours to remove any residual calcium carbonate contained within the organic matter. The filters were then oven-dried again at 45°C for 1-3 hours. The filters were folded in half and cored with a 20 mm metal punch, and the cored subsamples (each comprising two 20 mm diameter filter fractions, one from each side of the folded filter) were placed in tin cups. The filters were folded in half in order to account for any transfer of particulate matter from the one side of the filter to the other prior to freezing. All surfaces and forceps were cleaned with ethanol between samples to prevent contamination with organic material.

The filters were combusted in a Flash 2000 organic Elemental Analyzer and the isotope ratios of the resulting gases ($N_2$) analysed with an in-line Delta V Plus IRMS via a Conflo IV gas control unit. A blank combustion followed every filter sample to ensure carry over from one sample to the next is reduced as much as possible. Three in-house standards were run at regular intervals: Merck Gel, a proteinaceous gel produced by Merck with a $\delta^{15}N$ of 7.5‰, Valine, a branch chain amino acid with a $\delta^{15}N$ of 12.1‰ purchased from Sigma, and an $NH_4Cl$ standard, with a $\delta^{15}N$ of -0.6‰. These standards have been calibrated against IAEA reference materials. The samples were run in batches of 30-50 samples with standards run after every 10 samples.

The $\delta^{15}N$ of PON on the filters was calculated using equation 2.6, with $R_{standard}$ being an $N_2$ reference gas in this gas. These $\delta$ values were then converted to $\delta^{15}N$ vs. $N_2$ in air using equation 2.7.

## 2.3 Derived variables

Throughout the results and discussion of this thesis, various variables have been derived in order to assist with the interpretation of the measurements. These variables are defined below:

### a. Apparent Oxygen Utilisation

Apparent oxygen utilisation (AOU; µM) is used to quantify the amount of oxygen added to or removed from a water parcel by biological activity since it last equilibrated with the atmosphere.

$$AOU = O_2' - O_2 \quad (2.8)$$

AOU is the difference between the oxygen concentration at saturation ($O_2'$), which is controlled by the salinity and temperature of the water parcel, and the measured oxygen concentration ($O_2$) (Redfield 1934, 1942; Redfield et al. 1963). If AOU is high, oxygen has been removed from a water parcel by biological activity. If, by contrast, AOU is negative, oxygen has been added to a water parcel by biological activity.

### b. N*

N* (µM) is a tracer used to understand the changes in nitrogen relative to phosphorous in a nutrient pool, therefore providing information as to whether nitrogen is being added to or lost from the system (Gruber and Sarmiento 1997). N* is defined as:

$$N^* = [\text{Total dissolved nitrogen}] - 16 \times [PO_4^{3-}] + 2.9 \quad (2.9)$$

Where total dissolved nitrogen is the sum of all dissolved nitrogen forms, i.e. nitrate, nitrite and ammonium, 16 is the stoichiometric N:P ratio observed during the remineralization of organic matter (Redfield et al. 1963; Gruber and Sarmiento 1997), and 2.9 is a constant that represents the observed mean global excess of phosphate relative to nitrate (Gruber and Sarmiento 1997).

**c. Si***

Si* (µM) is used to track water masses, in particular Subantarctic Mode Water (SAMW), which is the source water mass that upwells onto the SBUS shelf, as well as to understand the nutrient requirements of specific phytoplankton species (Sarmiento et al. 2004). Si* is defined, based on the assumption that non-limited silicic acid-using phytoplankton (i.e., diatoms) consume silicic acid and nitrate in a ratio of ~1 (Ragueneau et al. 2000), as:

$$Si^* = [Si(OH)_4] - [NO_3^-] \quad (2.10)$$

SAMW has a low Si* in its formation region (-10 µM to -15 µM; Sarmiento et al. 2004) and is therefore a good tracer of understanding any biological changes SAMW might have undergone on the shelf in the SBUS.

**d. $\Delta NO_3^-$, $\Delta Si(OH)_4$ and $\Delta PO_4^{3-}$**

$\Delta NO_3^-$, $\Delta Si(OH)_4$ and $\Delta PO_4^{3-}$ **(**µM) are used to quantify the difference between the *in situ* nitrate, silicic acid and phosphate concentrations of a water parcel versus those present in the source water prior to upwelling (i.e., SAMW). If $\Delta NO_3^-$, $\Delta Si(OH)_4$ and $\Delta PO_4^{3-}$ are positive, the implication is that post-upwelling processes occurring on the shelf are acting to raise the nutrient concentrations above those of SAMW. $\Delta NO_3^-$, $\Delta Si(OH)_4$ and $\Delta PO_4^{3-}$ are defined as:

$$\Delta X = [X]_{measured} - [X]_{SAMW} \quad (2.11)$$

Where X is nitrate, silicic acid or phosphate, $[X]_{measured}$ is the *in situ* concentration, and $[X]_{SAMW}$ is the average SAMW concentration, calculated within the SAMW density range at the stations west of the OF. Here, SAMW is present below the mixed layer depth and euphotic zone.

### e. Regenerated nitrate from $\delta^{18}O$

Regenerated nitrate is often defined as the stoichiometric-quantity of nitrate expected from AOU (i.e., regenerated nitrate = 16/138 x AOU; Redfield et al. 1963). However, in regions where nitrate may be lost from the water column/sediment-water interface by processes that are decoupled from oxygen (e.g., denitrification), this definition of regenerated nitrate is no longer appropriate. Using the measured $\delta^{18}O$ of nitrate and a two end-member mixing model, the fraction of nitrate regenerated on the SBUS shelf can be calculated as follows:

$$\delta^{18}O_{mix} = \delta^{18}O_A\,(f_A) + \delta^{18}O_B\,(1\text{-}f_A) \quad (2.12)$$

Where $\delta^{18}O_{mix}$ is the measured $\delta^{18}O$ of nitrate, $\delta^{18}O_A$ is the $\delta^{18}O$ of newly nitrified nitrate ($\delta^{18}O_{nitrification}$, taken here to be ~1.4‰ given the observed range in $\delta^{18}O_{seawater}$ (~0-0.5‰; Meredith et al. 1999) and the fact that $\delta^{18}O_{nitrification} = \delta^{18}O_{seawater} + 1.15‰$ (Sigman et al. 2009; Buchwald et al. 2012)), $\delta^{18}O_B$ is the average $\delta^{18}O$ of nitrate in SAMW ($\delta^{18}O_{source}$), and $f_A$ is the fraction of nitrate that is regenerated.

### f. N deficit

The amount of nitrate lost from the system by denitrification (N deficit; µM) can be estimated using the equation below:

$$\text{N deficit} = [NO_3^-]_{expected} - [NO_3^-]_{measured} \quad (2.13)$$

Where $[NO_3^-]_{expected}$ was calculated using AOU in SAMW (i.e., $[NO_3^-]_{expected}$ = AOU x (16/138) + 10 µM, where 10 µM is the preformed nitrate present in SAMW before it upwells onto the shelf (i.e., the nitrate concentration measured in SAMW when AOU = 0 µM)).

### g. Δ(15-18)

To further interpret the nitrate $\delta^{15}N$ and $\delta^{18}O$ data, we investigate the parameter Δ(15-18) (‰), a tracer of remineralization defined as:

$$\Delta(15\text{-}18) = \delta^{15}N - \delta^{18}O \quad (2.14)$$

Δ(15-18) remains unaffected by phytoplankton assimilation and therefore any deviations in Δ(15-18) from the SAMW and SASTMW end-members is due to other potentially overlapping biological processes, as described in chapter 1 (Sigman et al. 2005; Rafter et al. 2013).

## 3. Results

### 3.1. Water column hydrography

The temperature and salinity sections along the four hydrographic lines surveyed in February (summer) and May (winter) 2017 showed seasonal features characteristic of the SBUS. Using the temperature data, four prominent fronts were identified in summer and three were apparent in winter (Figure 2.1 and 3.1). At Scarborough, the southern-most monitoring line, the equatorward Cape Jet (CJ; Shannon 1985) was identified by the 15ºC isotherm and 14ºC isotherm during summer and winter, respectively. The CJ separated the inshore station from the offshore regions. The CJ bifurcated north of Cape Columbine into two jets in summer (Shannon 1985): the Columbine Front (CF) which separated the inshore and midshore regions and was identified by the 15ºC isotherm (Lamont et al. 2015). The Shelf Break Front (SBF) in turn, separated the midshore from the offshore regions and was identified by the 17ºC isotherm and was situated along the 300 m isobath (Lamont et al. 2015). During the wintertime, the SBF could no longer be identified in the SBUS as it had merged with the CF, delineated by a 14ºC isotherm (Lamont et al. 2015). In both seasons, the Oceanic Front (OF) separated the upwelling zone inshore from the oceanic, subtropical gyre (Barange and Pillar 1992; Shannon and Nelson 1996; Lamont et al. 2015). While the OF usually dissipates between April and August (Lamont et al. 2015), it was observed to persist during early winter in 2017, as evidenced by the distinctive 18ºC isotherm (Figure 3.1; Lamont et al. 2015). From here on, we refer to February 2017 as the summer and May 2017 as the winter.

In both summer and winter of 2017, colder sea surface temperatures (SST) were observed at the inshore stations along all monitoring lines compared to the stations further from the shore. The inshore stations were characterized by colder SSTs in summer compared to winter (10ºC vs. 13ºC), whereas the oceanic stations had warmer SSTs in summer compared to winter (21ºC vs. 18 ºC). The warmer offshore SSTs extended shoreward until the CF, therefore penetrating further inshore during winter, particularly along the Namaqualand monitoring line (Figure 3.1F).

The mixed layer depth (MLD) decreased inshore in both seasons. A deepening of the MLD was observed westwards of each front, with the deepest MLDs occurring west of the OF. The shallow MLD observed at the inshore stations was due to the upwelling (active or quiescent) of cooler waters inshore, while offshore increased warming of surface waters and mixing of warmer waters laterally (now uninfluenced by upwelling) led to a deepening of the MLD, with the oceanic stations having the highest observed SST (Figure 3.1). A greater number of stations had deeper MLD in the winter compared to the summer, as indicated by warmer SSTs extending further inshore during the winter.

During summer and winter, six water masses were identifiable in the SBUS on the basis of their salinity and temperatures characteristics (Figure 3.2 and 3.3). At depth, Upper Circumpolar Deep Water (UCDW; $\sigma_\theta$ >27.3 kg.m$^{-3}$; Donners et al. 2005) was overlain by Antarctic Intermediate Water (AAIW; 27.0 kg.m$^{-3}$ < $\sigma_\theta$ < 27.3 kg.m$^{-3}$). Subantarctic Mode Water (SAMW; 26.6 kg.m$^{-3}$ < $\sigma_\theta$ < 27.0 kg.m$^{-3}$) off-shelf occurred between 200-600 m depending on the monitoring line. SAMW was present over the shelf break, and outcropped inshore in summer. SAMW has been identified as the source water mass that is upwelled to the surface inshore (Lamont et al. 2015). South Atlantic Subtropical Mode Water (SASTMW; 26.2 kg.m$^{-3}$ < $\sigma_\theta$ < 26.6 kg.m$^{-3}$) overlays SAMW. It appeared to outcrop between SAMW and the CF front in summer, and directly inshore in winter. Modified Upwelled Water (MUW; 25.5 kg.m$^{-3}$ < $\sigma_\theta$ < 26.2 kg.m$^{-3}$) extended from the surface at the inshore stations towards the OF in both seasons. MUW derived from upwelled SAMW and SASTMW that had warmed and been modified by evaporation, and potentially precipitation, at the surface (Donners et al. 2005; Figure 3.3). Warmer Oceanic Surface Water (OSW; $\sigma_\theta$ < 25.5 kg.m$^{-3}$; Donners et al. 2005; Duncombe Rae 2005) extended beyond the OF. OSW originated from South Atlantic Central Water (SACW) that had warmed and been modified by evaporation (Donners, Drijfhout, and Hazeleger 2005).

## 3.2. Chemical properties of the SBUS

### *Nutrient concentrations*

In both seasons, nutrient concentrations at the off-shelf stations were elevated at depth and more deplete at the surface (Figures 3.4-3.6). The concentrations were highest in UCDW

followed by AAIW, decreasing in SAMW and SASTMW above, and were lower in surface waters, with nutrient deplete conditions observed west of the OF in all cases (MUW and OSW; Table 3.1).

On-shelf, surface nitrate concentrations were highest at the inshore stations in summer, decreasing offshore (Figure 3.4A-D). Surface nitrate concentrations in winter were also elevated at the inshore stations, decreasing offshore (Figure 3.4E-H), with the exception of the St Helena Bay monitoring line where nitrate was low at the two most inshore stations (Figure 3.4G).

Subsurface nutrient concentrations along isopycnal surfaces inshore of the OF were generally greater than in the corresponding waters offshore. In summer, the average nitrate concentration in SAMW off-shelf was 21.3 $\pm$ 5.4 µM (Table 3.1) and the on-shelf nitrate concentration was 23.2 $\pm$ 4.9 µM. The highest nitrate concentrations ($\geq$ 30 µM) were observed inshore of the CF along the northern-most Kleinsee monitoring line, which is located where the continental shelf is widest (~200 km between the coast and the 300 m isobath; Figure 3.4A). Conversely, nitrate concentrations along the southern-most Scarborough monitoring line, which has the narrowest shelf area of the four monitoring lines (~40 km between the coast and the 300 m isobath; Figure 3.4D), were most similar to the SAMW end-member, although concentrations reached 25 µM. There appears to be a small contribution of SASTMW to upwelling, at least at the most inshore stations of the Namaqualand and Scarborough monitoring lines. In summer, the average nitrate concentration in SASTMW off-shelf was 8.7 $\pm$ 2.6 µM (Table 3.1) and the on-shelf nitrate concentration was 11.6 $\pm$ 3.8 µM, with a maximum along the Namaqualand monitoring line ($[NO_3^-]$ = 17.5 µM). Across the SBUS, the elevated sub-surface nitrate concentrations were apparent as far west as the SBF, with the highest concentrations observed inshore of the CF.

The patterns in subsurface nitrate concentrations in winter were similar to the summer, with concentrations on-shelf increasing above those in the source waters. Concentrations in the SAMW density range increased from 21.3 ± 5.4 µM off-shelf to 22.4 $\pm$ 4.8 µM on-shelf, with the highest concentrations observed at the midshore stations along the St Helena Bay monitoring line (Figure 3.4G). As in summer, nitrate concentrations along the Scarborough

monitoring line were not appreciably higher than those measured in SAMW offshore (Figure 3.4H). In contrast to summer, the elevated on-shelf nitrate concentrations propagated as far west as the OF along the Kleinsee, Namaqualand and St Helena Bay monitoring lines in winter. The vertical extent of SAMW on the shelf, however, was lower in winter than summer (Figure 3.2), although the vertically-integrated nutrient inventory was higher in winter. The inshore stations were characterised by nitrate concentrations above that of SASTMW, the water mass that appears to be upwelled to the inshore surface in winter. Off-shelf SASTMW had an average nitrate concentration of 8.7 $\pm$ 2.6 µM, while inshore, the average nitrate concentrations were 16.1 $\pm$ 5.6 µM in the SASTMW density range, and were highest along the Kleinsee and Namaqualand monitoring lines (Figure 3.4E and F).

As for nitrate, silicic acid and phosphate concentrations at the surface during the summer and winter decreased with distance from the coast (Figures 3.5 and 3.6). At depth, silicic acid and phosphate concentrations on-shelf were higher than those measured in SAMW off-shelf. In both seasons, the average silicic acid and phosphate concentrations in SAMW were 11.6 ± 5.7 µM (Table 3.1) and 1.4 $\pm$ 0.4 µM, respectively. In summer, the concentrations increased on-shelf in the SAMW density range to 22.6 $\pm$ 13.2 µM and 2.1 $\pm$ 0.7 for silicic acid and phosphate, respectively. The highest concentrations were observed inshore of the CF along the St Helena Bay monitoring line for both nutrients ($[Si(OH)_4] \leq 40$ µM and $[PO_4^{3-}] \leq 3.5$ µM; Figures 3.5C and 3.6C). The lowest accumulation of silicic acid and phosphate was observed along the Scarborough monitoring line ($[Si(OH)_4] \leq 20$ µM and $[PO_4^{3-}] \leq 2$ µM; Figures 3.5D and 3.6D). Although the highest subsurface nutrient concentrations were observed inshore of the CF along all monitoring lines, the signal propagated as far west as the SBF; this was most clearly observed along the Kleinsee monitoring line (Figures 3.5A and 3.6A).

Winter concentrations of silicic acid and phosphate were similarly elevated above those of the SAMW end-member on-shelf at the sediment interface. Unlike the nitrate concentrations, the highest silicic acid and phosphate concentrations were observed inshore of the CF along all lines (Figure 3.5 and 3.6; E-H only). The elevated concentrations extended west to the OF, as was observed for the wintertime nitrate concentrations. As per nitrate, the elevated silicic acid and phosphate concentrations did not extend as shallow in the water column as in summer, coinciding with the narrower vertical extent of SAMW above the shelf sediments. The highest

wintertime silicic acid concentrations were observed along the Kleinsee monitoring line (≤ 40 µM; Figure 3.5E). The Scarborough monitoring line once again showed the lowest on-shelf increase in silicic acid concentration, with an average [$Si(OH)_4$] of 20 µM (Figure 3.5H). The highest phosphate concentrations occurred along the St Helena Bay monitoring line (≤ 3 µM; Figure 3.6G). The lowest on-shelf phosphate concentrations were observed along the Namaqualand monitoring line (maximum [$PO_4^{3-}$] of ~2 µM; Figure 3.6F), while the Scarborough monitoring line had an average phosphate concentration of 2.2 µM (Figure 3.6H).

***Oxygen concentrations and Apparent Oxygen Utilization***

Surface oxygen concentrations were at or in excess of atmospheric equilibrium at all but the inshore stations along the Kleinsee and St Helena Bay monitoring lines in summer (data shown in Appendix A; Figure A1). Subsurface oxygen concentrations were lowest at the inshore stations along the Kleinsee, Namaqualand and St Helena Bay monitoring lines. Oxygen concentrations below that of SAMW propagated as far west as the SBF for the Kleinsee, Namaqualand and St Helena Bay monitoring lines and to the 400 m isobath along the Scarborough monitoring line. During the winter, oxic conditions (i.e. oxygen concentrations ≥ 60 µmol.kg$^{-1}$) were present throughout the water column at the inshore stations, with only the St Helena Bay monitoring line experienced oxygen concentrations below 60 µmol kg$^{-1}$ (data shown in Appendix A; Figure A1). As in summer, oxygen concentrations along the shelf were lower than those measured in SAMW offshore, and the low oxygen concentrations propagated further west in winter, reaching the OF. West of the SBF in summer and the OF in winter, oxygen concentrations were indistinct from those in the off-shelf water masses.

The corresponding AOU increased on-shelf compared to the SAMW end-member of 91.9 ± 28.3 µmol.kg$^{-1}$ (Figure 3.7; Table 3.1). In summer, the highest AOU was observed along the St Helena Bay monitoring line inshore of the CF (≤ 220 µmol.kg$^{-1}$; Figure 3.7C). AOU was lowest along the Scarborough monitoring line, with a maximum observed between the CF and OF (≤ 175 µmol.kg$^{-1}$; Figure 3.7D). For all monitoring lines, AOU was highest inshore of the CF and this signal was observed to extend west to the SBF, similar to the on-shelf nutrient concentrations (Figure 3.7A-D). In winter, the highest AOU was once again observed inshore of the CF (Figure 3.7E-H). The St Helena Bay monitoring line experienced the highest AOU, with concentrations inshore of the CF reaching 250 µmol.kg$^{-1}$ (Figure 3.7G). The lowest AOU

was observed along the Scarborough monitoring line ($\leq$ 150 µmol.kg$^{-1}$; Figure 3.7H), which also experienced the smallest increase in on-shelf nutrient concentrations above those of the SAMW end-member.

The spatial distribution of AOU on-shelf in both seasons is similar to that of phosphate, with a linear relationship existing between phosphate and AOU concentrations in summer and winter seasons (Figure 3.8A and B). A similar relationship is evident between nitrate and AOU (Figure 3.8C and D), and silicic acid and AOU (Figure 3.8E and F).

***N* and Si****

N* is used to identify a loss or gain in nitrogen relative to phosphate. A positive N* indicates a gain in nitrogen over the mean ocean value, while a negative N* indicates a loss (Gruber and Sarmiento 1997). Surface N* west of the CF in summer were ~0 µM along all lines except the Kleinsee monitoring line where the surface values were ~-2.5 µM (Figure 3.9A-D). Inshore of the CF, N* values were -8.44 $\pm$ 8.4 µM, with the lowest values observed at the inshore stations along the St Helena Bay monitoring line, -17.9 $\pm$ 9.8 µM (Figure 3.9C), and the highest inshore values along the Namaqualand monitoring line, -5.7 $\pm$ 6.5 µM (Figure 3.9B). Similar patterns were observed in winter. N* values of ~0 µM were observed west of the OF along all monitoring lines, with the lowest surface N* values observed inshore of the CF (Figure 3.9E-H). The lowest inshore values were observed at the inshore stations of the St Helena Bay monitoring line (-24.4 $\pm$ 15.5 µM; Figure 3.9G) while the highest values were observed along the Namaqualand monitoring line (14.9 $\pm$ 12.5 µM; Figure 3.9F).

In summer, SAMW off-shelf had a N* of -0.8 $\pm$ 2.6 µM. On-shelf N* decreased within the SAMW density range to -7 $\pm$ 8.7 µM. The lowest N* values were observed inshore of the CF along all monitoring lines (Figure 3.9A-D). The low N* values propagated until the SBF, whereby westwards of the SBF N* was indicative of SAMW. The lowest N* values were observed at the inshore stations along the St Helena Bay monitoring line (-10.2 $\pm$ 12.4 µM; Figure 3.9C) while the highest values were observed at the midshore stations along the Namaqualand monitoring line (-1.4 $\pm$ 3.7 µM; Figure 3.9B). The lowest values of N* coincide with the highest on-shelf concentrations of phosphate, silicic acid and AOU.

Subsurface values of N* in winter followed a similar trend as in summer. On-shelf N* decreased within the SAMW density range -9.4 ± 8.6 µM (Figure 3.9E-H). The lowest N* values were, as in summer, observed inshore of the CF along all monitoring lines. Along the Scarborough monitoring line, however, the lowest N* values were observed between 200-400 m at the midshore stations (-39.4 ± 2.8 µM; Figure 3.9H) and at the insh39.4 ore St Helena Bay monitoring line stations (-17.4 ± 9.5 µM; not all data shown). The low N* values propagated until the OF, and in certain instances N* values below the SAMW end-member were observed in off-shelf waters between 300-600 m (Figure 3.9E and F). The highest on-shelf values of N* were observed along the Namaqualand monitoring line, -5.4 ± 5.6 µM (Figure 3.9F). The low on-shelf values of N* coincide with the highest on-shelf concentrations of phosphate, silicic acid and AOU, as in summer.

Si* is used to identify changes in silicic acid relative to nitrate. A positive Si* indicates that there is more silicic acid present than nitrate while a negative Si* indicates the inverse (Sarmiento et al. 2004). Surface Si* values were ~0 µM westwards of the CF in both seasons, while inshore of the CF Si* was variable (Figure 3.10). In summer, positive Si* values of up to 20 µM, indicating excess silicic acid relative to nitrate, were observed at the inshore stations along the St Helena Bay monitoring line (Figure 3.10C), while negative values (-8.4 ± 8.5 µM) were observed inshore of the CF along the Kleinsee monitoring line (Figure 3.10A). At the most inshore stations in winter, surface Si* was elevated at the Kleinsee, Namaqualand and St Helena Bay monitoring lines (Figure 3.10E-G), decreasing westward towards the CF, with the largest decrease observed along the Kleinsee monitoring line. Surface Si* values along the Scarborough monitoring line were similar during the two seasons (Figure 3.10D and H).

In summer, on-shelf subsurface Si* concentrations varied relative to the SAMW end-member of -10 µM. Inshore of the CF, Si* concentrations within the SAMW density range were generally higher than that of SAMW with the highest concentrations observed along the St Helena Bay monitoring line (Figure 3.10C). Salient Si* concentrations (≥ 0 µM) were seen to extend as far west as the SBF along all monitoring lines, with a local Si* minimum (-20.9 µM) observed at the sediment-water interface at one station just east of the CF along the Namaqualand monitoring line (Figure 3.10B).

In winter, the on-shelf subsurface Si* concentrations followed similar trends to the summer. The highest Si* was once again observed inshore of the CF, with concentrations $\geq$ 15 µM for all monitoring lines. The elevated Si* concentrations extended westwards to the OF, as with the higher-than-source nutrient concentrations. The highest Si* concentrations were observed along the Kleinsee monitoring line, with an Si* of 20 µM observed at all midshore and offshore stations (Figure 3.10E). The lowest Si* concentrations occurred along the Scarborough monitoring line (0 µM); however, they were still elevated above that of the SAMW end-member (Figure 3.10H).

### 3.3. Nitrate isotope ratios

#### *$\delta^{15}N$ and $\delta^{18}O$ of nitrate*

In both seasons, the nitrate N and O isotope ratios showed characteristic depth distributions at the off-shelf stations (Figures 3.11 and 3.12). Ratios were lowest in UCDW, 5.7 ± 0.3‰ and 2.4 $\pm$ 0.2‰ for $\delta^{15}N$ and $\delta^{18}O$, respectively (Table 3.1; Figure 3.3). These increased characteristically in AAIW to 6.0 $\pm$ 0.3‰ and 2.7 $\pm$ 0.3‰, to 6.6 $\pm$ 0.2‰ and 3.1 $\pm$ 0.3‰ in SAMW and to 7.2 $\pm$ 0.3‰ and 3.9 $\pm$ 0.3‰ in SASTMW for $\delta^{15}N$ and $\delta^{18}O$, respectively (Table 3.1; Figure 3.3). In the surface layers (MUW and OSW) the nitrate isotope ratios were high due to isotopic fractionation during nitrate assimilation by phytoplankton (Mariotti et al. 1981) (Figure 3.3).

Surface nitrate $\delta^{15}N$ and $\delta^{18}O$ were generally higher than in the subsurface reservoir, and typically lowest inshore where nitrate concentrations were elevated, increasing offshore to relative maxima at lower nitrate concentrations (Figures 3.11 and 3.12). Nitrate was absent throughout OSW at the oceanic stations during both seasons, with the exception of in the deepest MLD samples from the St Helena Bay monitoring line. West of the SBF and the OF, subsurface OSW and SASTMW were relatively elevated in $\delta^{15}N$ and $\delta^{18}O$, particularly in summer, down to 150-200 m, well below the MLD (Figures 3.11C and 3.12C). One explanation for the elevated sub-mixed layer nitrate $\delta^{15}N$ and $\delta^{18}O$ is the downward mixing of the surface nitrate assimilation signal. However, this signal is held in a very low concentration of nitrate at the base of the mixed layer. A related and more likely option is that the high subsurface $\delta^{15}N$ and $\delta^{18}O$ is the remnant geochemical signal of phytoplankton nitrate assimilation in inshore

and midshore surface waters that has been subducted below the various fronts (Andrews and Hutchings 1980; Appendix D). At the Scarborough monitoring line in summer, nitrate $\delta^{15}N$ nitrate was particularly high at the inshore station while its $\delta^{18}O$ was only moderately elevated (Figures 3.11D and 3.12D).

On-shelf, the nitrate isotopes were not conservative with respect to the source water masses in either season. Below the surface mixed layer, $\delta^{15}N$ on-shelf in summer was slightly higher than the SAMW end-member, rising from 6.6‰ off-shelf to values between 6.7‰ and 7.1‰ on-shelf along all hydrographic lines (Fig 3.11A-D). The high $\delta^{15}N$ signal propagates west from the inshore stations to the SBF, with the highest values observed inshore of the CF and CJ. The increase in $\delta^{15}N$ at depth on the shelf was most distinct along the Kleinsee monitoring line (Figure 3.11A), and least evident along the Namaqualand monitoring line (Figure 3.11B).

Subsurface waters in winter showed an even higher on-shelf $\delta^{15}N$ relative to SAMW than in summer, with values ranging between 6.7‰ and 8.3‰ (Figure 3.11E-H). The highest on-shelf $\delta^{15}N$ was observed inshore of the CF and the CJ, coincident with the highest silicic acid and phosphate concentrations. The high on-shelf $\delta^{15}N$ signal was evident as far west as the OF, thus propagating further along the shelf in winter than in summer. The high on-shelf $\delta^{15}N$ was most apparent along the Kleinsee monitoring line (Figure 3.11E), and least so along the Scarborough monitoring line (Figure 3.11H).

The corresponding $\delta^{18}O$ of nitrate at the subsurface in summer was lower on-shelf relative to the SAMW off-shelf, decreasing from 3.1‰ in SAMW to values between 2.2‰ and 3.0‰ on-shelf (Figure 3.12A-D). The on-shelf decrease appeared to coincide with the higher-than-source water nutrient concentrations and AOU. The low $\delta^{18}O$ signal extended along the shelf until the SBF and was lowest along the Kleinsee monitoring line ($1.8 \pm 0.5$‰; Figure 3.12A). Nitrate $\delta^{18}O$ lower than SAMW was not evident along the Scarborough monitoring line (Figure 3.12D). Along the Kleinsee and St Helena Bay monitoring lines, where the highest on-shelf nutrient concentrations were observed, the lowest $\delta^{18}O$ values were measured between the CF and the SBF (Figure 3.12A and C).

In winter, on-shelf nitrate $\delta^{18}O$ was also lower than that of SAMW off-shelf, ranging between 1.9‰ and 3.0‰ (Figure 3.12E-H). The on-shelf average $\delta^{18}O$ was slightly lower in winter compared to the summer, with an average of 2.5 $\pm$ 0.3‰ in winter and 2.6 $\pm$ 0.3‰ in summer. The low on-shelf $\delta^{18}O$ signal was observed across the shelf inshore of the OF. The lowest on-shelf nitrate $\delta^{18}O$ was observed along the Kleinsee monitoring line (Figure 3.12E), with the smallest change in $\delta^{18}O$ from that of SAMW observed along the Scarborough monitoring line (Figure 3.12H). Furthermore, the lowering of the on-shelf $\delta^{18}O$ overlapped with the elevated on-shelf nutrient concentrations and AOU (Figure 3.13).

In both seasons, the decrease in subsurface nitrate $\delta^{18}O$ on the shelf coincided with an increase in AOU (Figure 3.13). The decrease in $\delta^{18}O$ was greater in winter than summer (up to 1‰ lower than the SAMW end-member in winter and 0.8‰ in summer).

Nitrate isotope ratios measured for sample nitrate+nitrite differed slightly from those measured for nitrate only (i.e., following nitrite removal). For the on-shelf summer samples, nitrate $\delta^{15}N$ and $\delta^{18}O$ throughout the water column decreased after nitrite removal. The surface values decreased by 0.4 $\pm$ 1.0‰ and 0.5 $\pm$ 0.9‰ for $\delta^{15}N$ and $\delta^{18}O$, respectively, while subsurface values decreased by 0.2 $\pm$ 0.5‰ and 0.3 $\pm$ 0.9‰ for $\delta^{15}N$ and $\delta^{18}O$, respectively. Off-shelf, nitrate-only $\delta^{15}N$ and $\delta^{18}O$ decreased by 0.3 $\pm$ 1.2‰ and 0.1 $\pm$ 0.7‰, respectively, relative to the corresponding nitrate+nitrite samples. Surface on-shelf winter values of $\delta^{15}N$ decreased by 0.1 $\pm$ 0.6‰ and $\delta^{18}O$ increased by 0.1 $\pm$ 0.6‰, while subsurface average nitrate $\delta^{15}N$ did not change (0 $\pm$ 0.1‰) and $\delta^{18}O$ increased by 0.1 $\pm$ 0.3‰. Off-shelf, the average nitrate $\delta^{15}N$ did not change (0 $\pm$ 0.2‰) and $\delta^{18}O$ increased by 0.1 $\pm$ 0.4‰ (Appendix B; Figure B1-B4).

### *Δ(15-18) of nitrate*

At the off-shelf stations, the Δ(15-18) of nitrate was 3.5‰ in SAMW and slightly lower in SASTMW at 3.3‰ (Table 3.1; Figure 3.14). On-shelf, subsurface Δ(15-18) values higher than the SAMW end-member were observed during both seasons (average of 3.8 $\pm$ 0.4‰ in summer and 4.0 $\pm$ 0.7‰ in winter). Larger excursions in Δ(15-18) coincided with the stations where nutrient concentrations and AOU were highest (Figures 3.4-3.7 and 3.14), with Δ(15-18) above that of the SAMW end-member extending west to the SBF in summer and the OF in winter.

Nitrate Δ(15-18) in summer reached 4.4‰ at the Kleinsee monitoring line, with values as high as 5.8‰ observed in winter. The on-shelf rise in Δ(15-18) above that of the source waters was due to both an increase in nitrate $\delta^{15}N$ and a decrease in nitrate $\delta^{18}O$, with a more pronounced rise in $\delta^{15}N$ and decline in $\delta^{18}O$ relative to SAMW and SASTMW observed in winter.

### 3.4. Particulate organic nitrogen isotopes

PON was collected during both cruises, with wintertime samples constituting the majority of the data set. Figure 3.15 shows surface nitrate and PON $\delta^{15}N$ ($\delta^{15}N_{NO3}$ and $\delta^{15}N_{PON}$, respectively) and nitrate concentration at nine stations sampled in the SBUS in the summer. On average, $\delta^{15}N_{PON}$ and the nitrate concentrations are higher inshore of the shelf-break (Figure 3.15; vertical dashed grey line) than offshore. $\delta^{15}N_{NO3}$ is also high inshore but could not be measured for the offshore stations because the ambient nitrate concentration was so low.

In winter, surface $\delta^{15}N_{NO3}$ increases from the inshore stations towards the shelf break, while $\delta^{15}N_{PON}$ remains fairly uniform and the nitrate concentrations decrease (Figure 3.16). Beyond the shelf break (Figure 3.16; vertical dashed grey line), the northern and southern lines appear to follow different patterns. The northern Kleinsee and Namaqualand monitoring lines show an increase in $\delta^{15}N_{PON}$ with a decrease in the nitrate concentration at the offshore and oceanic stations (Figure 3.16A and B), while at the southern St Helena Bay and Scarborough monitoring lines, a decrease in all three parameters is observed from the shelf break into offshore waters (Figure 3.16C and D). The difference between the $\delta^{15}N_{PON}$ and $\delta^{15}N_{NO3}$ at all winter stations is 2-6‰, except at the inshore and midshore stations along the St Helena Bay monitoring line where $\delta^{15}N_{PON}$ is similar to $\delta^{15}N_{NO3}$. Here, the inshore $\delta^{15}N_{PON}$ is the highest of all the stations sampled (Figure 3.16C). $\delta^{15}N_{PON}$ is lowest at the oceanic stations along the Scarborough line (Figure 3.16D).

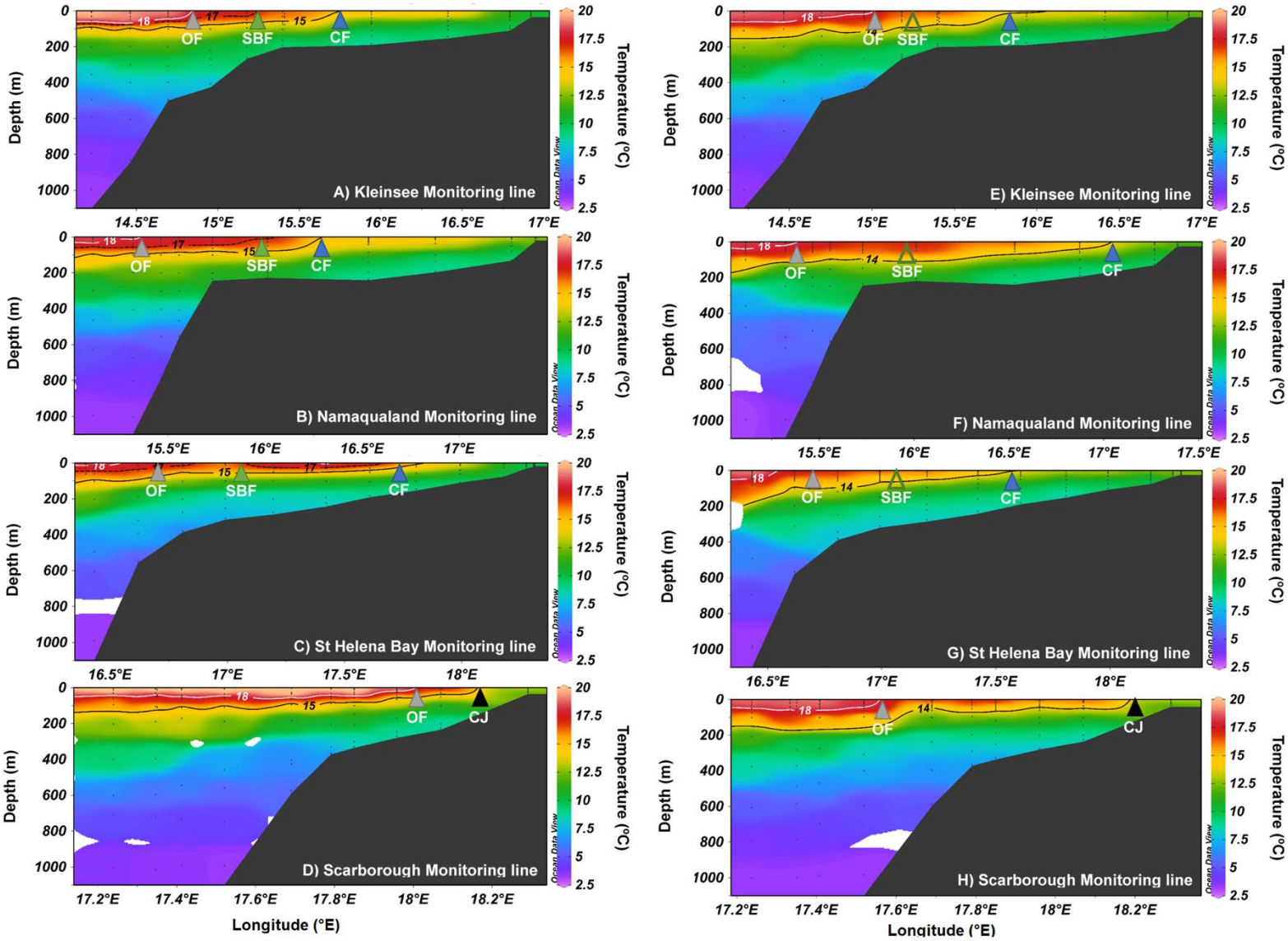


**Figure 3.1** Section plots of temperature for the **summer** (A-D) and **winter** (E-H) for (from north to south) A and E) Kleinsee monitoring line, B and F) Namaqualand monitoring line, C and G) St Helena Bay monitoring line and D and H) Scarborough monitoring line. The various fronts that occur in the SBUS are identified at the top of each of the contour plots. These include the Columbine Front (CF; blue triangle), the Shelf Break Front (SBF; green triangle), the Oceanic Front (OF; grey triangle) and the Cape Jet (CJ; black triangle). The SBF is not present during winter; however the summertime position is shown on the winter plots by the empty green triangle for context. The isotherms indicative of the positions of the fronts (14ºC, 15ºC, 17ºC) are shown as black contours, with the 18ºC isotherm that characterizes the OF shown in white (Lamont et al. 2015; see text for details). The black dots show the position of the stations along each monitoring line. Note the changes in longitudinal scale between panels.

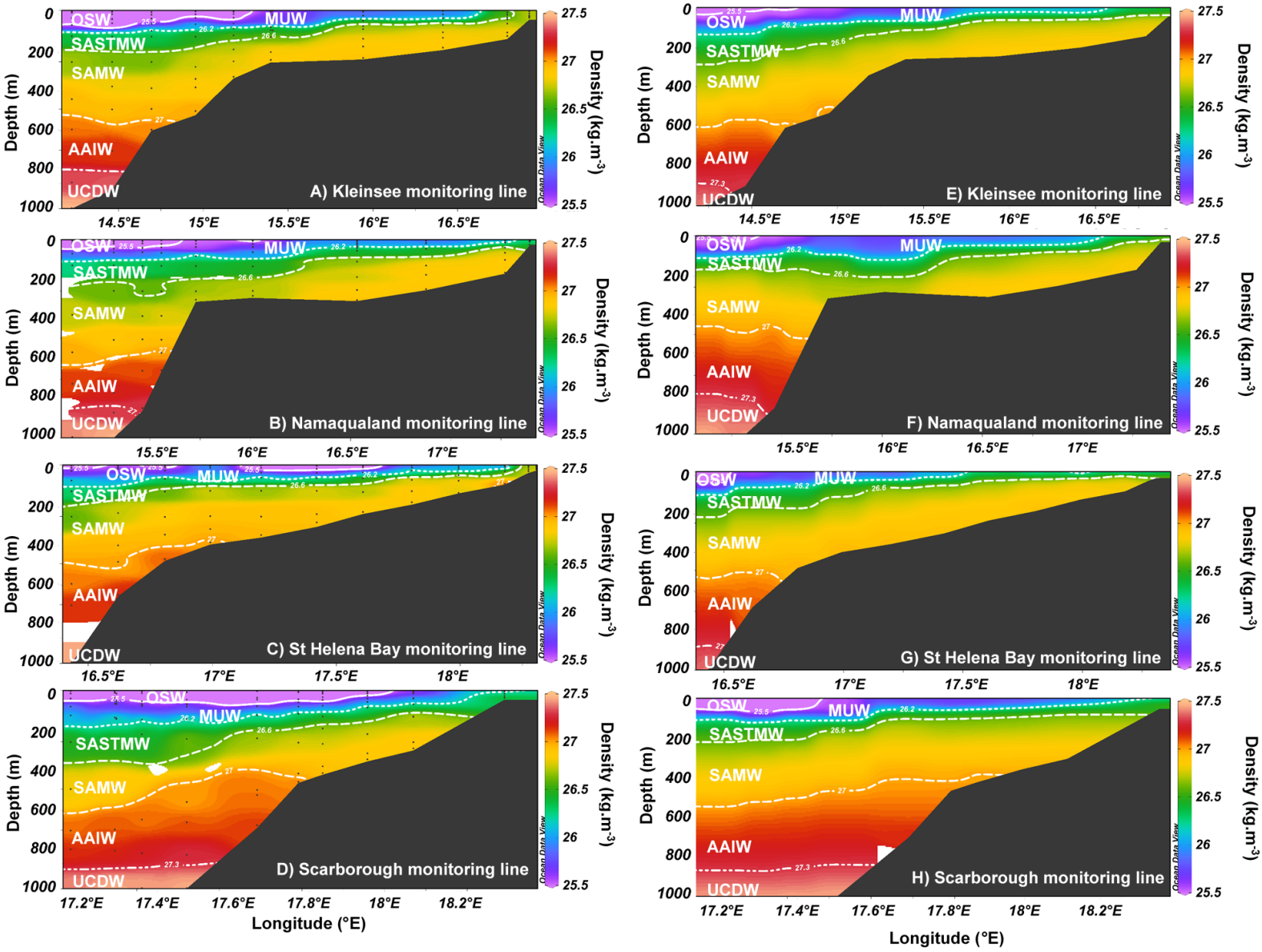


**Figure 3.2** Potential density ($\sigma_\theta$) section plots showing the vertical distribution of the water masses in the SBUS during **summer** (A-D) and **winter** (E-H) along the four IEP monitoring lines: A and E) Kleinsee monitoring line, B and F) Namaqualand monitoring line, C and G) St Helena Bay monitoring line and D and H) Scarborough monitoring line. The water masses are identified by their respective density ranges (UCDW - Upper Circumpolar Deep Water, AAIW - Antarctic Intermediate Water, SAMW - Subantarctic Mode Water, SASTMW - South Atlantic Subtropical Mode Water, MUW - Modified Upwelled Water and OSW - Oceanic Surface Water). The black dots show the position of the stations along each monitoring line. Note the changes in longitudinal scale between panels.

**Table 3.1** Average values of select parameters for water masses off-shelf in the SBUS. Averages are calculated using all measurements that fall within the potential density ranges that characterize the various water masses (see text for details).

| **Water mass** | **Nitrate (µM)** | **Silicic Acid (µM)** | **AOU (µmol.kg$^{-1}$)** | **$\delta^{15}N$ (‰)** | **$\delta^{18}O$ (‰)** | **$\Delta$(15-18) (‰)** |
|---|---|---|---|---|---|---|
| UCDW | 33 $\pm$ 1.3 | 55 $\pm$ 1.7 | 148.8 $\pm$ 7.8 | 5.7 $\pm$ 0.3 | 2.4 $\pm$ 0.2 | 3.3 $\pm$ 0.5 |
| AAIW | 27 $\pm$ 3.5 | 23.5 $\pm$ 9.6 | 106.2 $\pm$ 10.3 | 6.0 $\pm$ 0.3 | 2.7 $\pm$ 0.3 | 3.3 $\pm$ 0.5 |
| SAMW | 21.3 $\pm$ 5.4 | 11.6 $\pm$ 5.7 | 91.9 $\pm$ 28.3 | 6.6 $\pm$ 0.2 | 3.1 $\pm$ 0.3 | 3.5 $\pm$ 0.5 |
| SASTMW | 8.7 $\pm$ 2.6 | 3.9 $\pm$ 1.5 | 49.1 $\pm$ 10.9 | 7.2 $\pm$ 0.3 | 3.9 $\pm$ 0.3 | 3.3 $\pm$ 0.5 |

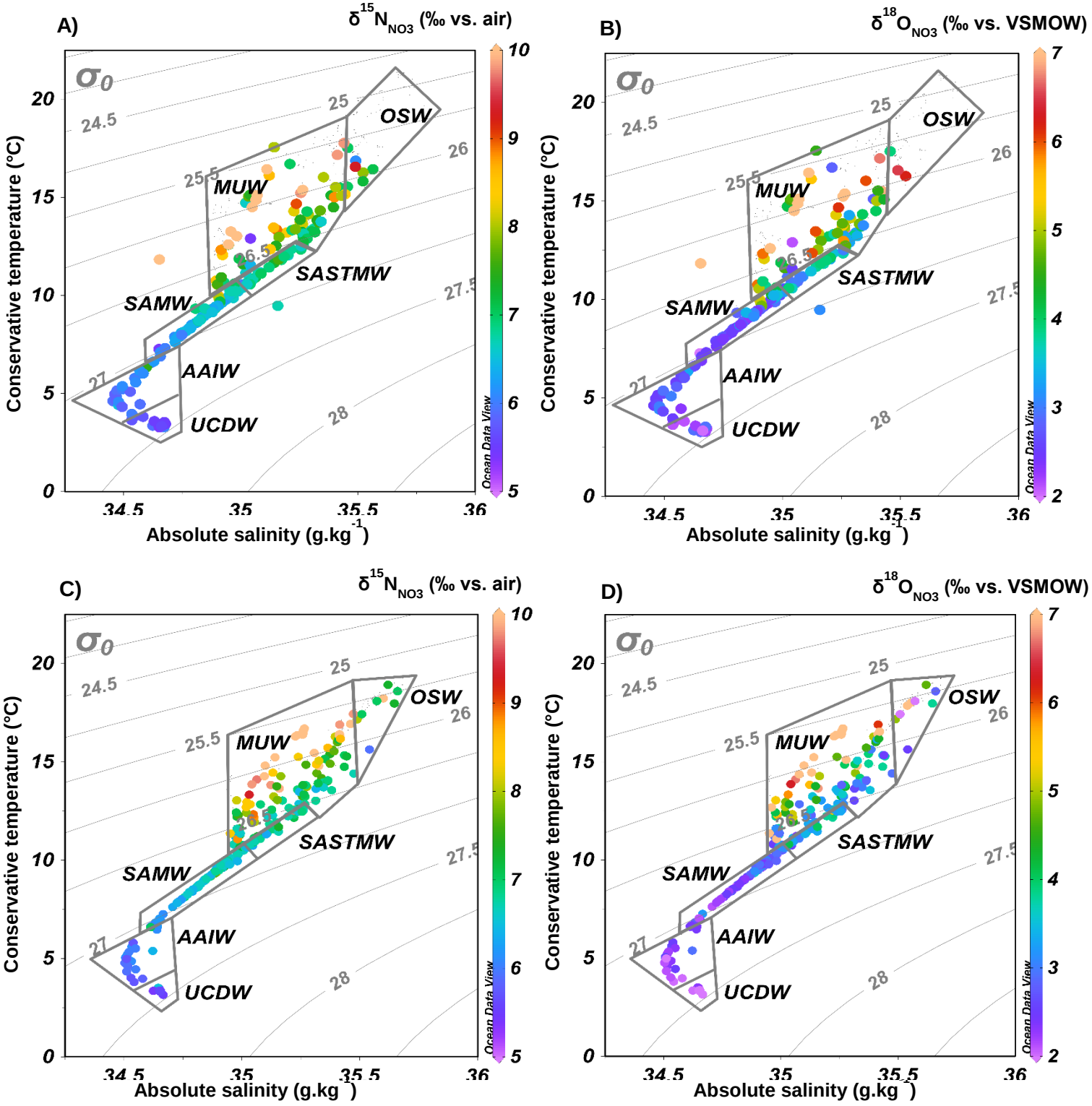


**Figure 3.3** Conservative temperature (°C) and absolute salinity (g.kg$^{-1}$) plots with nitrate-only isotope data overlaid in colour. A) $\delta^{15}N_{NO3}$ and B) $\delta^{18}O_{NO3}$ in **summer** and C) $\delta^{15}N_{NO3}$ and D) $\delta^{18}O_{NO3}$ in **winter**. The water masses, identified according to Lamont et al. (2015) (see text for details), are indicated by the grey boxes and labeled on the plots: UCDW (Upper Circumpolar Deep Water), AAIW (Antarctic Intermediate Water), SAMW (Subantarctic Mode Water), SASTMW (South Atlantic Subtropical Mode Water), MUW (Modified Upwelling Water) and OSW (Ocean Surface Water).

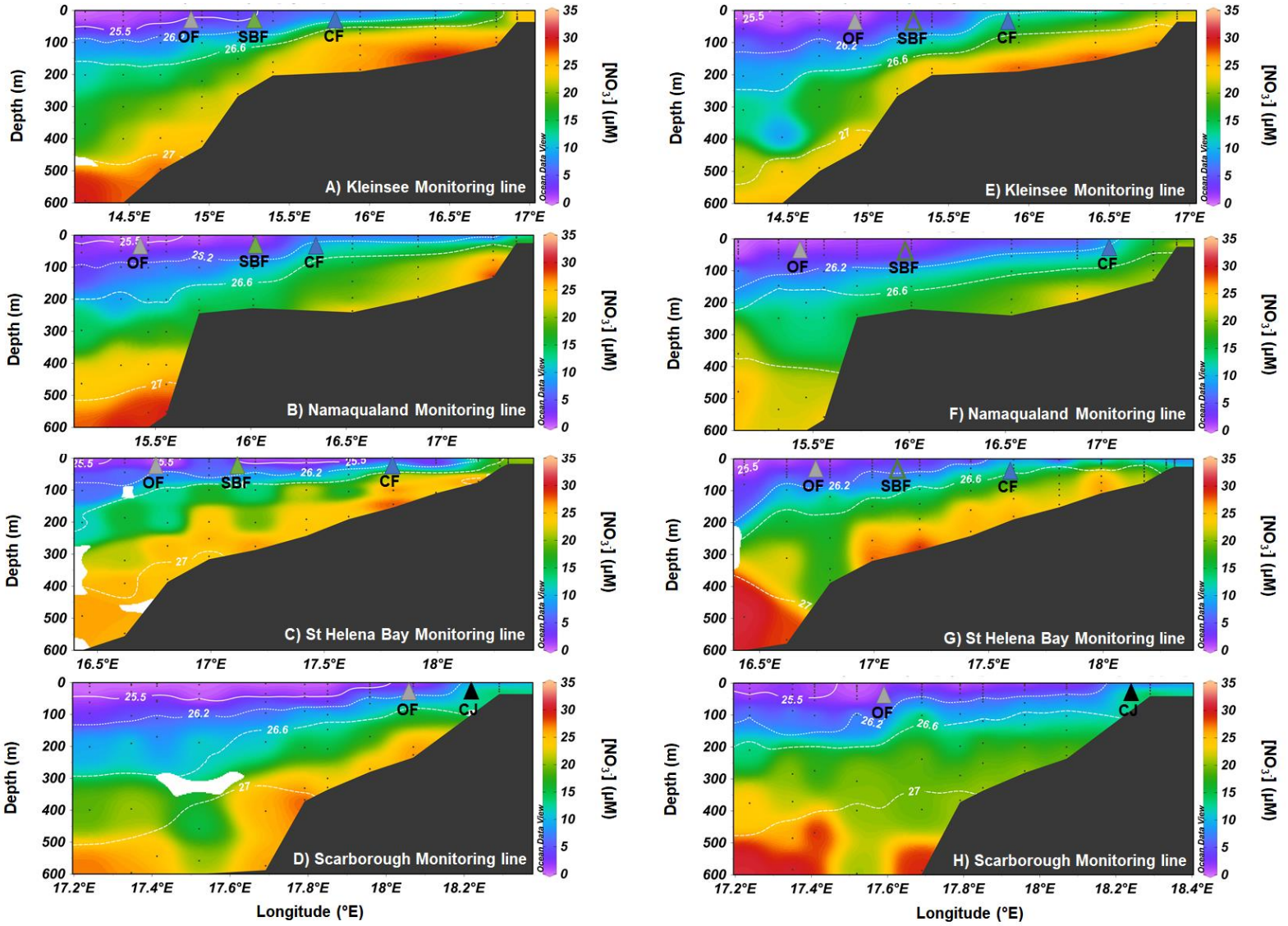


**Figure 3.4** Section plots of nitrate concentration ($[NO_3^-]$ (µM); colours) and potential density ($\sigma_\theta$; contours) for **summer** (A-D) and **winter** (E-H) along (from north to south) A and E) Kleinsee monitoring line, B and F) Namaqualand monitoring line, C and G) St Helena Bay monitoring line and D and H) Scarborough monitoring line. Note the changes in longitudinal scale between panels. The positions of the fronts identified in Figure 3.1 are shown on each figure. The density contours denote the water masses identified in Figure 3.2. The black dots show the position of the stations and the depths at which discrete nutrient samples were collected along each monitoring line. Note the changes in longitudinal scale between panels.

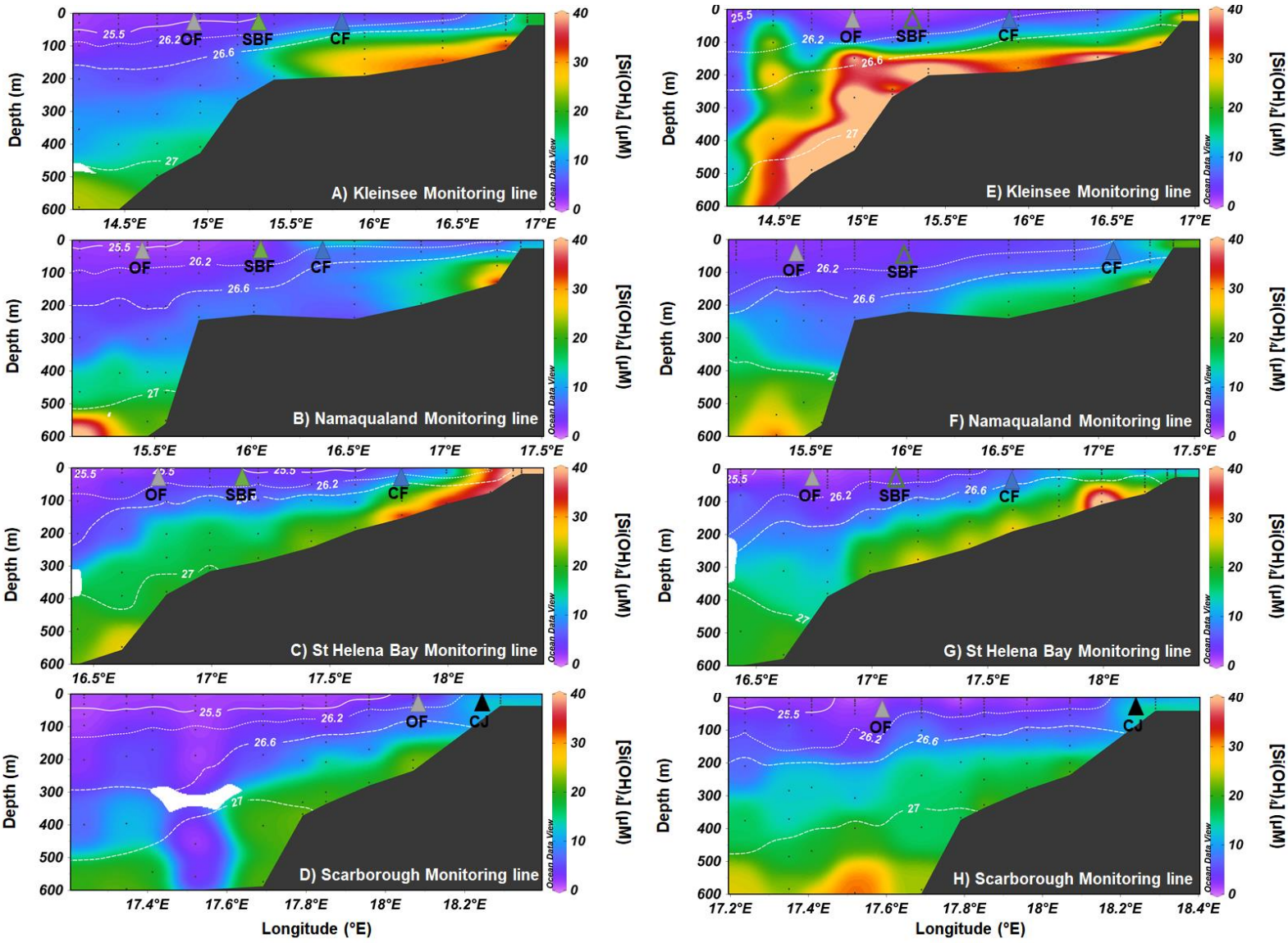


**Figure 3.5** Section plots of silicic acid concentration ([Si(OH)$_4$] (µM); colours) and potential density ($\sigma_\theta$; contours) for **summer** (A-D) and **winter** (E-H) along (from north to south) A and E) Kleinsee monitoring line, B and F) Namaqualand monitoring line, C and G) St Helena Bay monitoring line and D and H) Scarborough monitoring line. Note the changes in longitudinal scale between panels. The positions of the fronts identified in Figure 3.1 are shown on each figure. The density contours denote the water masses identified in Figure 3.2. The black dots show the position of the stations and the depths at which discrete nutrient samples were collected along each monitoring line. Note the changes in longitudinal scale between panels.

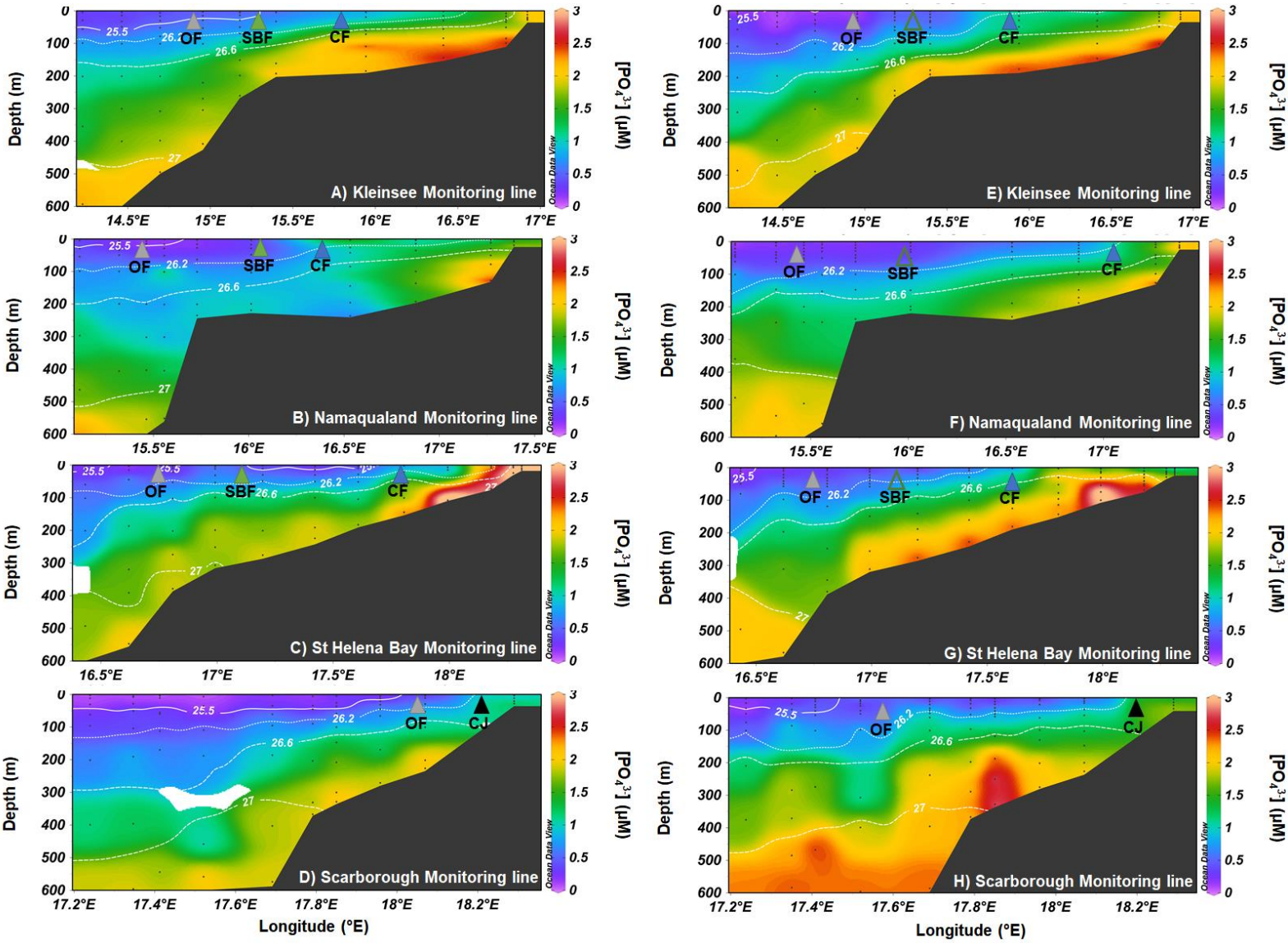


**Figure 3.6** Section plots of phosphate concentration ($[PO_4^{3-}]$ (µM); colours) and potential density ($\sigma_\theta$; contours) for **summer** (A-D) and **winter** (E-H) along (from north to south) A and E) Kleinsee monitoring line, B and F) Namaqualand monitoring line, C and G) St Helena Bay monitoring line and D and H) Scarborough monitoring line. Note the changes in longitudinal scale between panels. The positions of the fronts identified in Figure 3.1 are denoted on each figure. The density contours show the water masses identified in Figure 3.2. The black dots show the position of the stations and the depths at which discrete nutrient samples were collected along each monitoring line. Note the changes in longitudinal scale between panels.

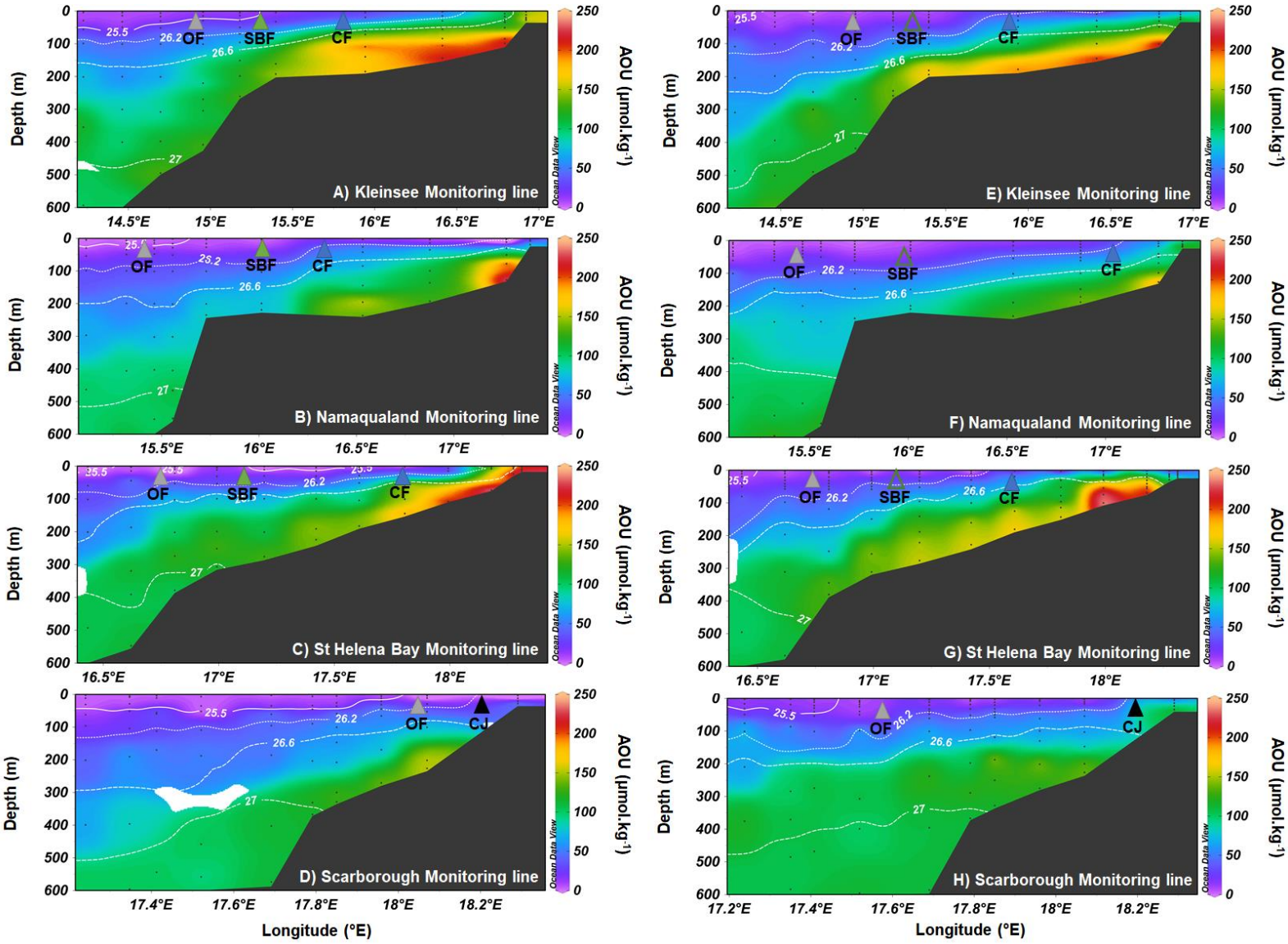


**Figure 3.7** Section plots of apparent oxygen utilisation (AOU (µmol.kg$^{-1}$; colours)) and potential density ($\sigma_\theta$; contours) for **summer** (A-D) and **winter** (E-H) along (from north to south) A and E) Kleinsee monitoring line, B and F) Namaqualand monitoring line, C and G) St Helena Bay monitoring line and D and H) Scarborough monitoring line. The positions of the fronts identified in Figure 3.1 are shown on each figure. The density contours denote the water masses identified in Figure 3.2. The black dots show the position of the stations along each monitoring line. Note the changes in longitudinal scale between panels.

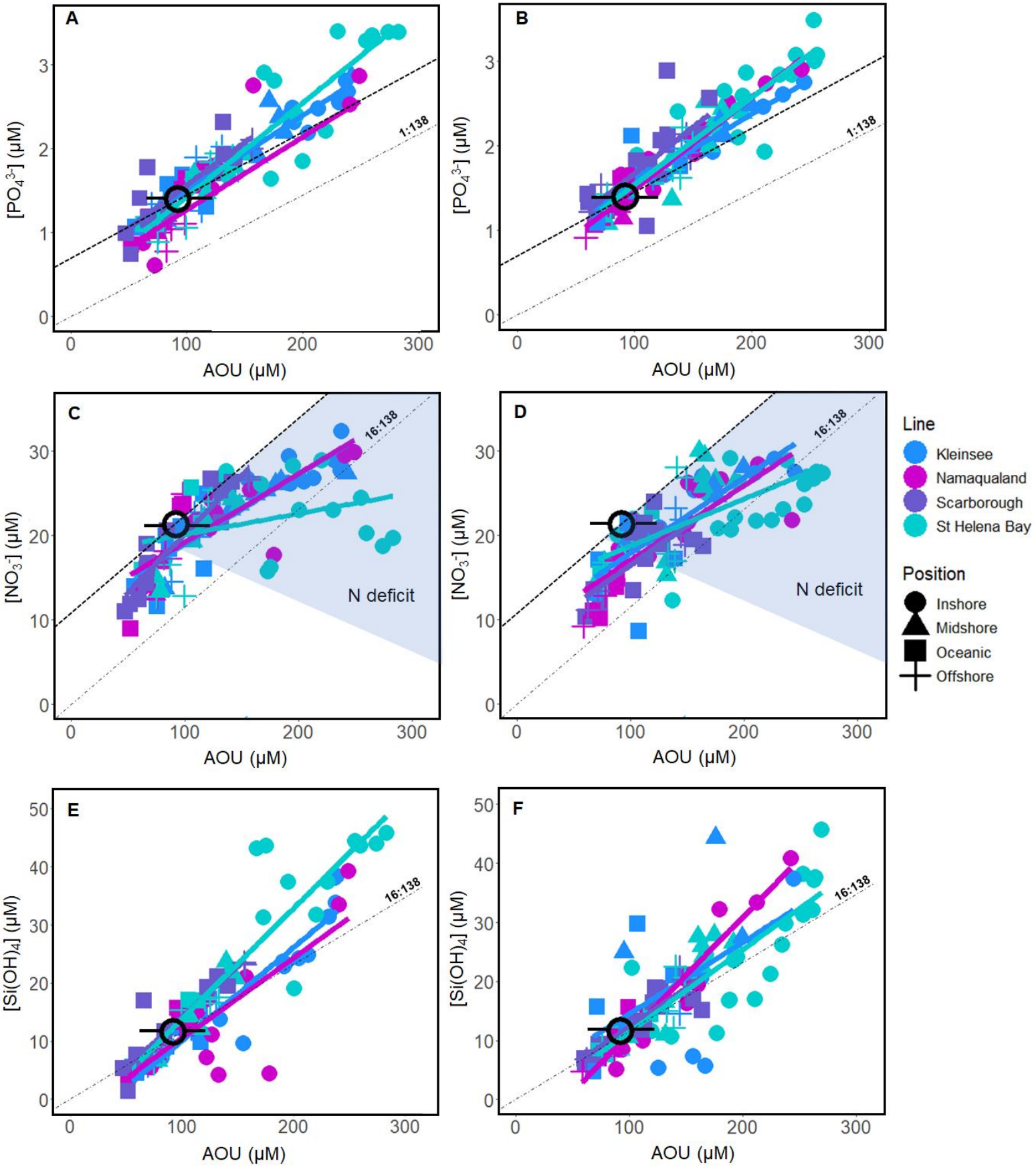


**Figure 3.8** AOU vs. phosphate (A-B), nitrate (C-D) and silicic acid (E-F) for all samples that fall into the SAMW density range for **summer** (A, C and E) and **winter** (B, D and F). The black circle represents the average the SAMW end-member values. The black dashed line shows the expected phosphate and nitrate concentrations for a given AOU if they evolve from

the SAMW end-member at a constant (Redfieldian) ratio (1:138 and 16:138 for phosphate:AOU and nitrate:AOU, respectively). The grey dotted-dashed line shows the Redfield ratio for regeneration (i.e., assuming no preformed nutrients in SAMW, such that the starting ratios of phosphate:AOU and nitrate:AOU are 0:0). For silicic acid:AOU (panels E and F), a Redfield ratio of 16:138 is shown (grey dotted-dashed line), which assumes that nitrate and silicic acid are consumed and produced in a ratio of 1:1 (i.e., Si* = 0). For all panels, the coloured lines show the linear regressions for each of the monitoring lines and the blue area on panels C and D denotes the stations with a nitrate deficit (i.e., N deficit).

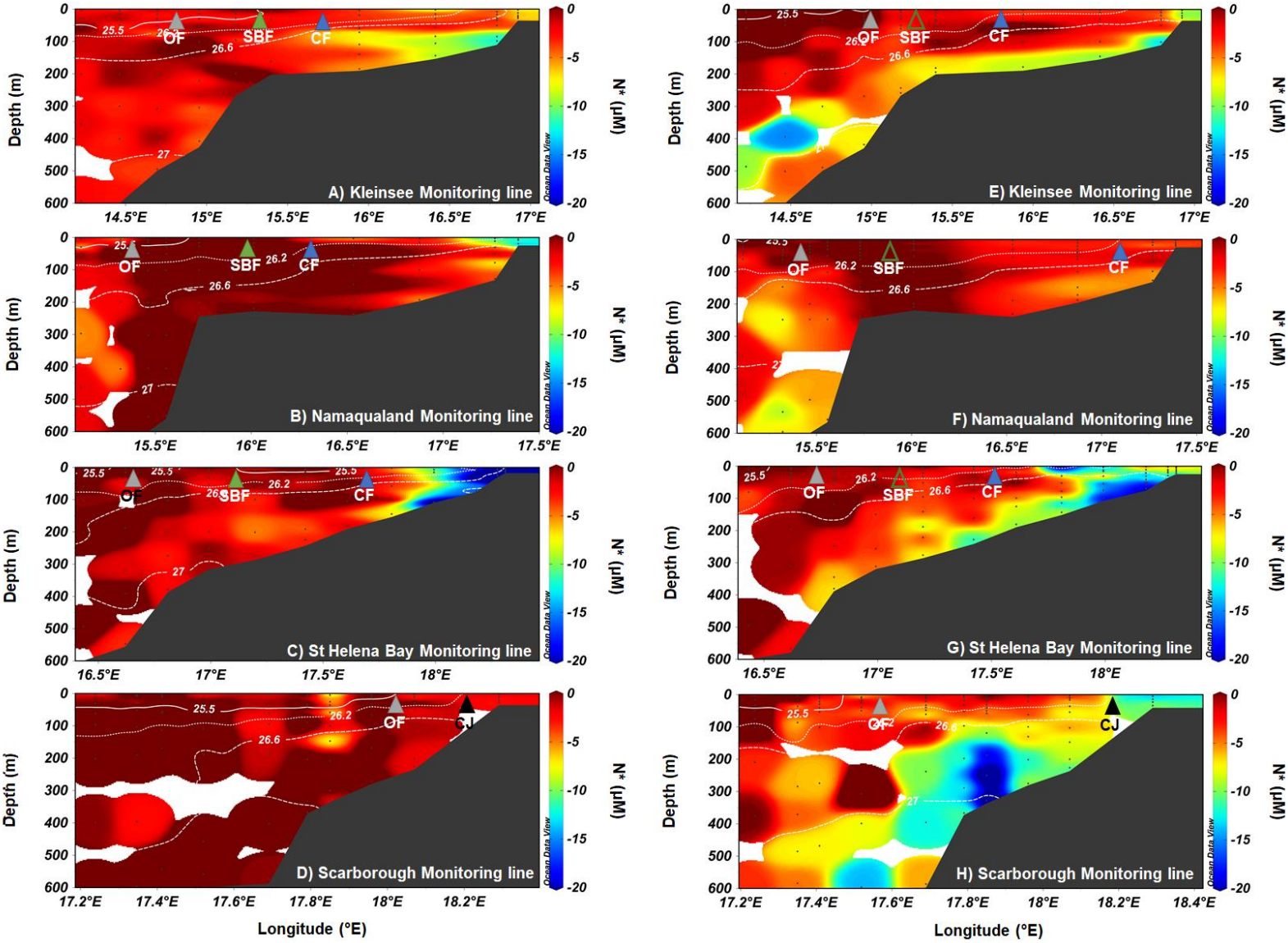


**Figure 3.9** Section plots of N* (colour) and potential density ($\sigma_\theta$; contours) for **summer** (A-D) and **winter** (E-H) along (from north to south) A and E) Kleinsee monitoring line, B and F)

Namaqualand monitoring line, C and G) St Helena Bay monitoring line and D and H) Scarborough monitoring line. The positions of the fronts identified in Figure 3.1 are shown on each figure. The density contours denote the water masses identified in Figure 3.2. The black dots show the position of the stations along each monitoring line and the depths at which discrete nutrient samples were collected. Note the changes in longitudinal scale between panels.

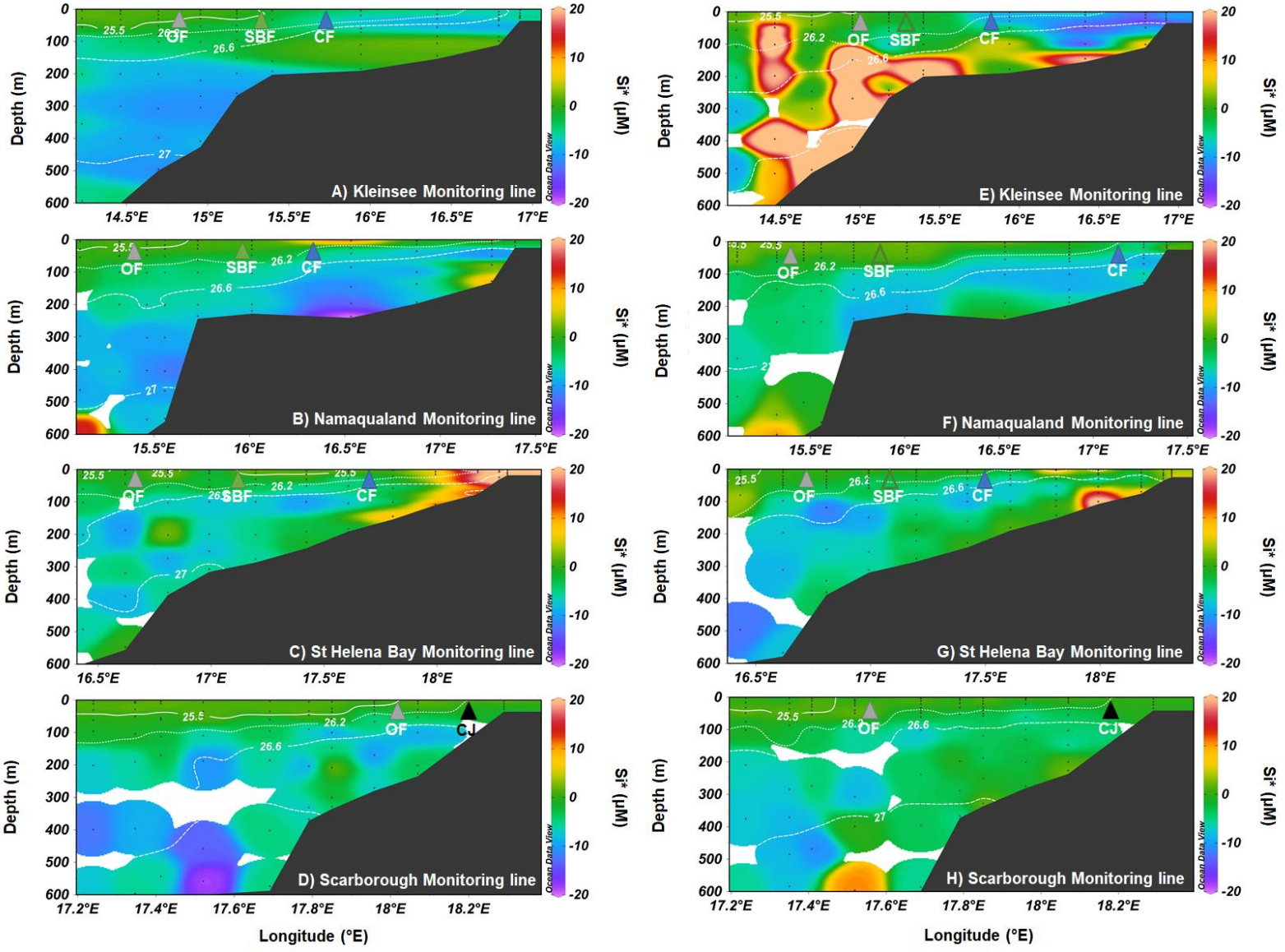


**Figure 3.10** Section plots of Si* (colour) and potential density ($\sigma_\theta$; contours) for **summer** (A-D) and **winter** (E-H) along (from north to south) A and E) Kleinsee monitoring line, B and F) Namaqualand monitoring line, C and G) St Helena Bay monitoring line and D and H) Scarborough monitoring line. The positions of the fronts identified in Figure 3.1 are shown on each figure. The density contours denote the water masses identified in Figure 3.2. The black

dots show the position of the stations along each monitoring line and the depths at which discrete nutrient samples were collected. Note the changes in longitudinal scale between panels.

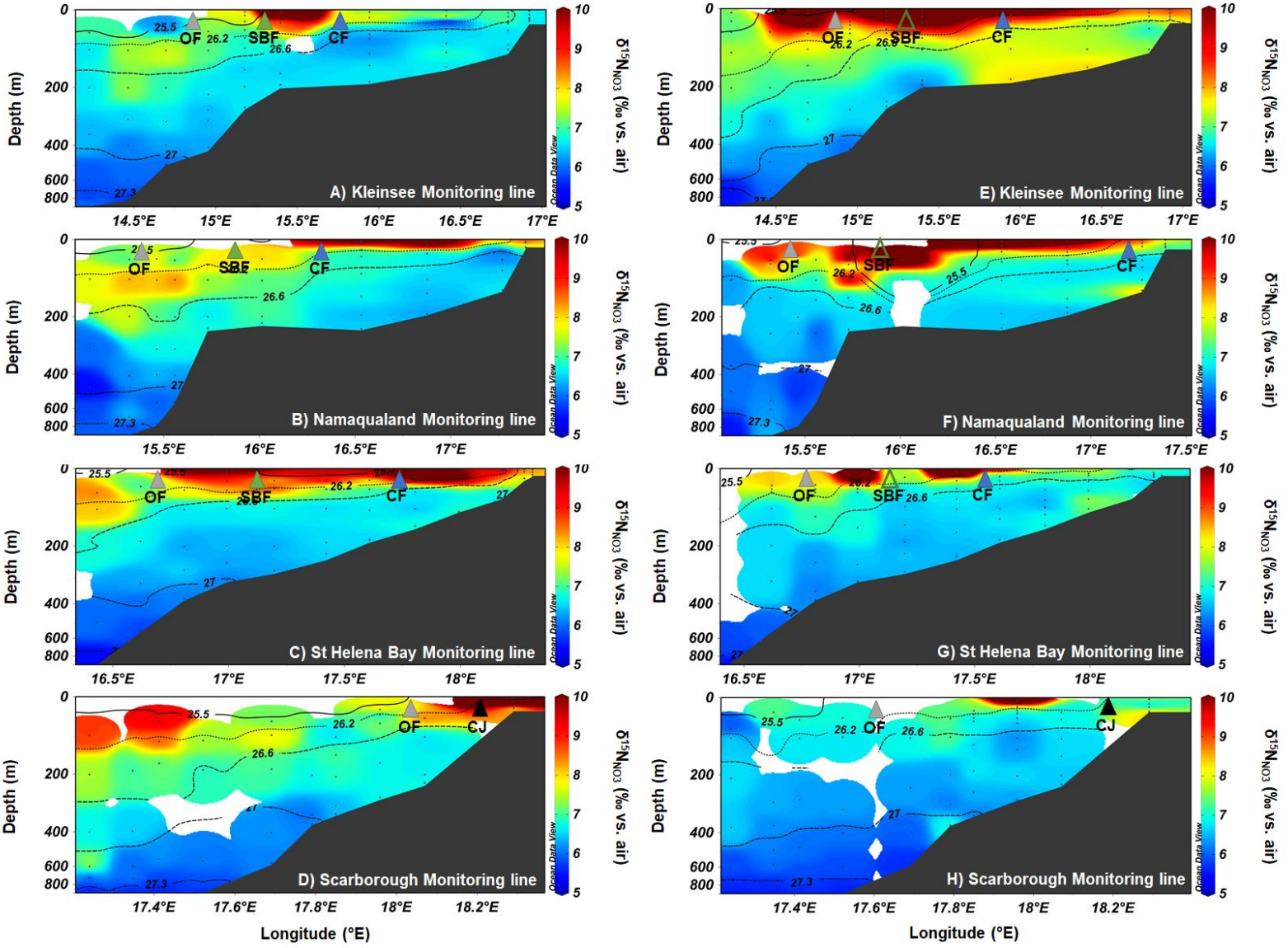


**Figure 3.11** Section plots of nitrate $\delta^{15}N$ ($\delta^{15}N_{NO3}$; colour) and potential density ($\sigma_\theta$; contours) for **summer** (A-D) and **winter** (E-H) along (from north to south) A and E) Kleinsee monitoring line, B and F) Namaqualand monitoring line, C and G) St Helena Bay monitoring line and D and H) Scarborough monitoring line. The positions of the fronts identified in Figure 3.1 are shown on each figure. The density contours denote the water masses identified in Figure 3.2.

The black dots show the position of the stations along each monitoring line and the depths at which discrete samples were collected. Note the changes in longitudinal scale between panels.

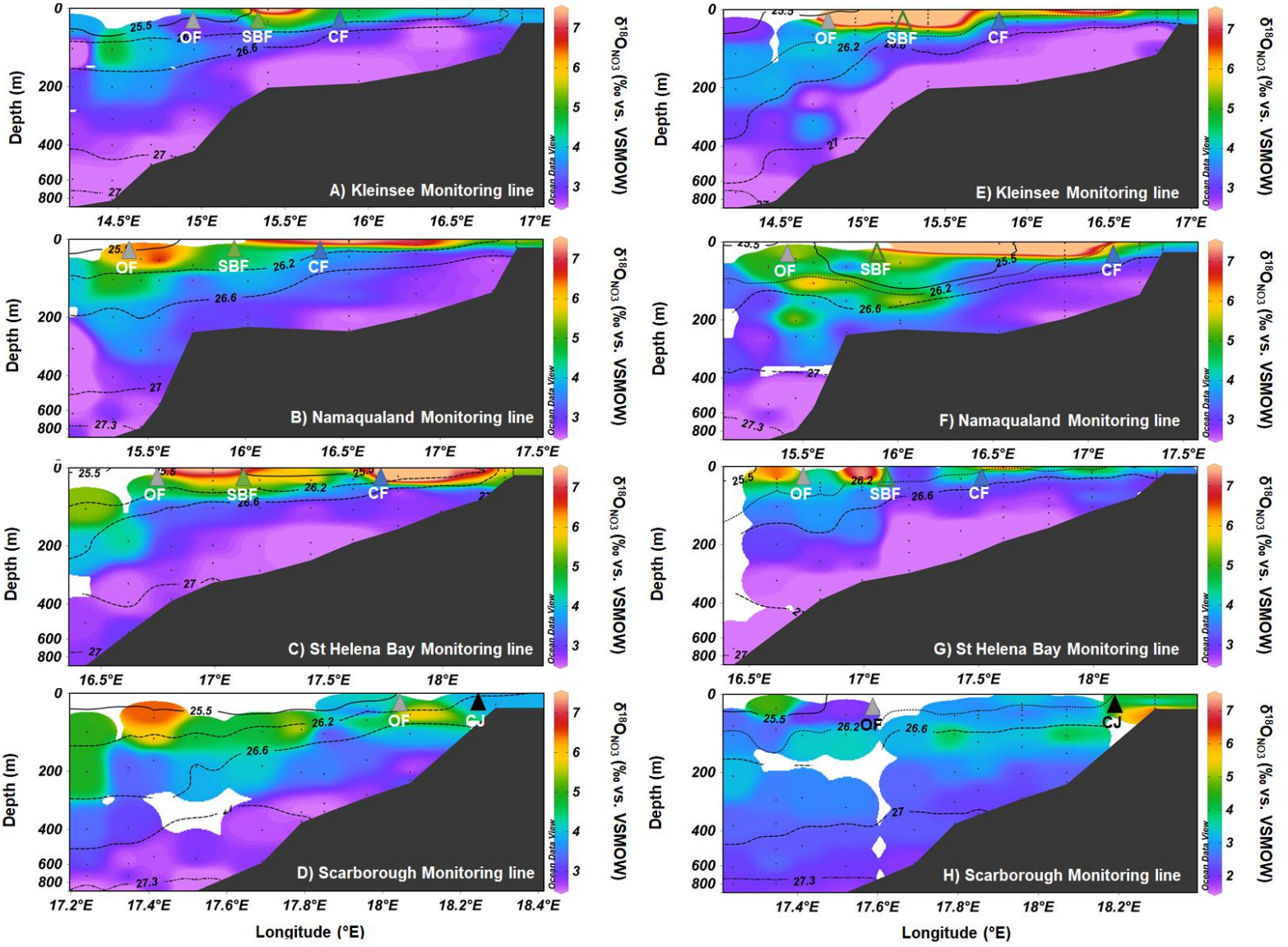


**Figure 3.12** Section plots of nitrate $\delta^{18}O$ ($\delta^{18}O_{NO3}$; colour) and potential density ($\sigma_\theta$; contours) for **summer** (A-D) and **winter** (E-H) along (from north to south) A and E) Kleinsee monitoring line, B and F) Namaqualand monitoring line, C and G) St Helena Bay monitoring line and D and H) Scarborough monitoring line. The positions of the fronts identified in Figure 3.1 are shown on each figure. The density contours denote the water masses identified in Figure 3.2. The black dots show the position of the stations along each monitoring line and the depths at which discrete samples were collected. Note the changes in longitudinal scale between panels.

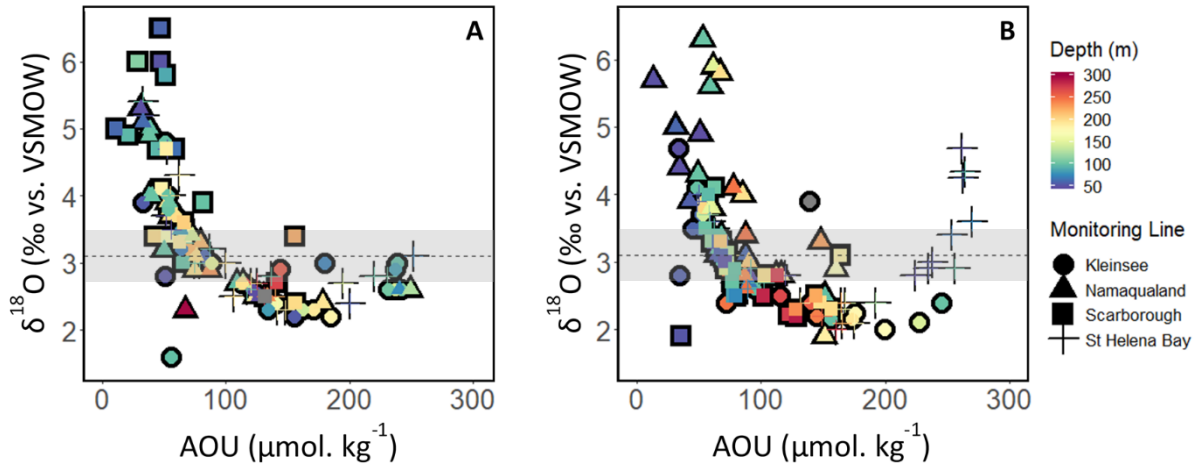


**Figure 3.13** $\delta^{18}O$ vs. AOU between 50-300 m in A) **summer** and B) **winter** 2017 at all on-shelf stations (i.e., inshore of the 300 m isobath). The grey box indicates the $\delta^{18}O$ range of SAMW nitrate (2.8‰ to 3.4‰) and dotted line indicates the average $\delta^{18}O$ of SAMW nitrate (3.1‰).

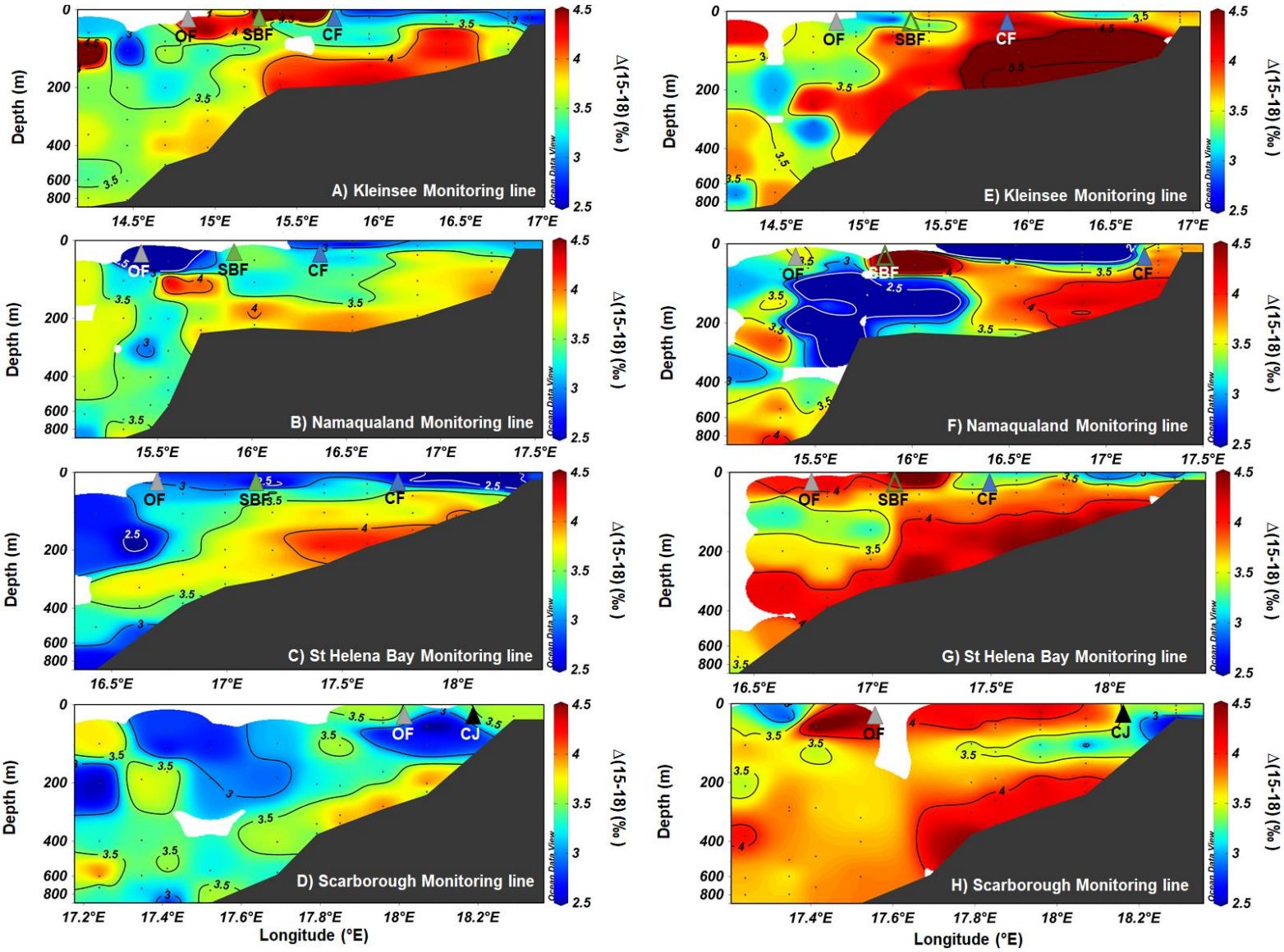


**Figure 3.14** Section plots of nitrate Δ(15-18) (colours and contours) for **summer** (A-D) and **winter** (E-H) along (from north to south) A and E) Kleinsee monitoring line, B and F)

Namaqualand monitoring line, C and G) St Helena Bay monitoring line and D and H) Scarborough monitoring line. The positions of the fronts identified in Figure 3.1 are shown on each figure. The black dots show the position of the stations along each monitoring line and the depths at which discrete samples were collected. Note the changes in longitudinal scale between panels.

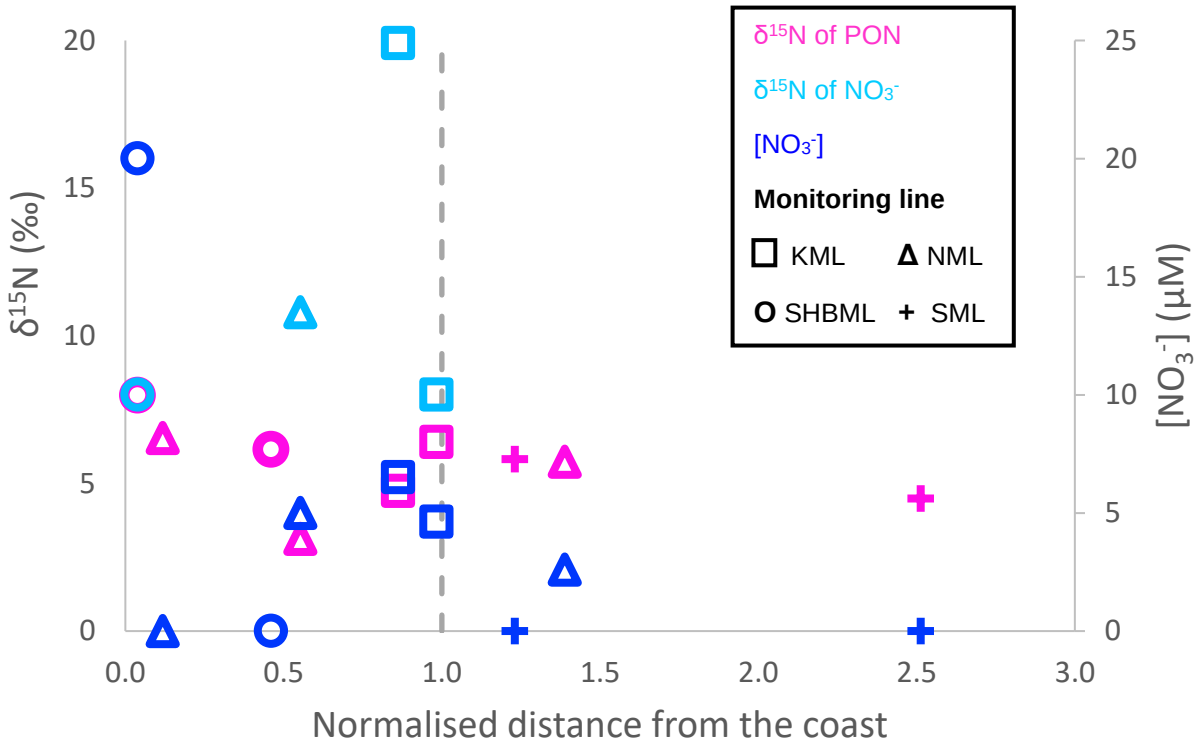


**Figure 3.15** Summertime surface $\delta^{15}N_{NO3}$ (pink), $\delta^{15}N_{PON}$ (light blue) and $[NO_3^-]$ (dark blue) at select stations along Kleinsee monitoring line (squares; KML), Namaqualand monitoring line (triangles; NML), St Helena Bay monitoring line (circles; SHBML) and Scarborough monitoring line (crosses; SML). Normalised distance from the coast was determined by dividing the distance of each station from shore by the width of the continental shelf at the station latitude; higher distances indicate stations further offshore. The grey dotted line indicates the location of the shelf break at the 300 m isobath. Note the different left and right y-axes. The PON data shown constitute all the data collected during the February 2017 cruise. Where $\delta^{15}N_{NO3}$ data are not shown, nitrate concentrations were <1 uM.

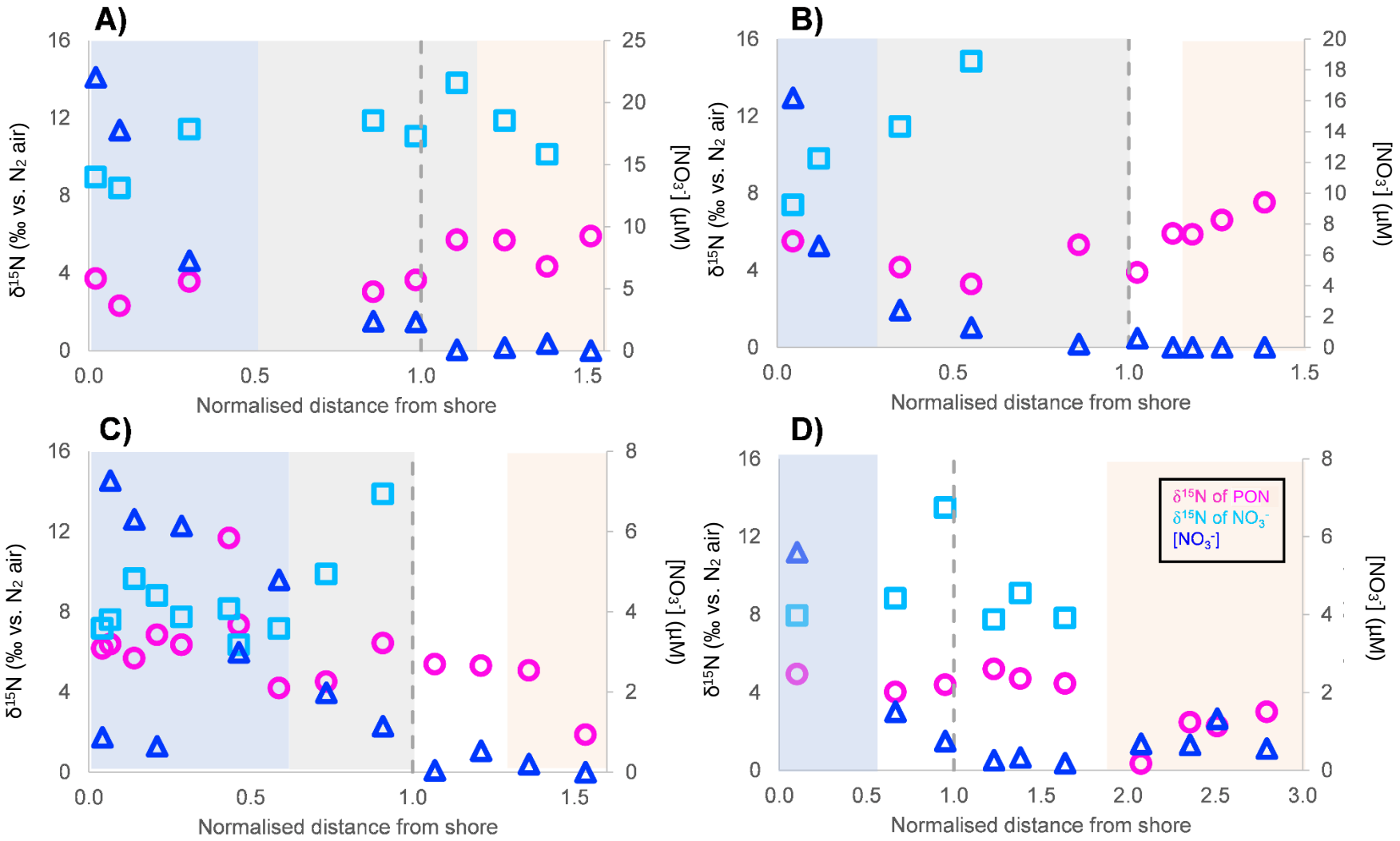


**Figure 3.16** Wintertime surface $\delta^{15}N_{NO3}$ (pink), $\delta^{15}N_{PON}$ (light blue) and $[NO_3^-]$ (dark blue) along (from north to south) A) Kleinsee monitoring line, B) Namaqualand monitoring line, C) St Helena Bay monitoring line and D) Scarborough monitoring line. Normalised distance from the coast is as described in Figure 3.15. The blue box highlights the stations inshore of the CF (i.e., the "inshore" stations), the grey box the stations between

the CF and the summertime position of the SBF (i.e., the “midshore” stations), the white box the stations between the SBF and the OF (i.e., the “offshore” stations) and the orange box stations west of the OF (i.e., the “oceanic” stations). Along the Scarborough monitoring line (D) only the CJ and the OF are present which is why there is no box denoting the midshore stations. The grey dotted line indicates the position of the shelf break at the 300 m isobath. Note the different left and right y-axes. The PON data shown constitutes all the data collected during the May 2017 cruise. Where nitrate $\delta^{15}N$ data are not shown, nitrate concentrations were <1 uM.

## 4. Discussion

Hydrographic sections from the SBUS in the summer and winter showed salient features. The surface layer became progressively more nutrient-deplete from the inshore towards the offshore, with a coincident increase in nitrate $\delta^{15}N$ and $\delta^{18}O$, which is characteristic of nitrate assimilation by phytoplankton. Relative to the winter, surface nutrients were more deplete at the inshore stations in the summer during the period of intense upwelling likely due to rapid uptake by phytoplankton. In the subsurface, the nitrate, phosphate and silicic acid concentrations on the continental shelf were higher than those in source waters off-shelf on the same isopycnals in both seasons, with the depth integrated on-shelf concentrations being more elevated in the winter. These elevated concentrations coincided with a slightly higher nitrate $\delta^{15}N$ and a lower $\delta^{18}O$ relative to SAMW off-shelf. The differences in $\delta^{15}N$ and $\delta^{18}O$ resulted in coincidently higher nitrate $\Delta$(15-18) on the shelf inshore of the SBF and the CF, which was most apparent in winter. The sum of these patterns suggests that nutrients upwelled to the SBUS surface in both seasons are assimilated into biomass that is subsequently exported to the shallow benthos, where its remineralization augments the nutrient reservoirs in the subsurface. This dynamic thus increases the concentration of nutrients that can be upwelled to the inshore surface waters. In order to support the hypothesis that benthic recycling in the SBUS enhances the concentrations of the nutrients available for upwelling relative to the SAMW source, the spatial evolution of the on-shelf biogeochemical tracers in relation to the seasonal physical dynamics is examined.

### 4.1. Nutrients upwelled in the SBUS

To a first approximation, nutrients upwelled in the SBUS should reflect the concentrations observed in source waters offshore. In summer, when upwelling in the SBUS is most vigorous, waters upwelled inshore at the Namaqualand, Cape Columbine and Cape Point upwelling cells derive from SAMW (Figure 1.5; Nelson and Hutchings 1983). Contrary to *a priori* expectations, however, summertime nutrients at the inshore and midshore stations in the density range of SAMW (26.6-27 $kg.m^{-3}$) were elevated in comparison to in offshore SAMW (Figures 3.4-3.6). To illustrate this dynamic, the concentration difference of on-shelf nitrate relative to that in SAMW, $\Delta NO_3^-$, is derived (Equation 2.11). This parameter shows that in summer, on-shelf nitrate concentrations were upwards of 10 µM higher than SAMW inshore of the CF along the Kleinsee monitoring line, with an average $\Delta NO_3^-$ concentration of 5.1 $\pm$ 3

µM for all the monitoring lines (Figure 4.1A-D). The elevation of on-shelf nutrients above those of off-shelf SAMW is further evidenced by $\Delta Si(OH)_4$ (Equation 2.11; Figure 4.2A-D; Figure 3.10A-D). Silicic acid concentrations in summer were up to 25 µM higher than those in SAMW (e.g., at the inshore St Helena Bay monitoring line stations; Figure 4.2C), with an average $\Delta Si(OH)_4$ of 10 µM for all the monitoring lines (Figure 4.2A-D). The highest $\Delta Si(OH)_4$ values were observed inshore of the CF, as was the case for $\Delta NO_3^-$. The elevated nutrient concentrations propagated westwards to roughly the SBF along the Kleinsee, Namaqualand and St Helena Bay monitoring lines and the OF along the Scarborough monitoring line (Figures 4.1 and 4.2; A-D only).

In winter, upwelling favorable winds persist north of the St Helena Bay monitoring line, with less defined winds in the southern region of the SBUS (Figure 1.7). Outcropping of the isopycnals contiguous with SASTMW suggests that surface nutrients in winter derived from a combination of SASTMW and SAMW (Figure 3.2). The nutrient concentrations below the surface on the shelf were in excess of both SASTMW and SAMW (Figures 4.1 and 4.2; E-H only) and as in summer, $\Delta NO_3^-$ and $\Delta Si(OH)_4$ were highest inshore of the CF. These elevated concentrations extended further offshore in winter than in summer, as is evident along the Kleinsee and St Helena Bay monitoring lines where a positive $\Delta NO_3^-$ and $\Delta Si(OH)_4$ propagated as far west as the OF, likely due to the dissipation of the SBF in this season.

### 4.2. Origin of the excess nutrients on the SBUS shelf

The on-shelf subsurface nutrient concentrations were in excess of those in SAMW and SASTMW in both summer and winter. Below, three mechanisms by which the excess nutrients could occur on the SBUS shelf are proposed: 1) Relatively elevated nutrient concentrations are entrained onto the shelf of the SBUS from the south by the CJ and the CF, 2) the nutrients are entrained onto the shelf from the north by the inshore poleward undercurrent, and 3) the nutrients are produced *in situ* by the remineralization of organic matter.

The waters within the CJ, and the CF which derives from the CJ, derive from the western Agulhas Bank and the Agulhas Current (Bang and Andrews 1974; Shelton and Hutchings 1982; Boyd et al. 1992; Largier et al. 1992; Boyd and Shillington 1994; Boyd and Nelson 1998). The CJ flows from the Agulhas Bank northwards, bringing nutrients from the Agulhas Bank into the SBUS. The source water mass to the western Agulhas Bank is a combination of SAMW

and SASTMW, with maximum observed nitrate concentrations of 25 µM (Lutjeharms et al. 1996). Nitrate concentrations in the CJ therefore cannot exceed 25 µM. The on-shelf nitrate concentrations observed in the present study were higher than this ($\geq$ 30 µM; Figure 3.4), providing evidence that the elevated nutrient signals cannot be imported by the CJ and the CF. Furthermore, these fronts are confined to the surface and midwater layers (Shannon and Nelson 1996), while the excess nutrients were observed at depths of up to 400 m. If a current had entrained the nutrients onto the shelf, it would therefore need to occupy depths of 50-400 m.

The poleward undercurrent has been postulated as a mechanism by which chemical properties such as nutrients and low oxygen are transported southwards from the coastal interior of the SBUS towards Cape Point (Nelson and Hutchings 1983). The poleward undercurrent occurs along the inshore region throughout the SBUS during periods of wind relaxation, particularly in winter (Nelson and Hutchings 1983; Holden 1987; Nelson 1989; Nelson and Polito 1987). If the poleward undercurrent had transported excess nutrients onto the shelf, a north-to-south gradient in the nutrient and AOU concentrations would be expected. However, this is not what was observed. The elevated on-shelf nutrient concentrations were highest along the northernmost Kleinsee monitoring line and the St Helena Bay monitoring line but reached far lower concentrations at the Namaqualand monitoring line that lies between them (Figures 3.4-3.7). Furthermore, previous studies have shown that the oxygen concentration, and therefore AOU concentration, of the poleward undercurrent is not distinct from that of the surrounding waters (Lamont et al. 2015). If the poleward undercurrent were responsible for transporting the observed excess nutrients onto the shelf, it would also have to transport low-oxygen water, for which there is no evidence. It is therefore unlikely that the poleward undercurrent is the mechanism by which elevated nutrient concentrations are introduced onto the shelf in the SBUS.

The excess on-shelf nutrients are thus best explained as deriving from *in situ* remineralization. The low oxygen concentrations overlying the inshore and midshore shelf sediments (data shown in Appendix A; Figure A1) were likely locally produced by the *in situ* remineralization of organic matter. This is evidenced by the overlap in multiple chemical parameters with the apparent oxygen utilization (AOU). AOU was observed to increase towards the inshore along all monitoring lines, with the largest increase occurring during the summer due to the decay of spring and summer upwelling-driven phytoplankton blooms (Bailey 1991).

AOU is positively correlated with phosphate, nitrate and silicic acid (Figure 3.8), as is expected for remineralization. In theory, therefore, it should be possible to calculate the quantity of remineralised nutrients on the shelf from AOU. However, this is not feasible for phosphate and nitrate in the SBUS. Phosphate versus AOU on the continental shelf integrates the immediate remineralised nutrients, phosphate buffering by sediments and remineralization by other oxidants such as nitrate and sulphate (Rozan et al. 2002). Thus, in order to observe changes in phosphate above that of the SAMW end-member, the parameter $\Delta PO_4^{3-}$ is used (Figure 4.3; Equation 2.11).

The regenerated nitrate concentration cannot be accurately computed because some portion of the on-shelf nitrate is being lost from the system by denitrification (Calvert and Price 1971; Bailey 1987; Tyrell and Lucas 2002). $\Delta NO_3^-$ is therefore used in order to show changes in nitrate above that of the SAMW end-member. Furthermore, if the theoretical regenerated nitrate concentration is calculated from AOU using the Redfield ratio of 16:138 (Redfield et al. 1963) then the difference between the theoretical regenerated nitrate concentration and $\Delta NO_3^-$ provides insight into the amount of nitrate lost to denitrification. This will be dealt with below in section 4.4. Finally, the amount of on-shelf nitrate that was remineralised *in situ* can be quantified using the O isotopes of nitrate.

The on-shelf rise in Si* above that of SAMW (Figure 3.10) provides strong evidence for *in situ* nutrient regeneration given that SAMW is characteristically low in Si* across the global ocean (Sarmiento et al. 2004). In addition to supporting the case for regeneration as a persistent feature of the on-shelf SBUS environment, at least in summer and early winter, the high Si* also implies that the organic matter being remineralized must include a large quantity of diatoms, as these phytoplankton synthesize biogenic silica tests from dissolved silicic acid while most other phytoplankton have no silicic acid requirements. Diatoms are known to dominate in the SBUS (Pitcher et al. 1989; Pitcher et al. 1991) and the remineralization of their biomass would lead to a rise in the on-shelf silicic acid concentration. However, under conditions of non-limiting iron, as is generally expected for the SBUS, diatoms have been shown to take up nitrate and silicic acid in a ratio close to 1:1 (Ragueneau et al. 2000). The subsequent remineralization of their biomass, which should have an organic N:Si ratio close to 1, would yield an equal rise in the subsurface nitrate and silicic acid pools, leading to no change in Si*. However, this is not the case for either summer or winter when the positive Si* suggests

that proportionally more silicic acid than nitrate has been remineralized. We propose that this is due to a number of (non-exclusive) reasons. First, SBUS diatoms may take up nitrogen and silicic acid in a ratio <1:1 despite not being iron-limited. Under conditions of light limitation, which occur in aged phytoplankton blooms due to self-shading (Brown and Field 1986), nitrogen and silicic acid have been shown to be consumed in a variable ratio (Ragueneau et al. 2000; Sarmiento et al. 2002). Second, some portion of the remineralised nitrate has been denitrified at the sediment-water interface (see section 4.4 below), which would decrease the on-shelf nitrate concentration with no effect on the silicic acid. Finally, the remineralization length scales for nitrate and silicic acid are different, with organic nitrogen being more rapidly decomposed (Grill and Richards 1964). Nitrate remineralized at shallower depths than the silicic acid could thus more easily to lost to re-assimilation and/or advection, leading to an increase in the Si* of the regenerated nutrient pool at depth on the shelf.

### 4.3. On-shelf nutrient regeneration *in situ*

The *in situ* regeneration of nutrients in waters overlying the shelf is further evidenced by the decrease in subsurface nitrate $\delta^{18}O$ below that of SAMW. This decrease is due to nitrification (i.e., nitrate regeneration; Sigman et al. 2009). When organic matter undergoes ammonification and nitrification, the newly nitrified nitrate will have a $\delta^{18}O$ that is ~1.15‰ above that of ambient seawater – on the order of 1.15-1.65‰ for the SBUS given the reported $\delta^{18}O_{seawater}$ values of ~0-0.5‰ (Meredith et al. 1999; Sigman et al. 2005; Buchwald and Casciotti 2012). The change in the on-shelf nitrate $\delta^{18}O$ compared to SAMW provides insight into the extent of nitrification, where a lower nitrate $\delta^{18}O$ indicates a greater fraction of newly nitrified nitrate.

The lower on-shelf nitrate $\delta^{18}O$ values coincide remarkably with the elevated nitrate concentrations and high AOU in both seasons (Figures 3.7, 3.12 and 4.1). During remineralisation and nitrification, AOU should increase due to an increase in oxygen utilisation. Figure 3.13 shows that with more remineralisation and nitrification (i.e., with decreasing nitrate $\delta^{18}O$), more and more oxygen is utilised. Indeed, nitrate $\delta^{18}O$ values of up to 1‰ lower than SAMW were observed, providing evidence for high proportions of the on-shelf nitrate reservoir being nitrified *in situ*. The data further suggest that relatively more nitrification occurs in the winter, as evidenced by the greater proportion of observations of low-$\delta^{18}O$ nitrate and high AOU in Figure 3.13B compared to Figure 3.13A.

Using the nitrate $\delta^{18}O$ and a two end-member mixing model, the fraction of nitrate regenerated on the shelf can be calculated (Equation 2.12). In summer, an average of 30% of the on-shelf nitrate was regenerated, with a maximum of 55% regenerated along the Kleinsee monitoring line. During winter, an even greater proportion of the on-shelf nitrate was regenerated, upwards of 70% along the Kleinsee monitoring line, with an average of 35% for all the monitoring lines (Figure 4.4). The average on-shelf regenerated nitrate was thus ~5% higher in winter than in summer. There was also a broader range in the fraction of the total nitrate reservoir that was regenerated in winter versus summer (0 to 0.75 versus 0 to 0.54). In both seasons, a similar linear trend was observed between AOU and regenerated nitrate at AOU concentrations below ~180 µmol.kg$^{-1}$ (Figure 4.4). The bottom waters at the most inshore stations deviated from this linear trend, however, with AOU concentrations above ~180-200 µmol.kg$^{-1}$ but a lower fraction of regenerated nitrate (Figure 4.4). The nitrate $\delta^{18}O$ in these bottom waters was higher than that at the depths above (Figure 3.12 and Figure 3.13), perhaps due to water column denitrification. During denitrification, $^{16}O$-bearing nitrate is preferentially reduced over $^{18}O$-bearing nitrate as it is more energetically efficient; thus, the $\delta^{18}O$ of the residual nitrate pool rises. The isotope effect for denitrification is large (~20-30‰; Granger et al. 2008; Sigman et al. 2009a). It would therefore only take a small amount of water column denitrification to elevate the nitrate $\delta^{18}O$ of the on-shelf bottom waters. Favourable conditions for denitrification were observed in these on-shelf bottom waters, with average oxygen concentrations of 47.2 $\pm$ 9.1 µM (Figure A1), which are low enough to support denitrification (Nakajima et al. 1984). This likely explains why the fraction of regenerated nitrate was lower than expected in the highest-AOU samples. Rather than nitrate being solely produced, as was observed for the shallower depths, denitrification acted to remove nitrate from the system by reducing it to $N_2$ gas. Therefore, the data suggest that under oxygen-deplete conditions, denitrification may occur in the water column of the SBUS. It will be limited in its extent by the occurrence of low oxygen concentrations and is likely to be confined to specific areas of the shelf (see section 4.7).

Another consideration with regards to the quantity of on-shelf regenerated nitrate is that both SAMW and SASTMW can upwell at the surface at the inshore stations, particularly in winter (Figure 3.2; Lamont et al. 2015). The $\delta^{18}O$ of upwelled water should therefore range from 3.1‰ to 3.9‰, depending on the relative proportions of SAMW and SASTMW (Table 3.1). It is possible, therefore, that by assuming SAMW nitrate $\delta^{18}O$ alone to be the source water into which newly nitrified nitrate is added, the fraction of nitrate that is regenerated on the shelf is underestimated. In other words, if regenerated nitrate is added to a mixture of SAMW and

SASTMW in the waters overlying the shelf, which is mostly likely at the shallow, inshore stations, then $\delta^{18}O_{source}$ (Equation 2.12) is actually higher than 3.1‰ and a greater fraction of regenerated nitrate is required to decrease the on-shelf nitrate $\delta^{18}O$ to the observed values. However, this effect is fairly small. For example, if $\delta^{18}O_{source}$ is set to the SASTMW end-member (3.9‰), the fraction of regenerated nitrate increases by 10%. Thus, denitrification is still required to decrease the quantity of regenerated nitrate below that expected from AOU.

The on-shelf regeneration of nutrients has been described previously for the SBUS and other upwelling regions (Hart and Currie 1960; Jones 1971; Calvert and Price 1971; Rowe et al. 1975; Bailey and Chapman 1985; Bailey 1991). The first study to identify this phenomenon in the SBUS was conducted by Jones (1971). The author observed elevated concentrations of phosphate and silicic acid in the on-shelf bottom waters throughout the SBUS, which they attributed to *in situ* remineralization of organic matter on the shelf. Interestingly, Jones (1971) did not observe commensurately elevated concentrations of nitrate during their sampling, which they attributed to the varying rates at which these nutrients are regenerated (Grill and Richards 1964). Calvert and Price (1971) deduced that the changes nutrient ratios in the SBUS are due to the varying residence times of waters on the shelf. They observed the lowest N:P and Si:P ratios in offshore waters, with an increase in the ratios towards the coast. They concluded that the offshore waters represented more recently upwelled waters, while those further inshore were older, such that nutrient regeneration had likely progressed further at the inshore stations. Similar patterns were observed during our sampling, with the highest concentrations of regenerated nutrients measured at the inshore stations, decreasing offshore towards the shelf-break (Figure 4.1-4.3).

### 4.4. On-shelf increase in $\delta^{15}N$ above that of SAMW

During both seasons, the subsurface nitrate $\delta^{15}N$ on-shelf was slightly higher than that in SAMW along all monitoring lines, with the greatest difference observed during the winter (Figure 3.11). The on-shelf increase in nitrate $\delta^{15}N$ is accompanied by a rise in the nitrate, silicic acid and phosphate concentrations, and, more importantly, by an increase in $\Delta NO_3^-$, $\Delta Si(OH)_4$ and $\Delta PO_4^{3-}$ (Figures 3.4-3.6, 3.11 and 4.1-4.3). The elevation of on-shelf nitrate $\delta^{15}N$ above that of SAMW may be due to three processes: 1) the incomplete remineralization of organic material, 2) the upwelling of SASTMW nitrate and the subsequent remineralization of

organic material derived from it and 3) isotopic N increase due to coupled nitrification-denitrification in the sediments.

The rise in nitrate $\delta^{15}N$ above SAMW, particularly at the northern lines, cannot solely be due to incomplete remineralization and nitrification of organic matter. Surface PON along the Kleinsee and Namaqualand monitoring lines had an average $\delta^{15}N$ below that of SAMW (Figure 3.16A and B), and incomplete remineralization is unlikely to drive the $\delta^{15}N$ of the regenerated nitrate to values as high as 8‰ (Figure 3.11E). In the case where consumption of the nitrate pool is complete, the $\delta^{15}N$ of the phytoplankton will be equal to the source nitrate $\delta^{15}N$ (6.6‰; Table 3.1). When this PON sinks and is remineralised and nitrified, the newly nitrified nitrate will also have a $\delta^{15}N$ of 6.6‰. This appears to be the case in summer (Figure 3.15). Surface nitrate concentrations were depleted at all but the most inshore stations along all the monitoring lines, consistent with complete nitrate consumption. The weighted average $\delta^{15}N$ of the surface PON, at stations where surface nitrate was depleted, was 4.9 $\pm$ 0.7‰. In winter, however, the $\delta^{15}N$ of on-shelf surface PON was higher than expected from the $\delta^{15}N$ and concentration of the co-occurring nitrate (average surface nitrate $\delta^{15}N$ of 9.5 $\pm$ 2.3‰ and $[NO_3^-]$ of 6.1 $\pm$ 6.1 µM for all lines; Figures 3.4 and 3.16). The weighted average $\delta^{15}N$ of the on-shelf surface PON was 4.8 $\pm$ 1.4‰, similar to that measured in summer, yet surface nitrate was not depleted in winter. This suggests that the PON was advected from inshore waters where it was generated during earlier (near)complete nitrate consumption. As the surface waters moved offshore, isotopically-light PON would have been initially remineralised (Saino and Hattori 1980; Altabet and McCarthy 1986). If the remaining PON was advected as far as the midshore before remineralization was complete, its $\delta^{15}N$ would be elevated. The subsequent remineralization of this high-$\delta^{15}N$ PON in the subsurface of the midshore region could then elevate the $\delta^{15}N$ of the combined nitrate pool above the source value. The increase in surface PON $\delta^{15}N$ from the inshore towards the midshore region is best illustrated by Figure 3.16C. Here, along the St Helena Bay monitoring line, the $\delta^{15}N$ of surface PON rises from the inshore to the midshore stations. The $\delta^{15}N$ of PON also increases with depth due to the preferential remineralization of $^{14}N$ over $^{15}N$ (Saino and Hattori 1980). This shows that if incomplete remineralization occurred at the inshore stations and the remaining PON was advected offshore and sank out of the surface, the newly nitrified nitrate produced on the midshore shelf could be high in $\delta^{15}N$ relative to SAMW.

It is still unlikely, however, that this process can explain the entire rise in subsurface nitrate $\delta^{15}N$ relative to the SAMW end-member. The isotope effect associated with PON remineralization is small (~3‰; Möbius 2013), such that a large fraction of the PON pool would have to be remineralized in order for the remaining portion to reach a $\delta^{15}N$ of 8‰. Moreover, such a rise in the $\delta^{15}N$ of the residual PON pool should be accompanied by a significant decline in its concentration, which is not observed; if anything, the concentration of PON tends to rise from the inshore to the midshore (data not shown). Finally, the concomitant *in situ* production of PON in midshore surface waters (i.e., due to phytoplankton growth on nitrate and/or ammonium, with the former having a $\delta^{15}N$ of ~6.6‰ and the latter inferred to be low in $\delta^{15}N$ (<<6.6‰) due to isotopic fractionation associated with its production; Macko et al. 1986; Checkley and Miller 1989; Silfer et al. 1992) would add relatively low-$\delta^{15}N$ PON to the partially-remineralized pool, effectively decreasing the $\delta^{15}N$ of the combined PON pool available for export. This means that to drive the $\delta^{15}N$ of subsurface nitrate to 8‰ through PON remineralization, the $\delta^{15}N$ the advected PON would have to be >8‰, which is not supported by the available data and is difficult to achieve with such a small isotope effect.

The higher subsurface $\delta^{15}N$ for nitrate on-shelf than in SAMW offshore may be attributed to a greater proportion of PON deriving from SASTMW, which is upwelled at the inshore during winter and contains nitrate with a higher $\delta^{15}N$ than SAMW (7.2‰ versus 6.6‰) (Figure 3.2 and Figure 3.11). The $\delta^{15}N$ of upwelled nitrate could therefore range from 6.6‰ to 7.2‰, depending on the relative proportions of SAMW and SASTMW. If only SASTMW were upwelled, the PON produced under conditions of complete nitrate consumption would have a maximum $\delta^{15}N$ of 7.2‰. The incomplete remineralization and offshore advection of this PON could drive the $\delta^{15}N$ of the regenerated nitrate as high as 8‰ (the highest nitrate $\delta^{15}N$ observed during winter); however, in addition to the argument outlined above, it does not appear that SASTMW alone was upwelled to the surface. Thus, another process must be acting to raise the $\delta^{15}N$ of the nitrate overlaying the shelf sediment above that of SAMW and SASTMW.

The most plausible explanation for the increase in on-shelf nitrate $\delta^{15}N$ above that of the source water is coupled nitrification-denitrification in the sediment followed by water column nitrification of ammonium released from the sediment (Granger et al. 2011, Brown et al. 2015). Coupled benthic nitrification-denitrification results in isotopically-light nitrogen being lost from the system, while the remaining isotopically-heavy nitrogen is nitrified in the oxygenated water column. When organic matter is exported to the sediments, it is decomposed by microbes,

producing ammonium. The ammonium is then nitrified to nitrite and nitrate at the surface sediment, in the presence of oxygen. The decay and nitrification of a large proportion of the exported organic matter leads to oxygen-deplete conditions in the sediments, which favour denitrification. The nitrate produced by nitrification in surface sediments can fuel this denitrification in the underlying, oxygen-deplete sediments (Christensen et al. 1987; Seitzinger 1988; Devol 1991; Devol and Christensen 1993; Jahnke and Jahnke 2000).

The biological oxidation of ammonium to nitrate (nitrification) is associated with a relatively large isotope effect, ranging from 14-38‰ for ammonium oxidizing bacteria (AOB) (Mariotti et al. 1981; Yoshida 1988; Casciotti et al. 2003) and 20-22‰ for ammonium oxidizing archaea (AOA) (Santoro and Casciotti 2011). This yields an average isotope effect of ~23‰ for AOB and AOA together. When ammonium is nitrified, the $\delta^{15}N$ of the nitrate produced will thus be ~23‰ lower than that of the nitrified ammonium. Given that ammonification is expected to be intense at the surface sediment (Prokopenko et al. 2006; Velinksy et al. 1991), the resultant ammonium pool will have a $\delta^{15}N$ equivalent to that of the ammonified PON. Isotopic discrimination during ammonium oxidation in surface sediments will then increase the $\delta^{15}N$ of the ammonium compared to the $\delta^{15}N$ of PON, while producing relatively $\delta^{15}N$-deplete nitrate (Casciotti et al. 2003). This nitrate is then respired by denitrifying bacteria in underlying sediment, producing $N_2$ gas that has a low $\delta^{15}N$ in comparison to the bulk shelf $\delta^{15}N$ (Brandes and Devol 1997). The isotopically-light $N_2$ gas is lost from the system to the atmosphere. Ammonium in organic-rich sediments is effluxed from into the water column (Kemp et al. 2005; McCarthy et al. 2008; Conley et al. 2007) where it is subsequently nitrified under oxygen-replete conditions, producing nitrate that is high in $\delta^{15}N$ compared to the source waters (Figures 3.11). Figure 4.5 shows a schematic of the processes hypothesized to occur in the surface sediment and bottom waters of the SBUS midshore and inshore regions. The branching isotope effect results in low-$\delta^{15}N$ nitrogen being subject to coupled nitrification-denitrification and the high-$\delta^{15}N$ nitrogen undergoing water column nitrification.

The argument above appears consistent with the observed N* values of subsurface nutrients on the shelf (Figure 3.9). During both seasons, N* is always less than zero on the shelf, with the greatest decrease in N* occurring in the winter, coincident with the highest nitrate $\delta^{15}N$ (Figure 3.11). Furthermore, the link between nitrogen loss and oxygen depletion is evident with the lowest values of N* occurring at the inshore stations and coinciding with the highest AOU (Figure 3.7). There are, however, additional processes that may be occurring simultaneously at

the inshore stations, acting to further lower N*. For example, not only is there a loss of nitrogen to denitrification but there is also a gain in phosphate from sedimentary organic matter remineralization and subsequent phosphate efflux. Under oxygen-deplete conditions, phosphate has been observed to efflux out of the sediments into the water column of the SBUS (Schulz and Schulz 2005; Bailey and Chapman 1991). The lowest values of N* overlap with the highest concentrations of $\Delta PO_4^{3-}$, consistent with a gain in phosphate (Figure 3.9 and 4.3).

N* provides evidence that nitrogen loss is occurring in the SBUS in both summer and winter. A relationship between N* and $\delta^{15}N$ is observed, with a rise in $\delta^{15}N$ associated with a decline in N* (Figure 4.6A and B; highest N* = inshore St Helena Bay monitoring line). This supports the hypothesis of coupled nitrification-denitrification in the sediments, which can both raise the $\delta^{15}N$ of the subsurface on-shelf nitrate pool and decrease N* due to a net loss of nitrogen to denitrification.

Figure 3.8C and D clearly show the nitrate deficit in the SBUS at the time of sampling. For a given AOU, less nitrate is observed than is expected (with the dashed black line on the Figure panels representing the expected nitrate concentration for a given AOU). In AOU versus nitrate space, the starting ratio for AOU:$NO_3^-$ in SAMW is ~91.9:21.3 (Table 3.1; black circle in Figure 3.8C and D). During aerobic remineralization, the ratio of AOU: $NO_3^-$ should remain constant, with all data falling along the dashed line. However, all the inshore samples fall below this line, indicating nitrate concentrations that are anomalously low for the values of AOU. Using the difference between the expected and observed nitrate concentrations for a given AOU, the quantity of nitrate lost from the system by denitrification (i.e., the N deficit; Equation 2.13) can be calculated.

In summer, the N deficit was on average 7.1 $\pm$ 6.3 µM and 3.9 $\pm$ 2.4 µM at the inshore and midshore stations, respectively (Figure 4.6C). The greatest N deficit was observed at the inshore stations along the St Helena Bay monitoring line, as was the case for N* (Figure 3.9C). In winter, the N deficit was on average 7.5 $\pm$ 4.9 µM and 3.9 $\pm$ 2.5 µM at the inshore and midshore stations respectively, (Figure 4.6D). Again, the greatest N deficit was observed at the inshore stations along the St Helena Bay monitoring line (~28 µM), as was the case for N* (Figure 3.9G). The $\delta^{15}N$ of nitrate increased in conjunction with both a decrease in N* and an increase in N deficit. There were, however, obvious differences between N* and N deficit. At the inshore St Helena Bay stations, N* and N deficit differed by 10 µM on average. This is

likely due to phosphate efflux at these stations, which has an effect on N* but not on the N deficit. Nonetheless, both N* and N deficit can be used as tracers for coupled nitrification-denitrification in the sediments.

### 4.5. Δ(15-18), a tracer of coupled nitrification-denitrification

Changes in Δ(15-18) (Equation 2.14) above or below that of the source water (SAMW Δ(15-18) ~3.5‰) allow us to identify overlapping biological processes such as nitrification and denitrification that alter the $\delta^{15}N$ and $\delta^{18}O$ of nitrate differently (Figure 1.4).

A rise in Δ(15-18) to values above 3.5‰ at depth on the shelf (50-300 m) is apparent in both seasons (Figures 3.14). This rise is accompanied by an increase in the nitrate, silicic acid and phosphate concentrations (Figures 3.4-3.6) and more importantly, the $\Delta NO_3^-$, $\Delta Si(OH)_4$ and $\Delta PO_4^{3-}$ concentrations (Figure 4.1-4.3). Δ(15-18) reaches values of up to 5.5‰ in winter, with maximum values of 4.2‰ in summer. In addition, the high-Δ(15-18) signal propagates further along the shelf towards the offshore stations in winter but is retained inshore of the SBF in summer. The overlap between the rise in nitrate Δ(15-18) and the elevated regenerated nutrient concentrations suggests intense remineralization on the shelf plays a role in increasing Δ(15-18).

The rise in Δ(15-18) above that of SAMW in summer, and both SAMW and SASTMW in winter, is due to a decrease in nitrate $\delta^{18}O$ and an increase in $\delta^{15}N$ (Figures 3.11 and 3.12). The decrease in $\delta^{18}O$ is driven by *in situ* nitrification, while the increase in $\delta^{15}N$ can be explained by coupled nitrification-denitrification, incomplete remineralization, and the relative importance of the two source water masses (i.e., only SAMW in summer and a combination of SAMW and SASTMW in winter). The larger increase in Δ(15-18) in winter can be explained by a greater proportion of water column nitrification and less sedimentary nitrification (i.e., due to enhanced low-oxygen conditions driven by the remineralization of a large quantity of organic matter). More ammonium will be effluxed from the sediments when sedimentary nitrification is reduced, and it will be higher in $\delta^{15}N$ than if more complete nitrification had occurred due to less of the $^{15}N$-ammonium being oxidized. A higher flux of ammonium out of the sediments in winter will lead, in turn, to increased rates of nitrification in bottom waters, which will lower the wintertime nitrate $\delta^{18}O$. In addition, the tight coupling between the decrease in N* and the rise in Δ(15-18), except at the inshore stations where phosphate efflux

likely occurs (Figures 3.9 and 3.14), provides evidence for coupled nitrification-denitrification in the sediments. This is because as Δ(15-18) rises due to both water column nitrification (which lowers nitrate $\delta^{18}O$) and coupled sedimentary nitrification-denitrification (which raises nitrate $\delta^{15}N$), N* decreases due to denitrification-driven fixed nitrogen loss. Δ(15-18) can therefore be used as a tracer for coupled nitrification-denitrification and *in situ* remineralisation.

The process of coupled nitrification-denitrification in the sediments has previously been inferred for the SBUS (Calvert and Price 1971; Bailey 1987; Tyrell and Lucas 2002). Under oxic conditions, a nitrate maximum ($[NO_3^-]$ up to 200 µM) was observed in SBUS porewaters down to 2 cm deep, while under oxygen-deplete conditions, porewater nitrate concentrations were lower ($[NO_3^-]$ = 2 µM) (Bailey 1987). These data suggest that when there is high loading of organic matter to the sediments there will be: 1) increased nitrogen loss from the system by sedimentary denitrification and/or 2) lower rates of nitrification relative to the quantity of ammonium available for oxidation due to increased remineralisation and thus increased oxygen depletion. This is best observed at the inshore stations of the St Helena Bay monitoring line, particularly in winter. $\Delta NO_3^-$ concentrations at the most inshore stations are $\leq$ 1 µM (Figure 4.1C), yet the highest $\Delta PO_4^{3-}$ concentrations were observed at these stations (Figure 4.3C). In addition, the low $\Delta NO_3^-$ concentrations overlap with low oxygen concentrations (Figure A1C). Although the water column throughout the SBUS does not experience anoxia at the time of our sampling, it is likely that the porewaters of the sediments do (Bailey 1991). Therefore, the low inshore $\Delta NO_3^-$ concentrations can be attributed to a loss of nitrogen via the process of denitrification. The best correlation between N* and the high-$\delta^{15}N$ nitrate in the subsurface is observed at these stations (Figure 4.6), likely because St Helena Bay monitoring line experiences the lowest oxygen concentrations that are near-permanently sustained (Lamont et al. 2015).

### 4.6. On-shelf nutrient trapping and the importance of hydrographic fronts

Our observations reveal that remineralised nutrients accrue inshore and on the shelf of the SBUS, increasing the nutrient pool that can be upwelled to the surface relative to the source waters offshore. The effective "trapping" of nutrients on the shallow shelf thus effects a positive feedback on shelf fertility. Inshore nutrient trapping in the SBUS has been invoked previously by Tyrell and Lucas (2002). As proposed therein, nutrient trapping occurs as PON

produced by primary production at the surface sinks to the benthos where it is remineralised. The nutrient-deplete surface waters that led to the production of the PON are advected offshore by Ekman transport (Figure 4.7), whereas nutrient-rich deep water from offshore can become further enriched in nutrients as it travels over the continental shelf sediments with their overlying burden of regenerated nutrients before upwelling to the surface.

The spatial distribution of regenerated nutrients (and AOU) on the SBUS shelf provides additional nuance to the potential dynamics promoting nutrient trapping, intimating a role for the incident hydrographic fronts in retaining nutrients inshore and on the mid-shelf. In summer, a distinct bolus of regenerated nutrients appeared to be sequestered inshore of the CF, and another between the CF and the SBF mid-shelf (Figures 4.1-4.3; A-D only). In winter, the larger buildup of regenerated nutrients similarly occurred inshore of the CF at all hydrographic lines, whereas a second pool of regenerated nutrients midshore appeared to extend to the OF, especially along the Kleinsee and St Helena Bay monitoring lines (Figures 4.1-4.3; E-H only), in keeping with the wintertime dissipation of the SBF.

The role of fronts acting as barriers to the transport of biological and chemical properties has been frequently documented in the SBUS. Multiple studies have identified the fronts as boundaries between the shelf and oceanic populations of organisms (Olivar 1987; 1988; Lleonart and Roel 1984; Mas-Riera et al. 1990; Barange et al. 1992). For example, a study conducted by Barange et al. (1992) found that different zooplankton communities inhabit either side of the SBF, and remain separated by this boundary. The SBF has also been documented as a boundary for fish larvae (Olivar 1987; 1988), demersal fish (Lleonart and Roel 1984; Mas-Riera et al. 1990), and phytoplankton communities (Probyn 1985). Barange et al. (1992) concluded that the SBF acts as a boundary to water exchange for three reasons: 1) a strong longshore equatorward jet current is associated with the SBF (Bang and Andrews 1974; Nelson 1989), which 2) gives way to a secondary upwelling at the shelf-break (Hart and Currie 1960), and to 3) downwelling along the inner boundary of the front (Figure 1.8; Hutchings et al. 1986). These observed features of the SBF are characteristic of areas of the Benguela that have a broad shelf and steep slope, namely, the Kleinsee, Namaqualand and St Helena Bay monitoring lines (Hart and Currie 1960; Bang 1971; Nelson and Hutchings 1983; Shannon et al. 1984; Shannon 1985; Barange et al. 1992). Barange et al. (1992) deduced that due to the mechanisms involved in driving this boundary, it should remain present year-round with the movement in the front's position based on the position of the OF (Barange et al. 1992). However, from April to August,

Lamont et al. (2015) observed the presence of the CF only. It is likely that under these conditions, the CF is the feature that separates the inshore and oceanic regions.

Seasonal shifts in the position of prominent fronts may explain the spatial distributions of the regenerated nutrients in the SBUS inter-seasonally. In summer during peak upwelling, the regenerated nutrients in the subsurface were evidently trapped inshore of the CF, and mid-shelf between the CF and SBF. In winter, the offshore propagation of nutrients at the shelf bottom may be due to the dissipation of the SBF. In later winter (i.e., August) when both the SBF and OF were not present, we observed elevated on-shelf AOU and nitrate propagating even further offshore, as far as the CF (Figures 4.8 and 4.9; this is most apparent along the Kleinsee monitoring line). The remineralization signal thus extended further offshore on the shelf throughout winter, in keeping with the dissipation of the SBF, which shifts the frontal boundary westwards and allows inshore waters to be advected further offshore. The prominent fronts on the SBUS shelf may therefore trap the nutrients inshore, allowing them to accrue on-shelf rather than being advected off-shelf.

Interestingly, the total remineralized nutrient burden in the SBUS was greater in winter in summer, implicating a longer residence time of bottom waters on the shelf in winter. Although confined to a narrower depth range above the sediments, depth integrated nutrients were higher in winter than summer. The average depth integrated nitrate concentration at all on-shelf stations in summer was 960 $\pm$ 788 mmol $m^{-2}$, while in winter it increased to 1160 $\pm$ 1270 mmol $m^{-2}$. The average depth integrated silicic acid and phosphate concentrations also increased from summer to winter, with concentrations of 1980 $\pm$ 614 mmol $m^{-2}$ and 76 $\pm$ 30 mmol $m^{-2}$ in summer and 2760 $\pm$ 1760 mmol $m^{-2}$ and 130 $\pm$ 100 mmol $m^{-2}$ in winter, respectively. Considering the greater aerial extent of the bolus of subsurface regenerated nutrients in winter combined with the higher depth integrated nutrient concentrations, the regenerated nutrient inventory was substantially larger during this season. That there is less net primary production in the SBUS in winter, evidenced by measured rates that are 1.5-2.4 times lower than in summer (Brown 1984; Barlow et al. 2009; Lamont et al. 2014; Flynn et al. 2018), suggests significant differences in the residence time of bottom waters between the two seasons. This is explained in part by greater recharge of bottom waters in summer due to more intense on-shore upwelling. Nonetheless, the rate at which the production and remineralization of sinking PON adds regenerated nutrients to the on-shelf subsurface must exceed the rate of upwelling in summer

in order that the upwelling of SAMW does not erase the elevated $\Delta NO_3^-$, $\Delta Si(OH)_4$ and $\Delta PO_4^{3-}$ concentrations.

The role of regenerated nutrients on the shallow shelf of the SBUS in increasing its fertility has been recognized previously (Bailey 1991; Waldron et al. 1992). The increased primary productivity of the BUS relative to the other major upwelling regions is explained by higher surface nutrient concentrations and the broad continental shelf (~200 km wide along the Kleinsee and Namaqualand monitoring lines; Patti et al. 2008; Lachkar and Gruber 2012). Surface nutrient concentrations are higher than in other upwelling regions because the BUS experiences high rates of nutrient trapping (Bailey 1991). Furthermore, the broader continental shelf increases the aerial extent over which this nutrient trapping can occur because it provides an increased opportunity for PON to sink to the benthos. On narrower continental shelves, such as those of the Canary and California upwelling systems, fewer nutrients are trapped on the shelf as PON is often advected offshore and lost to the open ocean (Patti et al. 2007; Lachkar and Gruber 2012). Similar loss processes are likely occurring along the Scarborough monitoring line where lower concentrations of AOU and regenerated nutrients were observed (Figures 3.7, 4.1-4.3, 4.8 and 4.9). Nutrient trapping therefore enhances the primary productivity of the SBUS, particularly in areas characterized by a broad continental shelf.

### 4.7. Implications of nutrient trapping for on-shelf oxygen conditions

Lower oxygen concentrations and elevated AOU were observed in the SBUS shelf bottom waters in both late summer and early winter. Hypoxic events are frequently observed in the SBUS, and in some instances have caused mass mortalities of commercially important species (Cockcroft 2001; Pitcher and Probyn 2011). St Helena Bay is the most extensively sampled region of the SBUS as it is an important nursery ground for various commercial fish species, such as anchovy and sardine (Cockcroft 2001; van der Lingen et al. 2006). This has, however, resulted in a deficit of data regarding the extent of hypoxia and its effects on marine organisms in the rest of the SBUS.

Early work indicated that hypoxic events are driven by the entrainment of low oxygen waters into the SBUS from either the NBUS (De Decker 1970) or from the low oxygen waters of South Atlantic Central Water (Stander 1964) via a poleward undercurrent. More recent work, however, has established that the low oxygen bottom waters observed throughout the SBUS

are not due to the entrainment of low oxygen water, but instead derive from physical processes such as stratification, retention and advection, and biogeochemical processes (Bailey 1979; Bailey et al. 1985; Monteiro and van der Plas 2006). Specifically, low oxygen bottom waters evolve *in situ* due to the decay of large phytoplankton blooms at the inshore and midshore, throughout the SBUS, during the upwelling season (Pitcher and Probyn 2011). The organic matter delivery to the sediments and its subsequent remineralization depletes bottom water oxygen (Bailey 1987; Bailey and Chapman 1985), with persistent hypoxia observed in the inshore bottom waters along the St Helena Bay monitoring line (Monteiro and van der Plas 2006; Lamont et al. 2015).

Low oxygen concentrations persist at bottom depths year-round along the St Helena Bay monitoring line, particularly inshore of the CF (Jarre et al. 2015; Lamont et al. 2015). Shelf bottom waters are most oxygenated following the onset of seasonal upwelling in late winter, when oxygen-replete SAMW is entrained shoreward (Monteiro and van der Plas 2006; Duncombe Rae 2005; Pitcher et al. 2014; Lamont et al. 2015). This is apparent in our dataset, with the highest concentrations of AOU observed inshore of the CF in late summer and the lowest values in late winter (i.e., August) (Figures 3.7 and 4.8). Through spring and summer, oxygen concentrations progressively decrease in the bottom waters overlying the shelf during the period of intense upwelling, decreasing further through to autumn following the cessation of intense upwelling (Jarre et al. 2015, Lamont et al. 2015; Figure 3.7), with hypoxic conditions becoming most severe in autumn. In the winter, as the hydrographic fronts dissipate, MUW at the surface becomes contiguous shelf-wide, and occupies a larger depth range, oxygenating the surface to ~100 m depth, whereas bottom water oxygen concentrations remain depleted until recharge in late winter at the onset of upwelling (Lamont et al. 2015; Figure 4.8).

Inshore along the St Helena Bay monitoring line (Lamont et al. 2015), the persistently low oxygen conditions are maintained by the cyclonic circulation in St Helena Bay and by a strongly stratified two-layer water column that is set-up by the cold upwelling waters overlain by warm surface waters (Pitcher and Nelson 2006). The subsequent remineralization of PON supplied from the surface (Bailey 1991), coupled with the strongly stratified water column, leads to the depletion of oxygen in the bottom waters (Bailey and Chapman 1991; Monteiro and van der Plas 2006). At the most inshore stations, winter mixing ventilates the bottom waters to 50 m, whereas bottom waters at deeper inshore stations are not ventilated during these events.

The propensity of subsurface waters to become severely hypoxic, particularly inshore of the CF, may result in part from the accumulated pool of remineralised nutrients in bottom waters that are upwelled to the surface. The greater the proportion of nutrients trapped, the more primary production that will be fueled in the subsequent upwelling (i.e., the nutrients trapped on-shelf condition the surface waters). A greater organic matter export flux, due to the increase in primary production, will result in proportionally greater oxygen consumption in bottom waters. Such a positive feedback would likely be modulated by physical and associated biogeochemical dynamics of the upwelling, including 1) the intensity of upwelling, 2) the degree of nutrient consumption and efficiency of organic matter export with respect to the position of fronts, and 3) the position of the fronts relative to the coast and shelf bathymetry.

To a first approximation, increased upwelling increases the nutrient flux into the euphotic zone, supporting higher rates of primary production and export, thus increasing the concentration of remineralised nutrients at the shelf bottom, and coincident AOU. This scenario, however, is nuanced by the consideration that faster upwelling leads to a shorter residence time of bottom waters, thus leaving less time for them to accrue remineralised nutrients and AOU. Nevertheless, repeated cycles of upwelling and remineralization will ultimately result in the successive trapping of nutrients, increasing the remineralised nutrient pool throughout the upwelling season – eventually, the organic material generated from the consumption of the upwelled nutrients will exceed the oxygen available for remineralization at the subsurface. However, given relatively rapid upwelling, the phytoplankton may not have sufficient time to utilize all surface nutrients prior to the subduction of the Ekman layer at the hydrographic fronts (e.g, here (Figures 3.11 and 3.12) Lachkar and Gruber 2011, and Evans et al. 2015). In this respect, the CF and the SBF have been observed to merge during prolonged intense upwelling (Nelson and Hutchings 1983; Shannon and Nelson 1996; Shannon 1985). The merging of the fronts likely increases the residence time of surface waters as inshore waters are advected further offshore rather than being subducted below the CF (Andrews and Hutchings 1980). The increased surface water residence time in turn, allow for more primary production and consequent remineralization at the shelf bottom. However, sinking particles may be remineralised over a greater aerial extent of the shelf, moderating the oxygen drawdown. Indeed, Jarre et al. (2015) observed a parabolic relationship between upwelling strength and the *areal extent* of oxygen depleted waters on the shelf in summer and autumn throughout the

SBUS, which could be explained by this. Whether upwelling intensity is related to more severe hypoxia inshore, however, it is unclear.

Thus, the position of the fronts relative to the upwelling center and to the intensity of upwelling may modulate the severity of shelf hypoxia. Conditions that promote high nutrient utilization and the subsequent export of organic material inshore of the CF will ostensibly result in severe hypoxia in this region. This is due to the smaller volume of water in which PON will be remineralised, relative to if the CF was further offshore. This smaller volume contains less oxygen available the breakdown of the PON, such that oxygen is depleted more rapidly (Bailey 1991).

Finally, shelf bathymetry is also an important factor influencing the propensity for seasonal hypoxia. The proportion of nutrients remineralised *in situ* among the monitoring lines appears to be correlated with the shelf surface area. The Kleinsee monitoring line has the broadest expanse of shallow continental shelf and showed both the highest concentrations of remineralised nutrients and the greatest spatial extent of elevated AOU in both summer and winter. In contrast, the Scarborough monitoring line, which has a narrow shelf and steep slope, had little evidence of *in situ* remineralised nutrients (Figures 4.1-4.3). This dynamic can be explained by the higher probability that PON from surface primary production will be retained along the shallower Kleinsee monitoring line, versus the propensity for more water column remineralization and PON export off-shelf along the Scarborough monitoring line, notwithstanding the potential differences in residence time of mid-shelf water at the Scarborough monitoring line (Hardman-Mountford et al. 2003). In this respect, shallow broad continental shelves are known to enhance nutrients from benthic-pelagic coupling and experience increased hypoxia in on-shelf bottom waters (Rowe et al. 1975; Bailey 1991; Tyrell and Lucas 2002).

The intensity of coastal upwelling is predicted to increase globally with climate change (Bakun 1990; Sydeman 2014). An increase in upwelling intensity could potentially enhance nutrient trapping and consequent shelf hypoxia. However, nutrient trapping is reliant on various overlapping conditions. The challenge moving forward will be to define the co-incidence of conditions that influence shelf oxygenation.

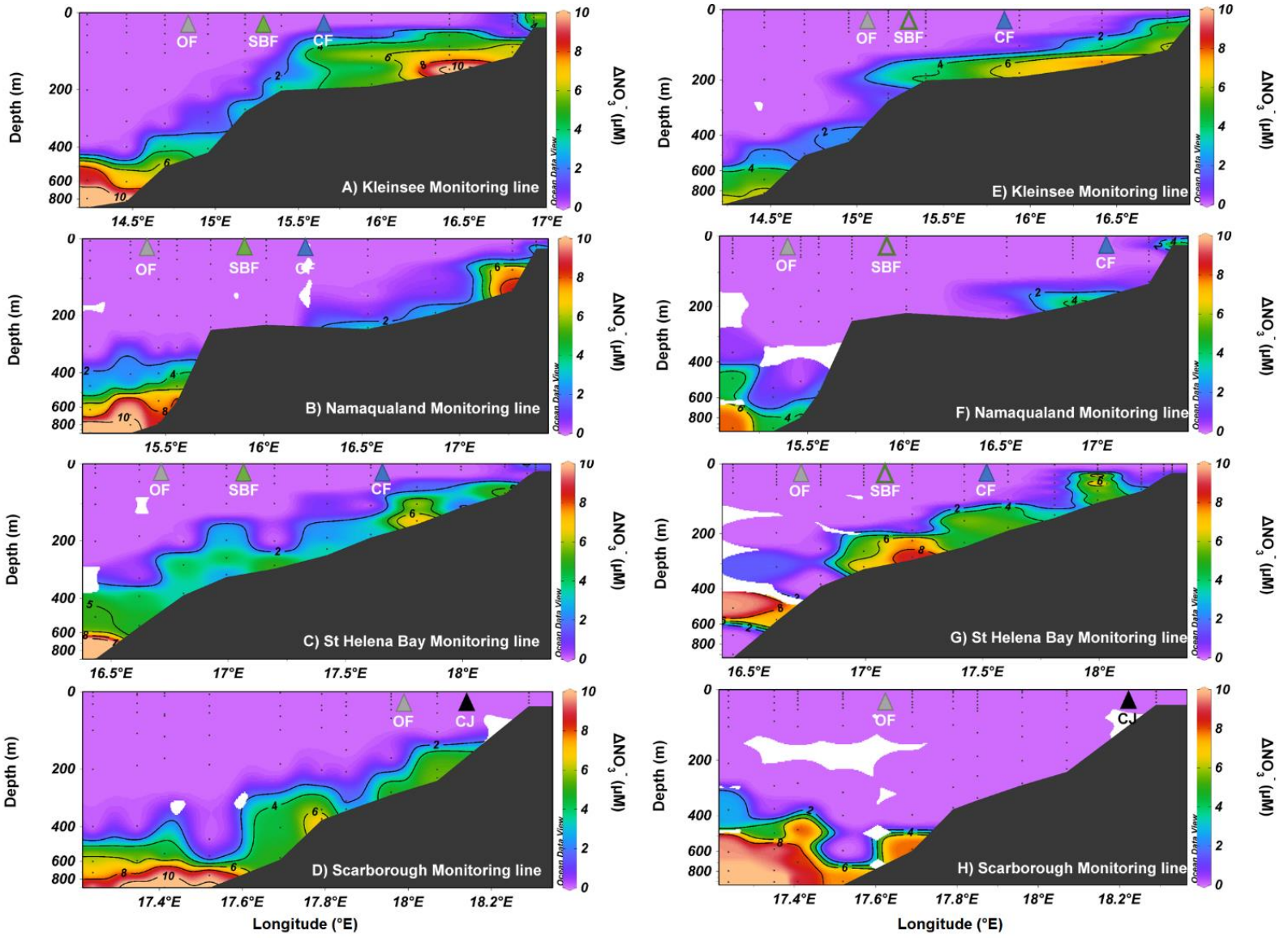


**Figure 4.1** Section plots of $\Delta NO_3^-$ (colours and contours) for **summer** (A-D) and **winter** (E-H) along (from north to south) A and E) Kleinsee monitoring line, B and F) Namaqualand monitoring line, C and G) St Helena Bay monitoring line and D and H) Scarborough monitoring line. Note the changes in longitudinal scale between panels. The position of the fronts identified in Figure 3.1 are shown on each figure. The black dots show the position of the stations and the depths at which discrete nutrient samples were collected along each monitoring line. $\Delta NO_3^-$ is calculated as $[NO_3^-]_{measured} - [NO_3^-]_{SAMW}$. Note the changes in longitudinal scale between panels.

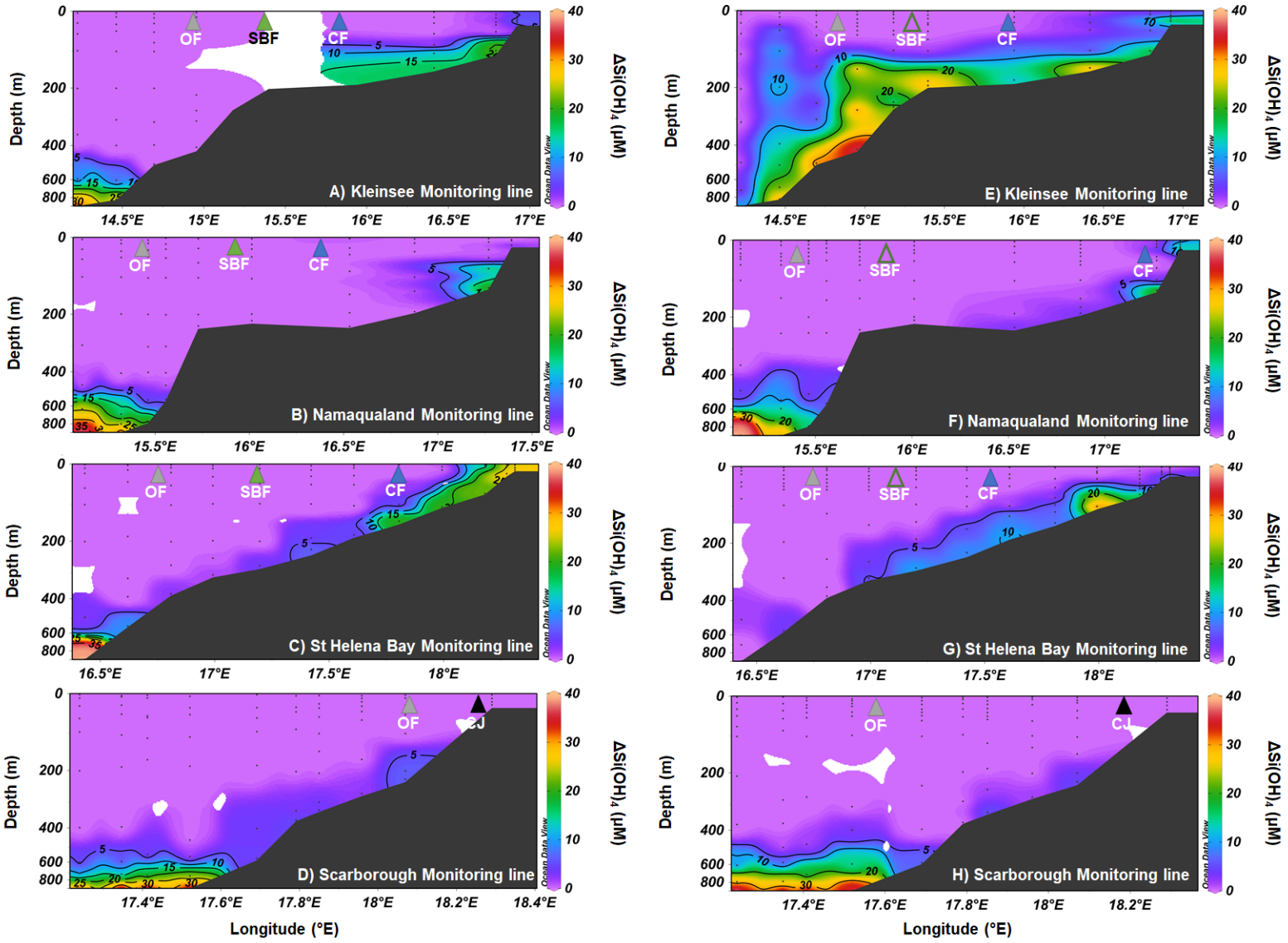


**Figure 4.2** Section plots of $\Delta Si(OH)_4$ (colours and contours) for **summer** (A-D) and **winter** (E-H) along (from north to south) A and E) Kleinsee monitoring line, B and F) Namaqualand monitoring line, C and G) St Helena Bay monitoring line and D and H) Scarborough monitoring line. Note the changes in longitudinal scale between panels. The position of the fronts identified in Figure 3.1 are shown on each figure. The black dots show the position of the stations and the depths at which discrete nutrient samples were collected along each monitoring line. $\Delta Si(OH)_4$ is calculated as $[\Delta Si(OH)_4]_{measured} - [\Delta Si(OH)_4]_{SAMW}$. Note the changes in longitudinal scale between panels.

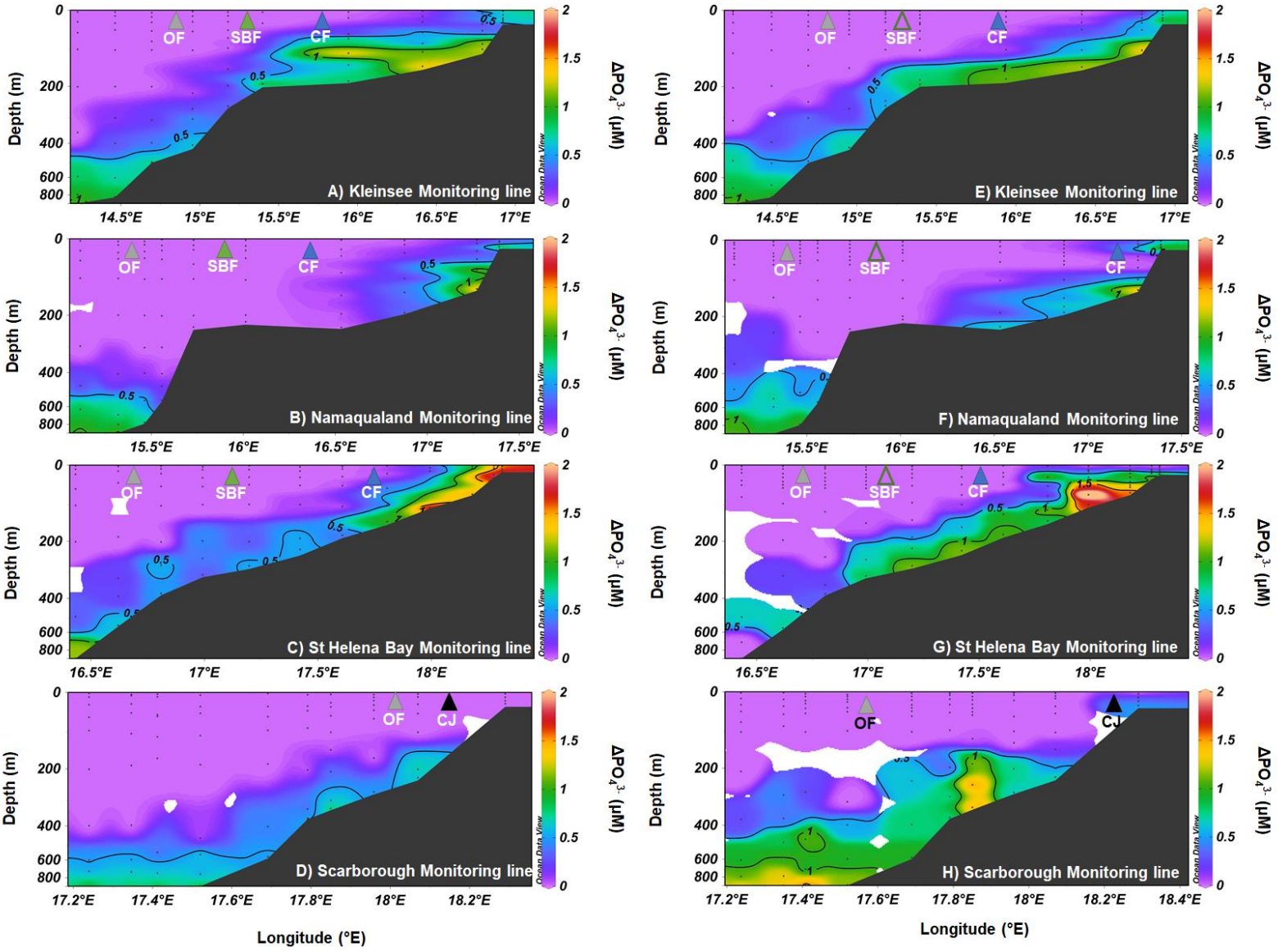


**Figure 4.3** Section plots of $\Delta PO_4^{3-}$ (colours and contours) for **summer** (A-D) and **winter** (E-H) along (from north to south) A and E) Kleinsee monitoring line, B and F) Namaqualand monitoring line, C and G) St Helena Bay monitoring line and D and H) Scarborough monitoring line. Note the changes in longitudinal scale between panels. The position of the fronts identified in Figure 3.1 are shown on each figure. The black dots show the position of the stations and the depths at which discrete nutrient samples were collected along each monitoring line. $\Delta PO_4^{3-}$ is calculated as $[\Delta PO_4^{3-}]_{measured} - [\Delta PO_4^{3-}]_{SAMW}$. Note the changes in longitudinal scale between panels.

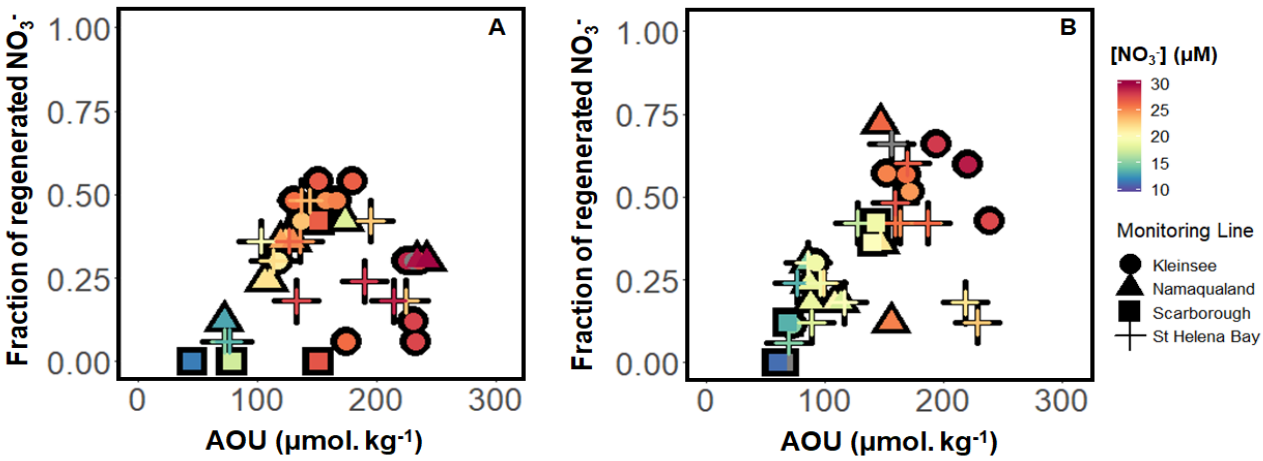


**Figure 4.4** The fraction of regenerated nitrate (from nitrate $\delta^{18}O$) vs. AOU between 50-300 m in A) summer and B) winter 2017 at all the on-shelf stations. The symbol shapes represent the various monitoring lines and the colours indicate the *in situ* $[NO_3^-]$.

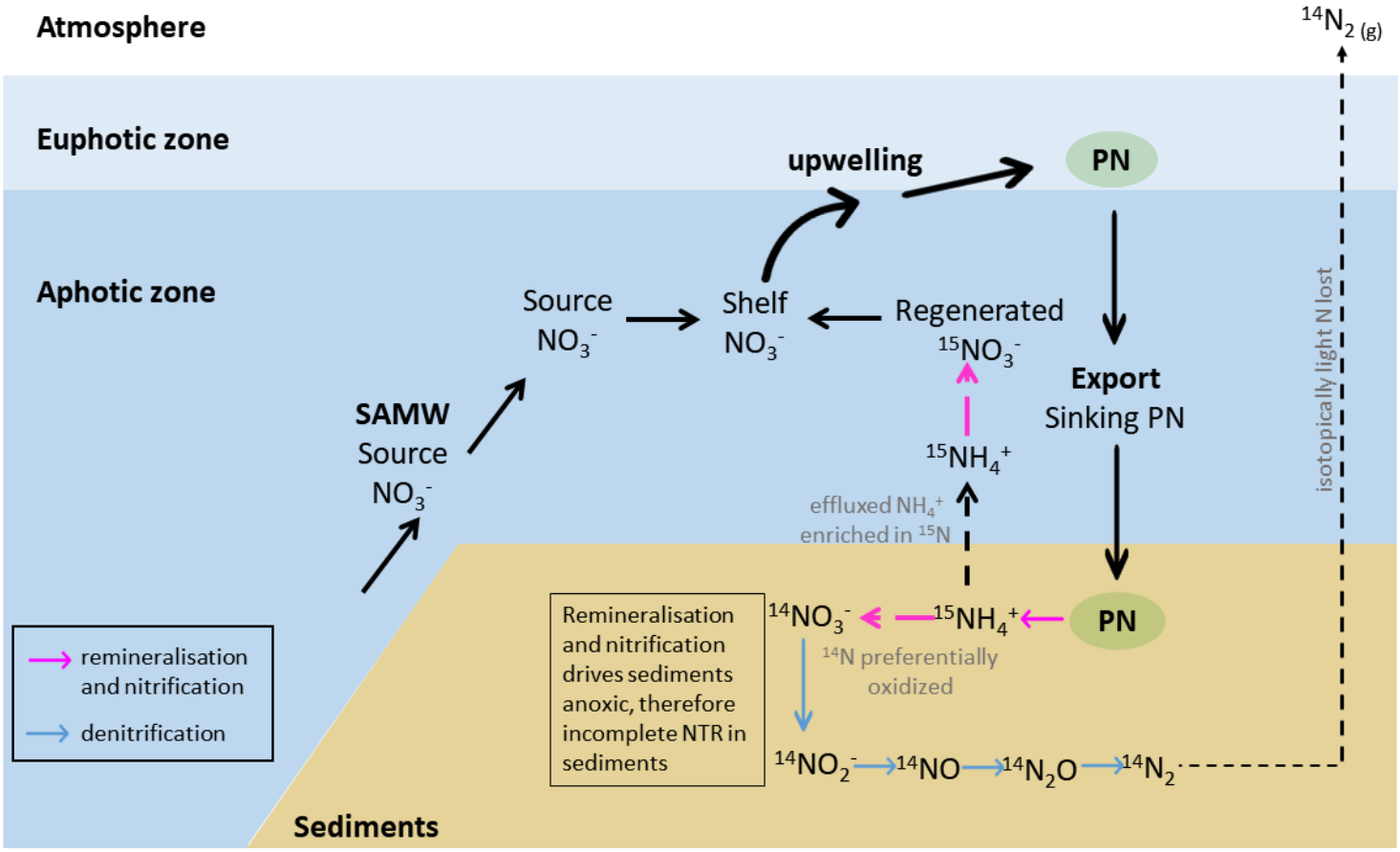


**Figure 4.5** A schematic of the $NO_3^-$ sources and sinks in the SBUS. The black arrows represent physical dynamics, while the coloured arrows represent various biological processes. Note that

the $NO_3^-$ that is upwelled into the euphotic zone is a mixture of SAMW and on-shelf regenerated $NO_3^-$. The branching isotope effect is identified, whereby low $^{14}NH_4^+$ is initially nitrified in the sediments, enriching the $\delta^{15}N$ of the $NH_4^+$ pool. Upon the depletion of oxygen in the sediments, the isotopically-heavy $NH_4^+$ is effluxed (i.e., it is not completely nitrified in the sediments). In the water column, the $NH_4^+$ is nitrified, producing $NO_3^-$ with a $\delta^{15}N$ above that of SAMW. In the oxygen-deplete sediments, some portion of the newly nitrified $NO_3^-$ is reduced to $N_2$ as denitrifiers are the second-most efficient energy-extractors after nitrifiers (Knowles 1982). This $N_2$ is ultimately lost from the system, representing a sink for low-$\delta^{15}N$ nitrogen.

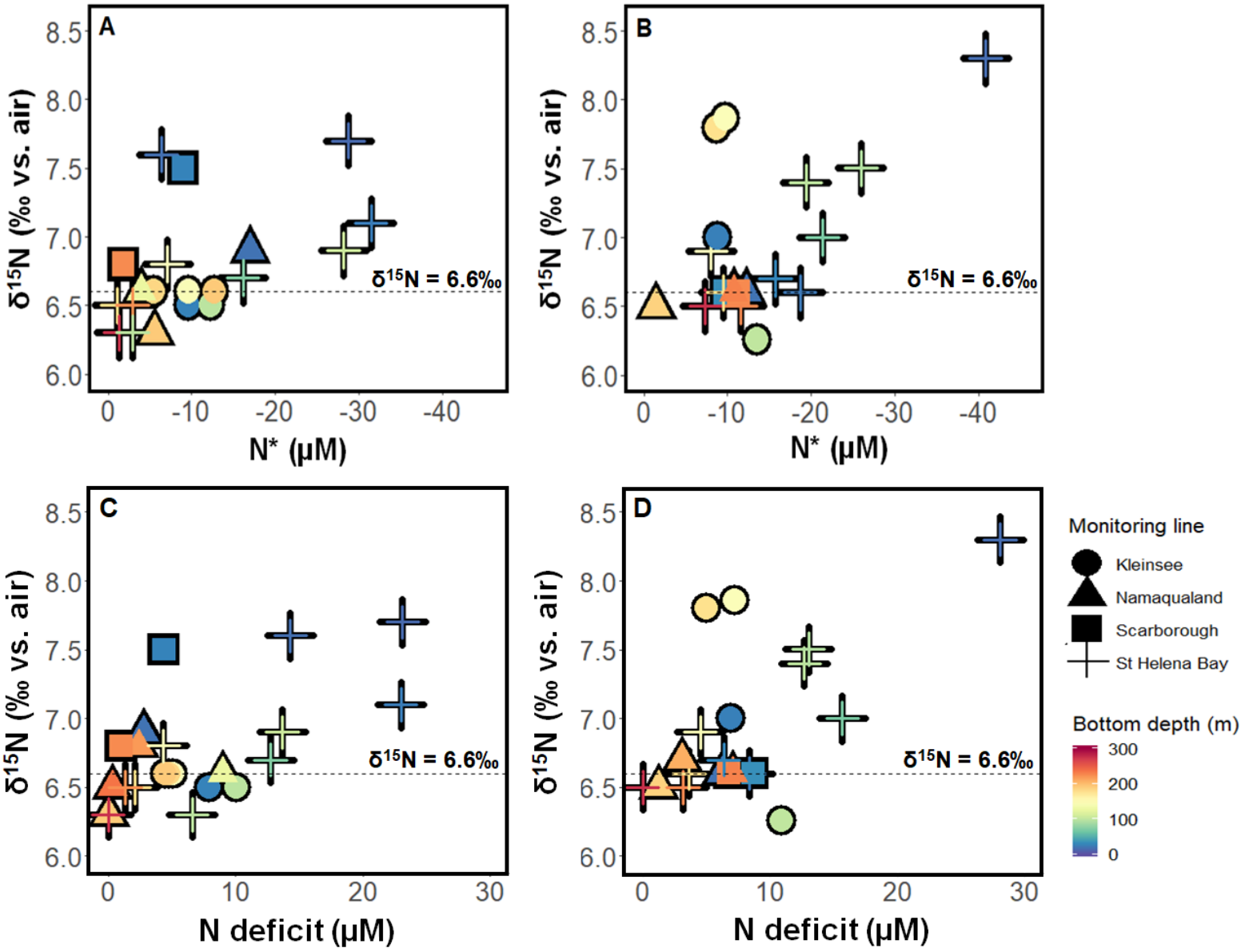


**Figure 4.6** Bottom depth values only for N* (A-B) and N deficit (C-D) vs. the $\delta^{15}N$ of nitrate for all inshore and midshore stations during A and C) summer and B and D) winter. The dotted line indicates the $\delta^{15}N$ of SAMW (6.6‰), while the colours represent the bottom depth.

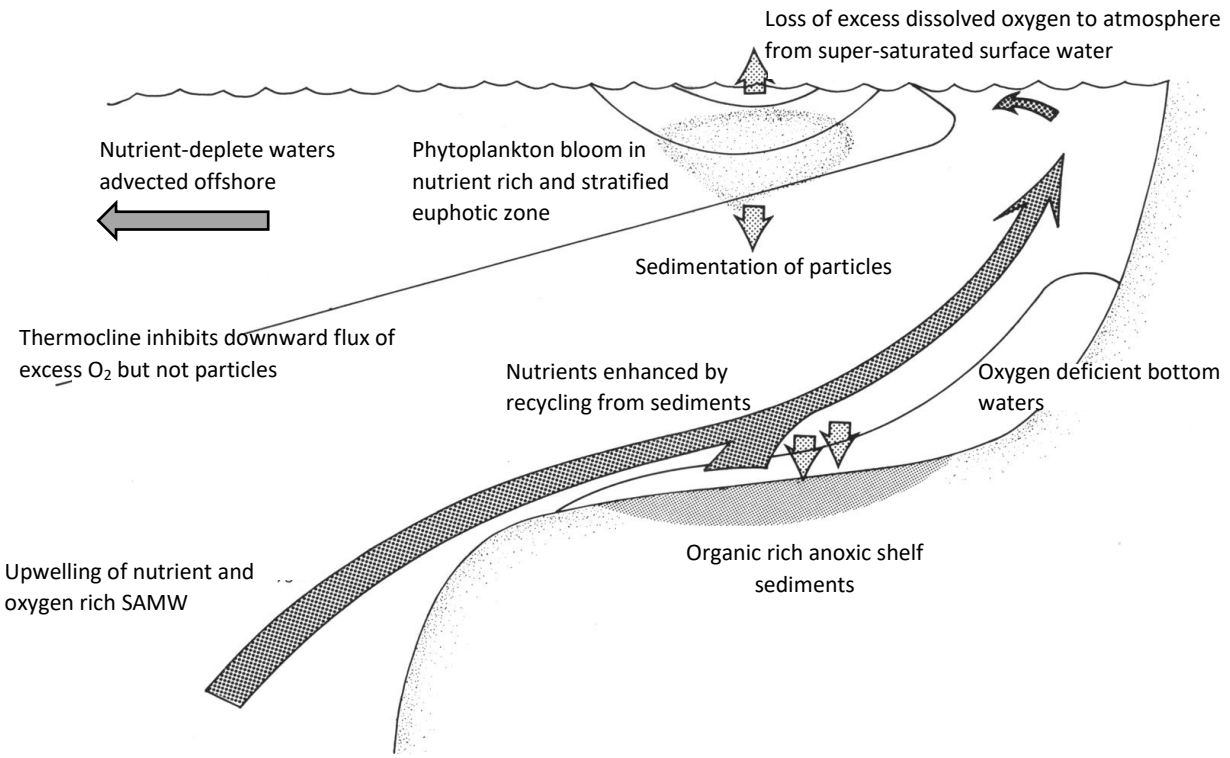


**Figure 4.7** Schematic of benthic-pelagic coupling between organic-rich sediments of the mid-shelf and the stratified euphotic zone [Figure adapted from Bailey 1991].

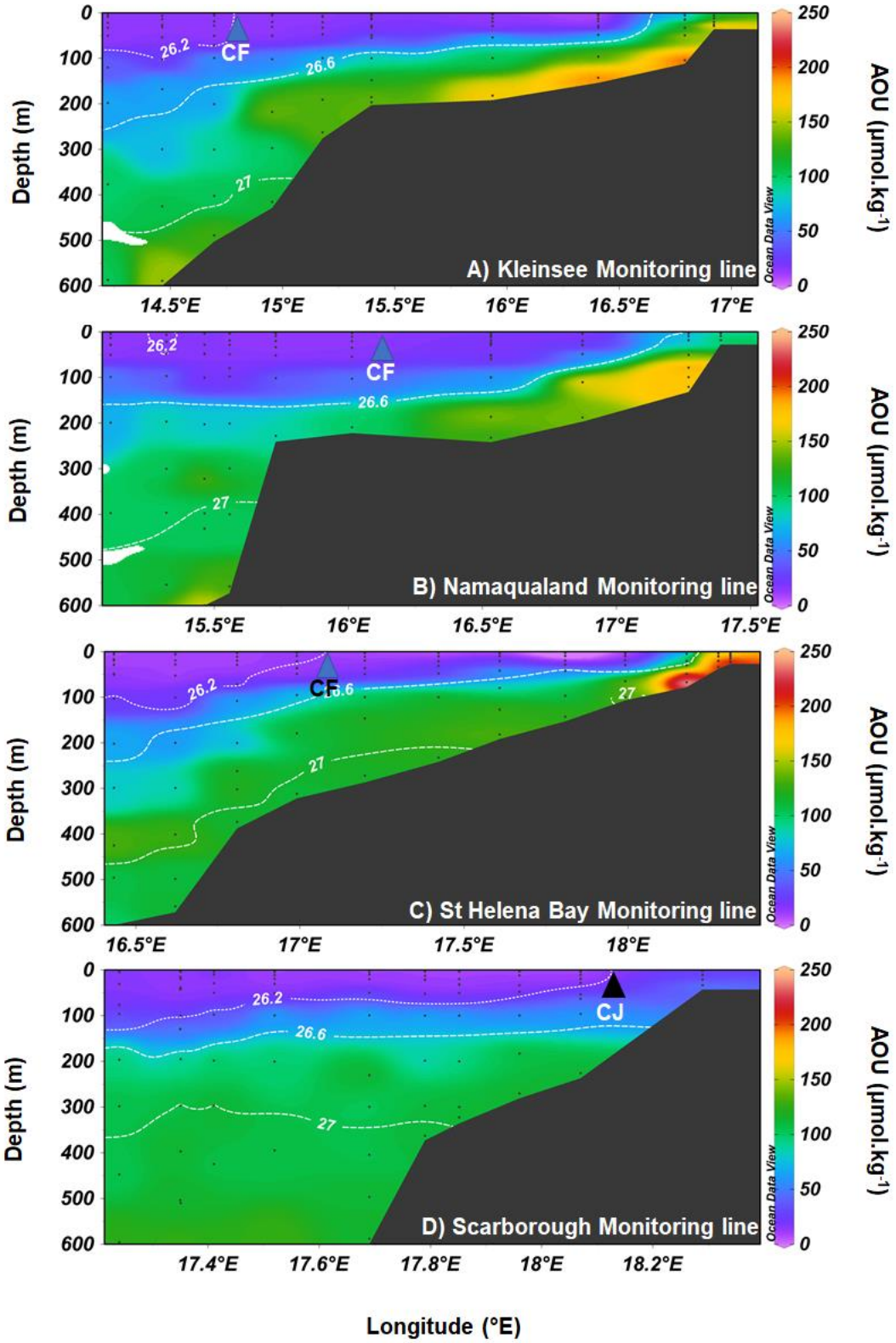


**Figure 4.8** Section plots of apparent oxygen utilisation, AOU (µmol.kg$^{-1}$), during **August** 2017 along (from north to south) A) Kleinsee monitoring line, B) Namaqualand monitoring line, C) St Helena Bay monitoring line and D) Scarborough monitoring line The fronts identified in the SBUS during this season are the Columbine Front (CF; blue triangle) and Cape Jet (CJ; black triangle). The density contours denote the water masses identified in Figure 3.2. The black dots show the position of the stations along each monitoring line. Note the changes in longitudinal scale between panels.

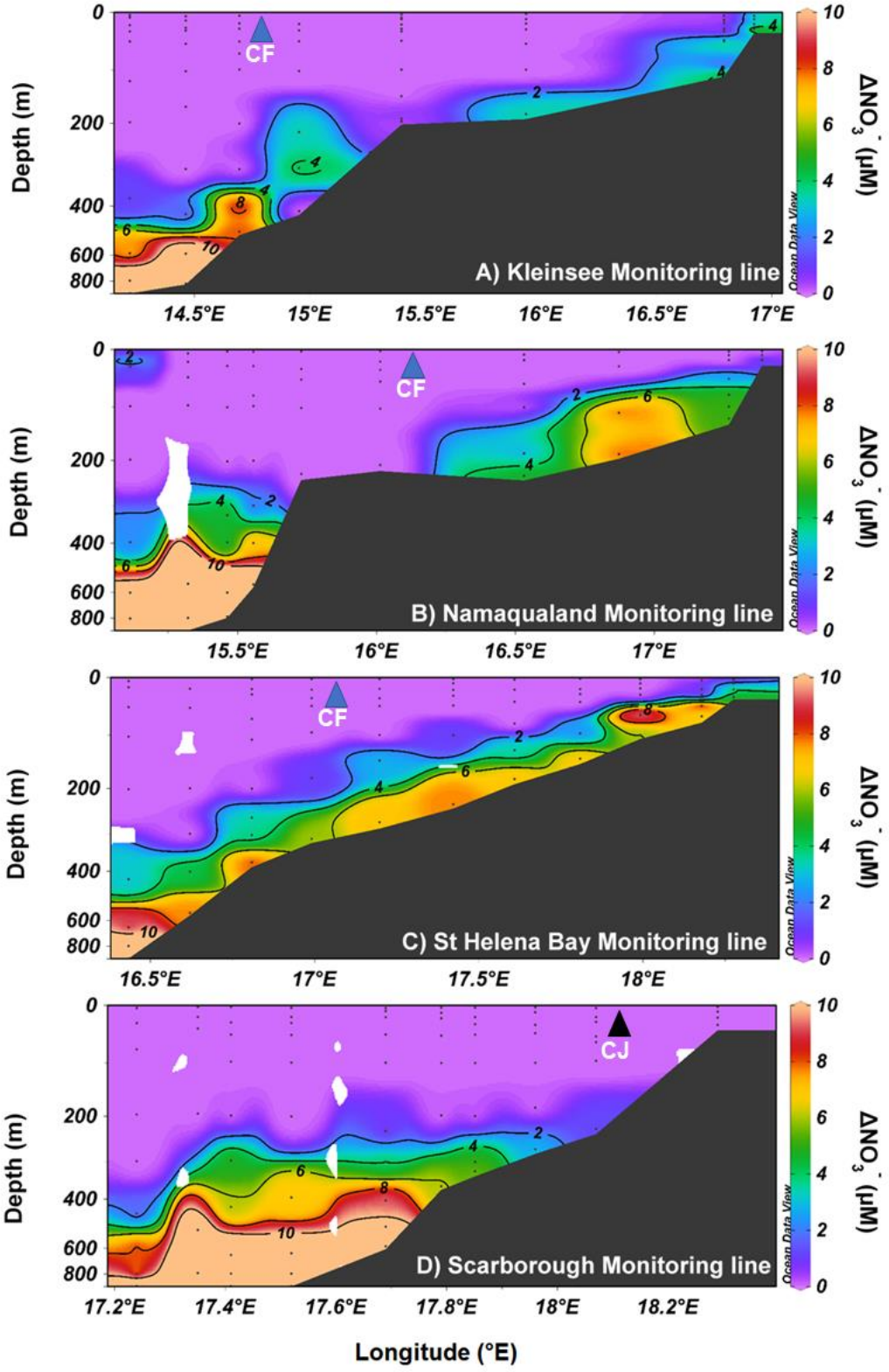


**Figure 4.9** Section plots of $\Delta NO_3^-$ during **August** 2017 along (from north to south) A) Kleinsee monitoring line, B) Namaqualand monitoring line, C) St Helena Bay monitoring line and E) Scarborough monitoring line. The fronts present in the system in August 2017 are identified as in Figure 4.8. The black dots show the position of the stations along each monitoring line. $\Delta NO_3^-$ is calculated as ($[NO_3^-]$-[SAMW $NO_3^-$]). Note the changes in longitude between panels.

## 5. Conclusions and future directions

Measurements of nutrient and oxygen concentrations, physical properties of the water column, and the dual isotopes of nitrate along four monitoring lines in the SBUS during summer and winter reveal that on-shelf nutrient trapping is a persistent feature of this region, likely explaining its exceptionally high fertility. While nutrient trapping is evident in both summer and winter, there are important seasonal differences. In winter, the SBUS hosts significant rates of nutrient regeneration on the shelf, while in summer there is higher entrainment of deep water due to upwelling, which erodes some of the on-shelf remineralization signal and at least partially "resets" the biogeochemistry of the system. However, the on-shelf regenerated nutrient pool is not erased by summertime upwelling, suggesting that the rate of organic matter export and remineralization in summer exceeds the rate of upwelling of SAMW. As the winter season progresses, the concentration of regenerated nutrients remains elevated on the shelf, even increasing from early to late winter in regions where the continental shelf is broad and shallow. The increase in the nutrient burden throughout the winter is likely due to the westward shift of the CF and the dissipation of the SBF and the OF, which increases the residence time of the on-shelf waters. The accrual of on-shelf regenerated nutrients during winter may pre-condition the following summer. This is because a greater proportion of nutrients regenerated during winter amounts to an increase in the nutrients available to support photosynthesis in the subsequent upwelling season. The on-shelf regenerated nutrients therefore enhance the fertility of the SBUS above that expected if offshore SAMW and SASTMW were the sole nutrient sources to the euphotic zone. The intensity of on-shelf nutrient regeneration also has implications for bottom water oxygen concentrations, with more nutrient trapping in winter potentially leading to more extreme hypoxia following the subsequent upwelling season.

Using nitrate $\delta^{18}O$, the proportion of nitrate regenerated *in situ* can be quantified, with approximately 5% more nitrate regenerated on-shelf in winter than in summer. This is, however, an underestimate due to the fact that some portion of the on-shelf nitrate is lost from the system by denitrification, which occurs in the sediments and possibly sometimes even in the water column. The oxygen-deplete conditions observed on-shelf that favour denitrification are driven by the remineralisation of PON. As outlined above, on-shelf nutrient trapping has been implicated in oxygen depletion in inshore and midshore bottom waters, with implications for the success of commercially important marine species in the SBUS. Using the proportion

of regenerated nutrients that have accrued on-shelf throughout the winter, coupled with information about the physical character of the SBUS (e.g., frontal positions, upwelling intensity), future studies may be able to predict the extent of hypoxia that is likely to occur following the subsequent upwelling season. This will ultimately require both *in situ* observations and a numerical model developed to investigate the interplay between the physical and biogeochemical dynamics of the SBUS.

## 6. Appendices

### Appendix A: Oxygen concentrations

The inshore St Helena Bay monitoring line stations were characterised by the lowest observed oxygen concentrations in the SBUS during summer and winter (Figure A1). Low oxygen concentrations were not restricted to the St Helena Bay monitoring line, however, during the summer, hypoxic waters, defined by $[O_2] \leq 60$ µmol.kg$^{-1}$ (Deuser 1975; Bailey et al. 1985), were also evident at the inshore stations of the Kleinsee and Namaqualand monitoring lines (Figure A1A and B). In the winter, hypoxic waters were only observed at the inshore stations along the St Helena Bay monitoring line (Figure A1G). At the time of sampling, it appears that no anoxic waters were present in the SBUS, with anoxia being defined as $[O_2] \leq 9$ µmol.kg$^{-1}$ (Demaison and Moore 1980).

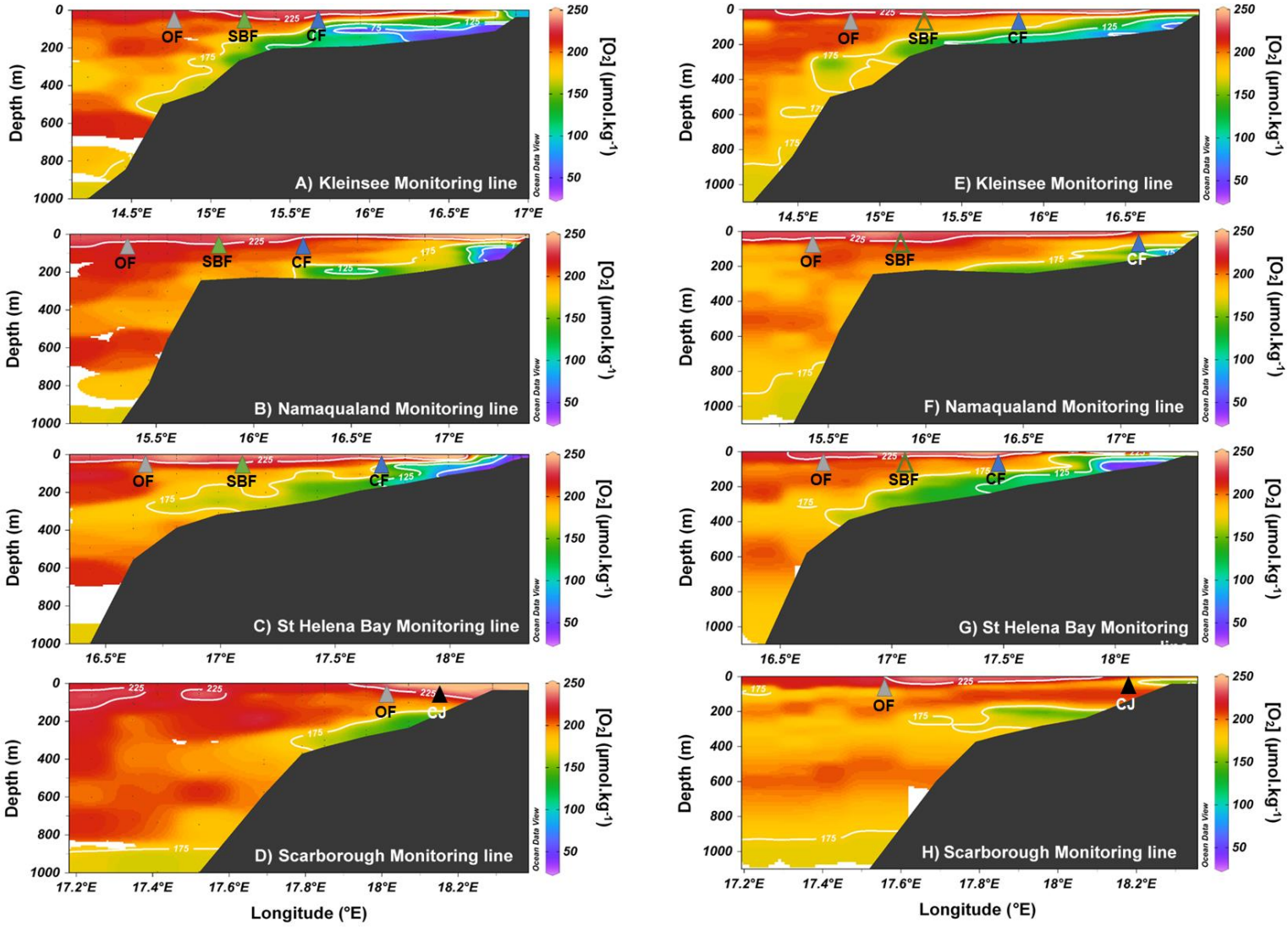


**Figure A1.** Section plots of oxygen concentration, $[O_2]$ (µM), for **summer** (A-D) and **winter** (E-H) for (from north to south) A and E) Kleinsee monitoring line, B and F) Namaqualand

monitoring line, C and G) St Helena Bay monitoring line and D and H) Scarborough monitoring line. The positions of the fronts identified in Figure 3.1 are shown on each figure. Note the changes in latitudinal scale between panels.

## Appendix B: Depth profiles of nitrate $\delta^{15}N$ and $\delta^{18}O$

Figures B1-B4 show depth profiles of nitrate $\delta^{15}N$ and $\delta^{18}O$ for the inshore, midshore, offshore and oceanic stations in summer and winter 2017. Nitrate $\delta^{15}N$ and $\delta^{18}O$ increased from depth (50-150 m, depending on the station) into the surface, with the highest values observed in the mixed layer. At the offshore and oceanic stations between 200-600 m, depending on the monitoring line, the $\delta^{15}N$ and $\delta^{18}O$ of nitrate tended towards the SAMW end-member values of 6.6‰ and 3.1‰, respectively. This is best observed in Figures B3 and B4.

The inshore stations followed similar trends in summer and winter, with the lowest nitrate $\delta^{15}N$ and $\delta^{18}O$ observed at the most inshore station, with values increasing towards the CF (Figure 3.10). At the midshore stations, there is an apparent seasonal difference in nitrate $\delta^{15}N$ and $\delta^{18}O$. Figure B2 shows higher surface values in winter compared to summer; with average surface values of 8‰ and 6‰ during summer and 12.5‰ and 7.5‰ during winter for nitrate $\delta^{15}N$ and $\delta^{18}O$, respectively. A similar trend was observed at the offshore and oceanic stations.

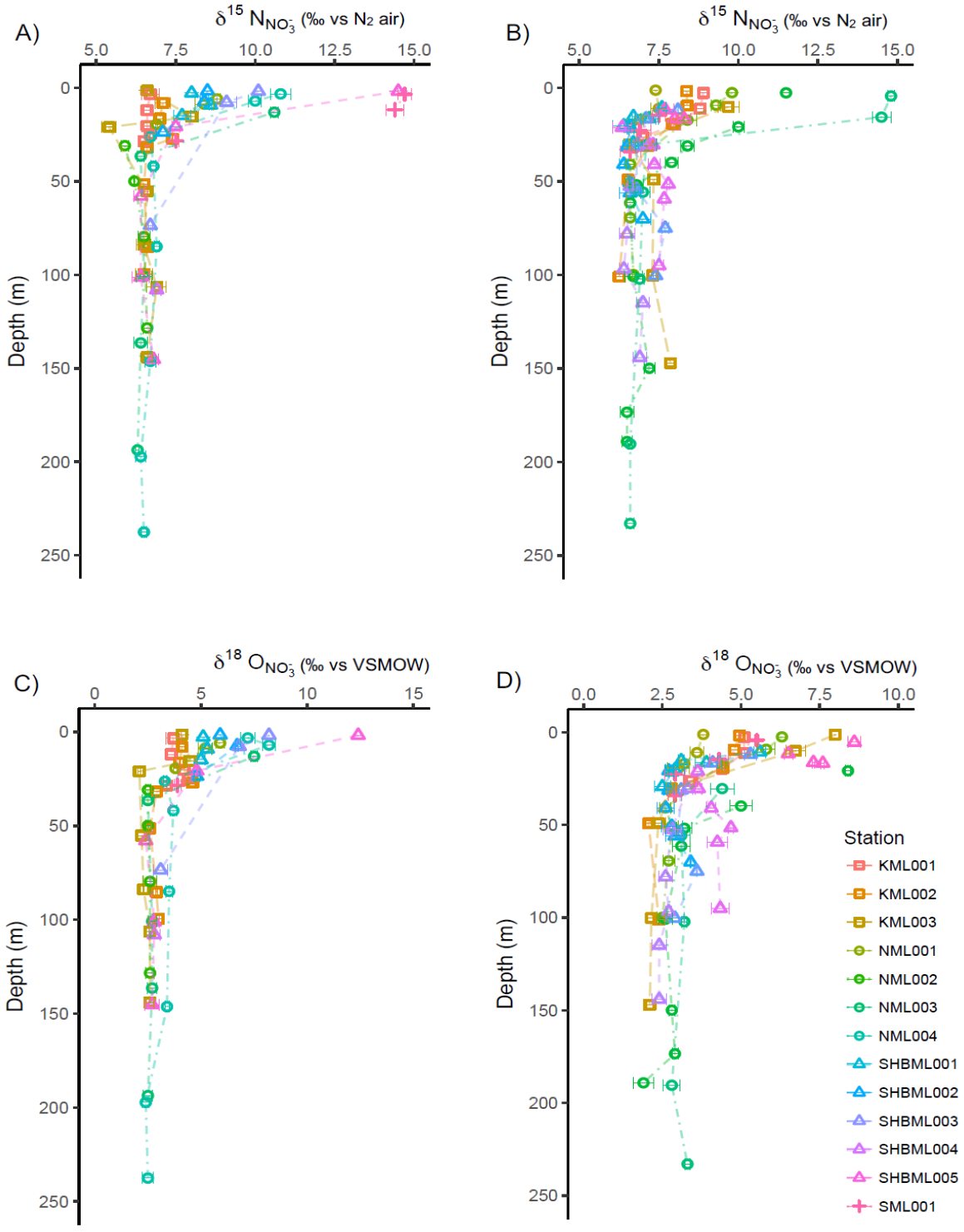


**Figure B1.** Depth profiles of A) $\delta^{15}N_{NO3}$ for summer, B) $\delta^{15}N_{NO3}$ for winter, C) $\delta^{18}O_{NO3}$ for summer and D) $\delta^{18}O_{NO3}$ for winter at the **inshore stations for all four monitoring lines**. Data shown are the nitrite-removed values (down to 250 m, below which nitrite concentration ~0 µM). Note the changes in the x-axis scale between the panels. The error bars indicate the measurement standard deviation ($n \geq 3$).

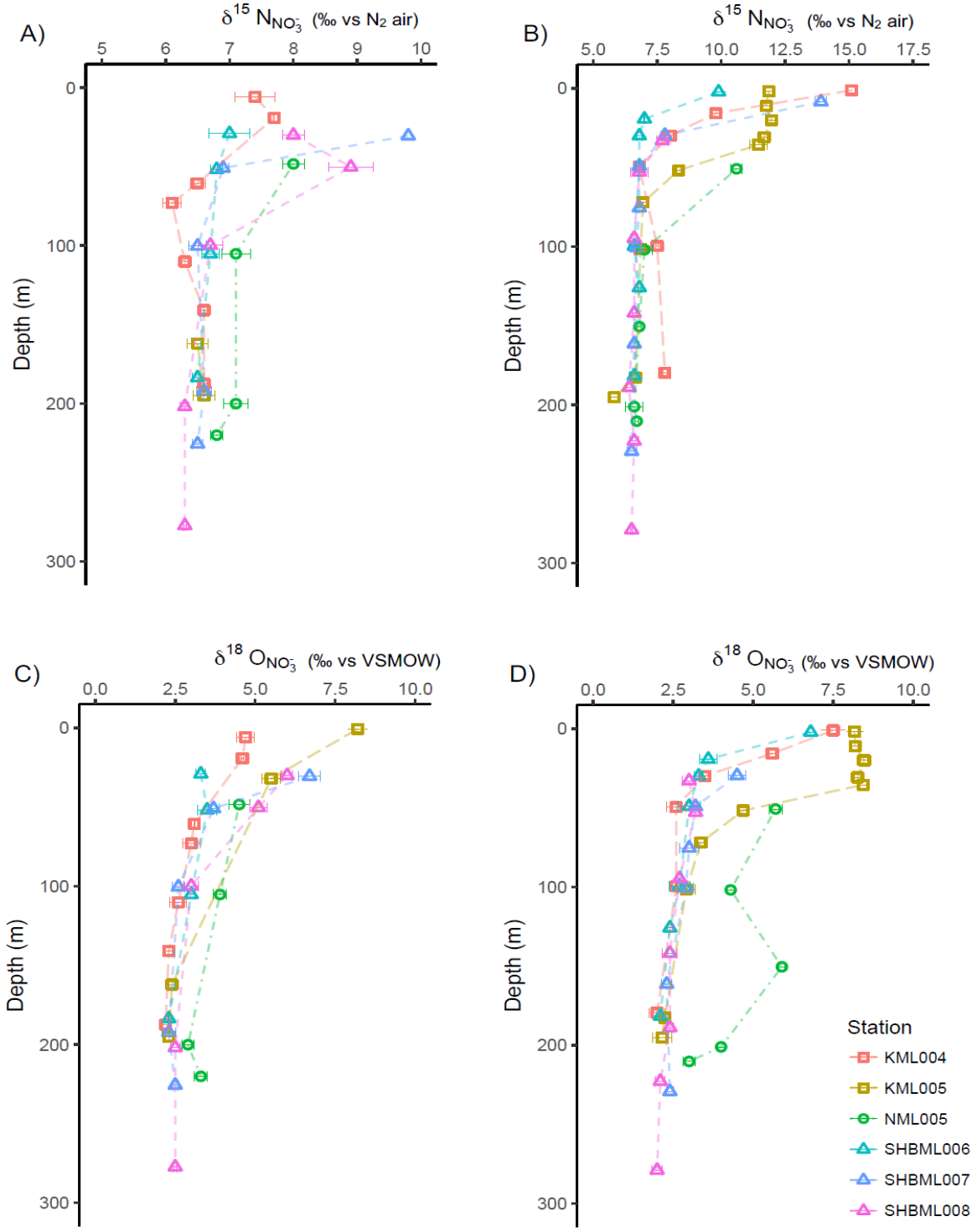


**Figure B2.** Depth profiles of A) $\delta^{15}N_{NO3}$ for summer, B) $\delta^{15}N_{NO3}$ for winter, C) $\delta^{18}O_{NO3}$ for summer and D) $\delta^{18}O_{NO3}$ for winter at the **midshore stations for all four monitoring lines**. Data shown are the nitrite-removed values (down to 250 m, below which nitrite concentration

~0 µM). Note the changes in the x-axis scale between the panels. The error bars indicate the measurement standard deviation (n ≥ 3).

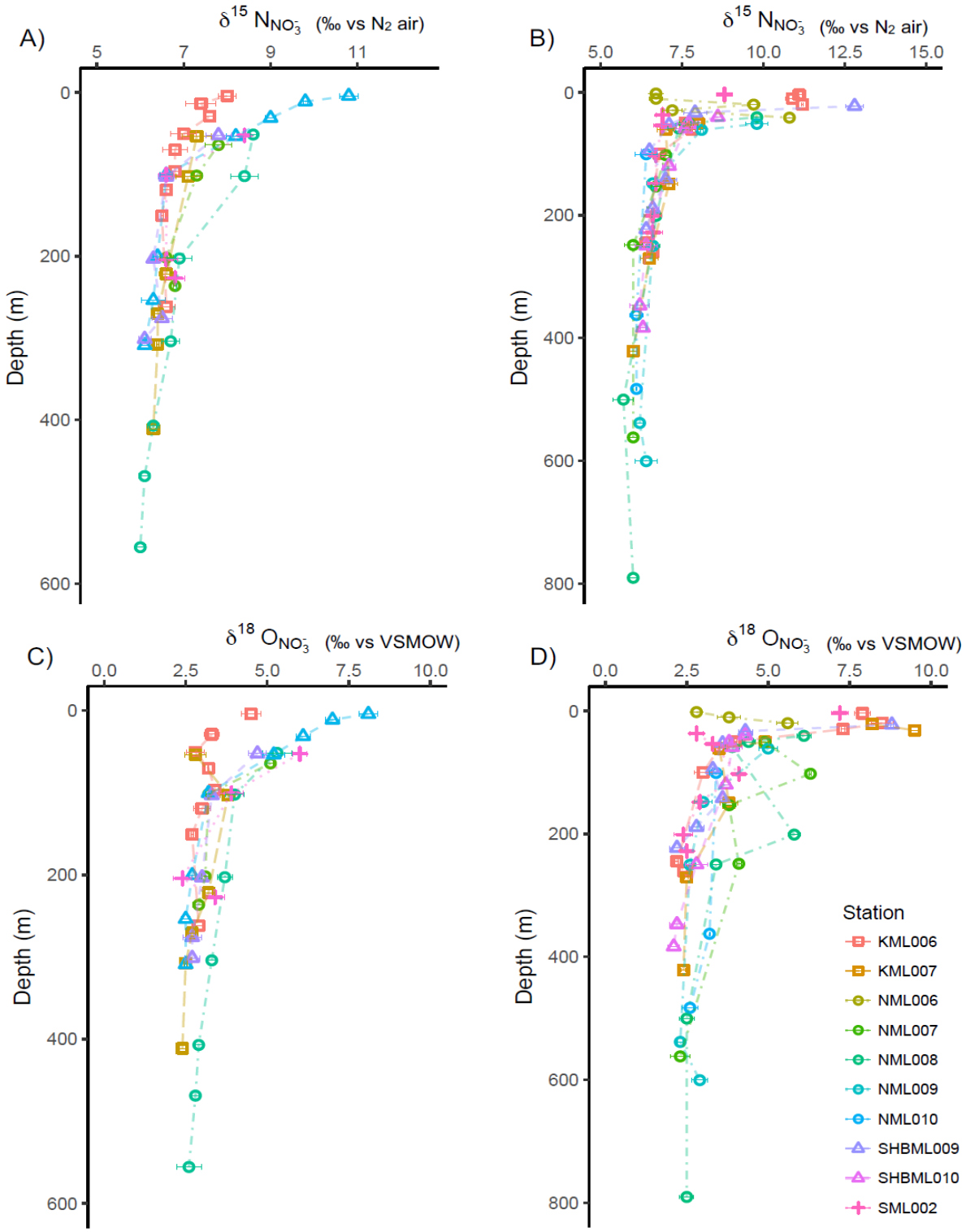


**Figure B3.** Depth profiles of A) $\delta^{15}N_{NO3}$ for summer, B) $\delta^{15}N_{NO3}$ for winter, C) $\delta^{18}O_{NO3}$ for summer and D) $\delta^{18}O_{NO3}$ for winter at the **offshore stations for all four monitoring lines**. Data shown are the nitrite-removed values (down to 250 m, below which nitrite concentration ~0

μM). Note the changes in the x-axis scale between the panels. The error bars indicate the measurement standard deviation (n ≥ 3).

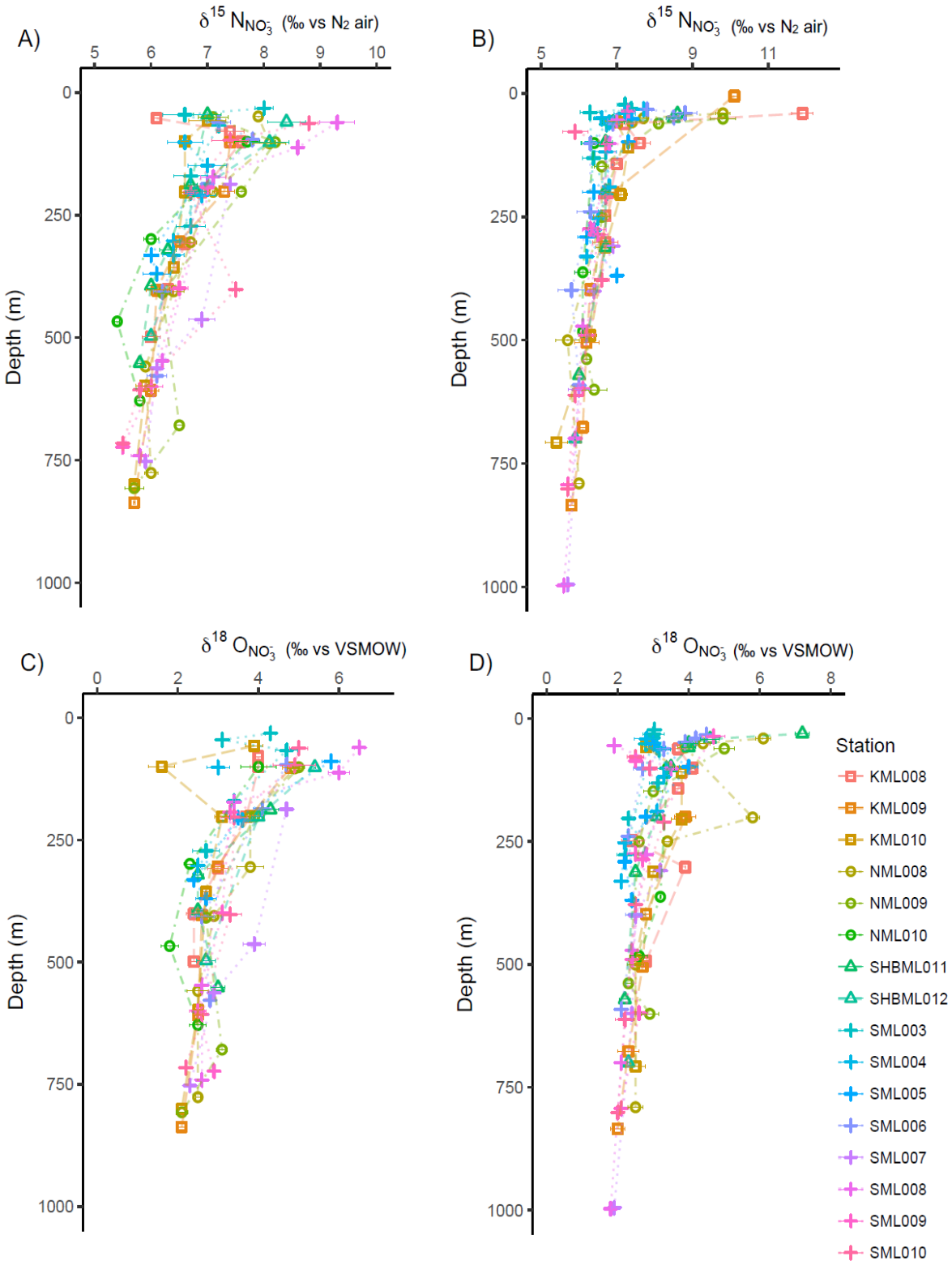


**Figure B4.** Depth profiles of A) $\delta^{15}N_{NO3}$ for summer, B) $\delta^{15}N_{NO3}$ for winter, C) $\delta^{18}O_{NO3}$ for summer and D) $\delta^{18}O_{NO3}$ for winter at the **oceanic stations for all four monitoring lines**. Data shown are the nitrite-removed values (down to 250 m, below which nitrite concentration ~0

μM). Note the changes in the x-axis scale between the panels. The error bars indicate the measurement standard deviation ($n \geq 3$)

## Appendix C: Depth profiles of nitrite $\delta^{15}N$

A Monte Carlo simulation was run using measurements of the $\delta^{15}N$ of the nitrate-only samples and the $\delta^{15}N$ of the nitrate+nitrite samples in order to estimate the $\delta^{15}N$ of nitrite for all samples with a nitrite concentration >1% of the nitrate+nitrite concentration. Figure C1 shows depth profiles of nitrite $\delta^{15}N$ for all stations in summer and winter 2017. Nitrite $\delta^{15}N$ was on average higher than 0‰ for all samples, which has implications for the nitrite-producing and consuming processes ongoing in the SBUS as the time of sampling.

In short, an average nitrite $\delta^{15}N$ >0‰ suggests that the primary nitrite source was phytoplankton efflux following incomplete nitrate consumption rather than ammonium oxidation. The $\delta^{15}N$ of nitrite produced by ammonium oxidation is low due to the fairly large isotope effect associated with this process (Mariotti et al. 1981; Yoshida 1988; Casciotti et al. 2003). The subsequent step in the nitrification pathway, nitrite oxidation, has an inverse isotope effect of -12.8‰ (Casciotti 2009). This means that $^{15}N$-bearing nitrite is preferentially oxidized over $^{14}N$-bearing nitrite, which further lowers the $\delta^{15}N$ of the residual nitrite pool. Assuming a starting $\delta^{15}N$ for the ammonium being oxidized of 5‰ (i.e., equivalent to the PON available for ammonification; Figures 3.15 and 3.16), the two steps of the nitrification pathway can yield nitrite with a $\delta^{15}N$ as low as -12‰, which is much lower than observed. If ammonium is being assimilated by phytoplankton concomitant with ammonium oxidation, nitrite $\delta^{15}N$ could be even lower (DiFiore et al. 2009; Smart et al. 2015; Kemeny et al. 2016).

The high $\delta^{15}N$ of nitrite likely derives from the efflux of nitrite by phytoplankton following the incomplete reduction of nitrate. Under stressful conditions such as light and iron limitation, phytoplankton have been observed to efflux nitrite (Milligan and Harrison 2000). This nitrite will have a $\delta^{15}N$ that is similar to the nitrate transported into the cell. Although there is a large isotope effect associated with the nitrate reductase enzyme that catalyzes the reduction of nitrate to nitrite (~25‰; Granger et al. 2008; Karsh et al. 2012; Treibergs and Granger 2016), this acts to significantly raise the $\delta^{15}N$ of the nitrate pool as it undergoes a high degree of

intracellular consumption, producing nitrite that, which much lower in $\delta^{15}N$ than the residual nitrate, will be only slightly lower than the starting nitrate $\delta^{15}N$ (SAMW with a $\delta^{15}N$ of 6.6‰ in the case of the SBUS). Nitrite $\delta^{15}N$ could be further raised if $^{14}N$-bearing nitrite is preferentially transported into the chloroplast and/or $^{14}N$-nitrite is preferentially reduced to ammonium within the chloroplast and some of the residual $^{15}N$-enriched nitrite is then effluxed out the chloroplast. This latter pathway is unlikely, however, as it would require nitrite to be effluxed across three membranes.

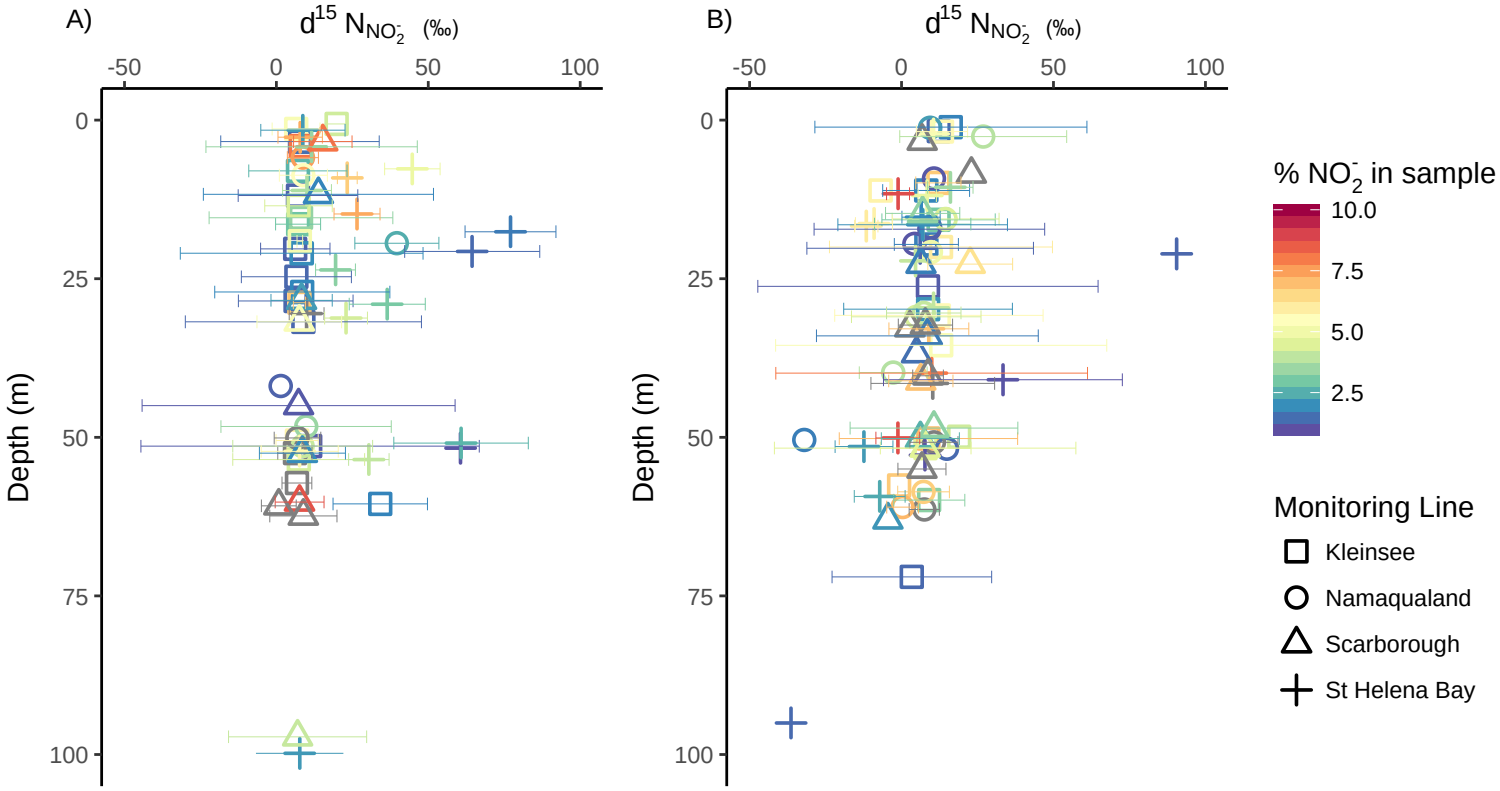


**Figure C1.** Depth profiles of estimated $\delta^{15}N_{NO2}$ for all samples with $NO_2^-$ concentration >1% of their respective $NO_3^-+NO_2^-$ concentrations for A) summer and B) winter at all stations in the SBUS. Error bars indicate the standard deviation of 100,000 Monte Carlo iterations run for each sample. Grey symbols represent samples with $[NO_2^-]$ >10% of $[NO_3^-+NO_2^-]$.

## Appendix D: Euphotic zone nitrogen cycle processes in the SBUS

### *Euphotic zone nitrification and nitrate assimilation: inshore and midshore stations*

The $\delta^{15}N$ and $\delta^{18}O$ of nitrate rise from the mid-depths towards the surface (Figure B1-4). This rise in nitrate $\delta^{15}N$ and $\delta^{18}O$ was observed at all stations during both seasons (Figures 3.10 and 3.11) and is coupled with a decrease in the nitrate, phosphate and silicic acid concentrations (Figures 3.3-3.5) and a rise in the oxygen concentrations (Figure A1). These changes are due to nitrate assimilation by phytoplankton in the euphotic zone (Granger et al. 2004; 2010). During nitrate assimilation, $^{14}N$- and $^{16}O$-bearing nitrate are preferentially taken up, enriching the residual nitrate pool in $^{15}N$ and $^{18}O$ and thus raising its $\delta^{15}N$ and $\delta^{18}O$ as nitrate is consumed.

If nitrate assimilation is the only process acting on the nitrate pool, nitrate $\delta^{15}N$ and $\delta^{18}O$ should change along a 1:1 line in $\delta^{15}N$ versus $\delta^{18}O$ space (Granger et al. 2004; 2010). However, in summer and winter, nitrate $\delta^{18}O$ rises more than its $\delta^{15}N$ in the surface at the inshore and midshore stations (Figures D1). This rise is more pronounced in the nitrate+nitrite data for both seasons. After nitrite removal in winter, the $\delta^{18}O$ rise disappears at all but the inshore stations. In summer, while nitrite removal brings the data much closer to the 1:1 line in $\delta^{15}N$ versus $\delta^{18}O$ space , nitrate $\Delta$(15-18) (symbol colour) indicates that a number of stations remain high in $\delta^{18}O$ relative to $\delta^{15}N$ in shallow waters, although this signal is still mainly observed inshore (Figures D1). The rise in nitrate $\delta^{18}O$ relative to $\delta^{15}N$ may be due to two processes: the nitrification of particles produced from 1) $N_2$ fixation or 2) partial assimilation of nitrate (Granger et al. 2004; Sigman et al. 2005; Granger et al. 2011; Rafter et al. 2013; Fawcett et al. 2015).

$N_2$ fixation produces PON with a low $\delta^{15}N$ of -2‰ to 0‰ (Minagawa and Wada 1986; Carpenter et al. 1997), introducing new low-$\delta^{15}N$ nitrate compared to the source nitrate once these particles have been remineralised and nitrified (Sigman et al. 2005). The inshore stations along all the monitoring lines are characterized by nutrient N:P ratios of ~12 (data not shown) which is below the Redfield ratio of 16 (Redfield 1934). This is evident in the low N* at these stations (Figure 3.9). A low N:P ratio in upwelled waters might be expected to stimulate $N_2$ fixation, which requires phosphorous (Deutsch et al. 2007). However, the nitrate concentrations were never below detection in the inshore surface waters (Figure 3.4). Under these conditions, it is unlikely that $N_2$ fixation would be favoured given that it requires more energy to convert $N_2$ into ammonium, the nitrogen form which the cell uses to build proteins (Raven et al. 1992; Warburg and Nagelein 1920), than does nitrate reduction. Furthermore, if $N_2$ fixation were

responsible for the low inshore nitrate Δ(15-18), why do we not observe the same signal elsewhere in the region? Indeed, the midshore, offshore and oceanic stations experienced more N-deplete conditions (Figure 3.4), which should favour $N_2$ fixation more than at the inshore stations. The inshore station surface waters were also colder than those offshore, and $N_2$ fixers have been observed to prefer warmer waters (Capone et al. 1997). Thus, if $N_2$ fixation were to occur in the SBUS, it would be more likely further offshore. Finally, while $N_2$ fixation and coupled partial nitrate assimilation-nitrification both yield a low Δ(15-18), this is driven by a decrease in nitrate $\delta^{15}N$ in the case of the former and an increase in nitrate $\delta^{18}O$ in the case of the latter. The data appear more consistent with a rise in $\delta^{18}O$ (Figures 3.11, 3.12 and D1) The deviation from 1:1 in $\delta^{15}N$ vs. $\delta^{18}O$ space is thus unlikely to be due to $N_2$ fixation. While there are no direct measurements of $N_2$ fixation from the SBSU, this conclusion is in agreement with studies from the northern Benguela (where the N:P ratio is similarly low or even lower; Flohr et al. 2014; Deutsch et al. 2007; Knapp et al. 2016) that have consistently found little evidence of significant rates of $N_2$ fixation (e.g., Sohm et al. 2011; Wasmund et al. 2015).

A more likely explanation for the rise in nitrate $\delta^{18}O$ relative to its $\delta^{15}N$ is euphotic zone nitrification of PON produced from the partial assimilation of nitrate. This process acts to raise the $\delta^{18}O$ of the combined nitrate pool (i.e., the partially consumed + newly nitrified nitrate) more than its $\delta^{15}N$. The $\delta^{18}O$ of the O atoms incorporated during nitrification is ~1.15‰ higher (Sigman et al. 2005; Buchwald and Casciotti 2012) than that of seawater (~0-0.5‰; Meredith et al. 1999), producing nitrate with a $\delta^{18}O$ ~1.15-1.55‰. The $\delta^{18}O$ of SAMW nitrate is 2.8-3.4‰. When this nitrate is assimilated, the $\delta^{18}O$ of the nitrate consumed ranges from -2.2‰ to -1.6‰ (based a nitrate assimilation O isotope effect of 5‰). The $\delta^{18}O$ produced by nitrification is therefore higher than that removed during assimilation (Sigman et al. 2009; Rafter et al. 2013; Fawcett et al. 2015). The $\delta^{15}N$ of newly nitrified nitrate, on the other hand, will equal the $\delta^{15}N$ of the PON produced during partial nitrate assimilation, which, when ammonified, nitrified, and combined with the partially-consumed nitrate, will yield a combined nitrate pool with the same $\delta^{15}N$ that is unchanged. (Sigman et al. 2005). In this way, partial nitrate assimilation followed by nitrification acts to decouple nitrate $\delta^{15}N$ and $\delta^{18}O$, leading to samples that fall above the 1:1 line in $\delta^{15}N$ vs. $\delta^{18}O$ space and that have a low Δ(15-18) (Sigman et al. 2000; Sigman et al. 2009a; Rafter et al. 2013)

The only nitrification data that exist for the SBUS were collected inshore and suggest that euphotic zone nitrate can be produced at rates of 4-9 nmol $L^{-1}$ $hr^{-1}$ (Rees et al. 2006). It is unclear exactly where in the SBUS the Rees et al. (2006) study was conducted, and the measurements are of ammonium oxidation, which usually occurs at a higher rate than nitrite oxidation (e.g., Ward and Zafiriou 1998; Dore and Karl 1996; Newell et al. 2013; Peng et al. 2016), with this latter step controlling the rate of nitrate production. Nonetheless, euphotic zone nitrification may be important in the inshore and midshore SBUS, as has been shown for other upwelling regions. For example, studies conducted in Monterey Bay have found that on average, 15-30% of nitrate-based productivity in surface waters is fueled by nitrate regenerated in the euphotic zone (Ward 2005; Wankel et al. 2007).

Figure 3.14 shows Δ(15-18) values of < 3‰ in the surface at the inshore and midshore stations along all the monitoring lines during both seasons, with a larger decrease in Δ(15-18) in summer. This may indicate that proportionally more nitrification is occurring in the euphotic zone in summer. However, it is also possible that in winter, the PON being remineralised is higher in $\delta^{15}N$ due to the offshore transport of high-$\delta^{15}N$ PON as discussed in section 4.4. In this cases, an equal or even higher rate of nitrification would lead to a smaller change in Δ(15-18). A final possibility is that the $\delta^{15}N$ of PON in summer is lower than that expected from fractionation during nitrate assimilation alone due to significant uptake of low-$\delta^{15}N$ ammonium. The latter options seem unlikely as the inshore St Helena Bay monitoring line has a weighted average PON $\delta^{15}N$ of 8‰ and 7.1‰ in summer and winter, respectively (Figures 3.15 and 3.16). The average $\delta^{15}N$ of PON for the summer may be biased towards higher values, however, as it is based only on data from two inshore stations.

***No evidence for euphotic zone nitrification at the offshore and oceanic stations***

The section plots of Δ(15-18) (Figure 3.14) show average surface values of 3‰ in summer and 4‰ in winter at the offshore and oceanic stations, which can be explained largely by phytoplankton assimilation, which raises nitrate $\delta^{15}N$ and $\delta^{18}O$ in unison (Sigman et al. 2005; Rafter et al. 2013), with no room for subsequent euphotic zone nitrification, which would decrease Δ(15-18). The increase in Δ(15-18) from summer to winter may be due to the system being dominated by regenerated shelf-nitrate in the winter (Figure 4.1), which is both anomalously low in $\delta^{18}O$ and at times high in $\delta^{15}N$, and propagates far further west in winter.

A second possibility is complete nitrate assimilation followed by surface nitrification, which acts to raise nitrate Δ(15-18) through the addition of newly nitrified nitrate that is lower in $\delta^{18}O$ than the nitrate that was consumed (Rafter et al. 2013). However, the present study and previous work has shown that while the nitrate concentrations at the offshore stations are low, they are not zero (Flynn et al. 2018). Furthermore, if surface nitrification were occurring, one might expect the regenerated and observed nitrate concentrations to be higher in these waters (Figure 3.4 and 4.1). In sum, while nitrate Δ(15-18) was slightly different in offshore and oceanic waters in winter relative to summer, the observed deviation from the 1:1 line in $\delta^{15}N$ vs. $\delta^{18}O$ space for surface waters was restricted to the inshore and midshore stations (Figure D1). This supports the hypothesis that euphotic zone nitrification is insignificant relative to autotrophic nitrate assimilation at the offshore and oceanic SBUS stations in summer and winter.

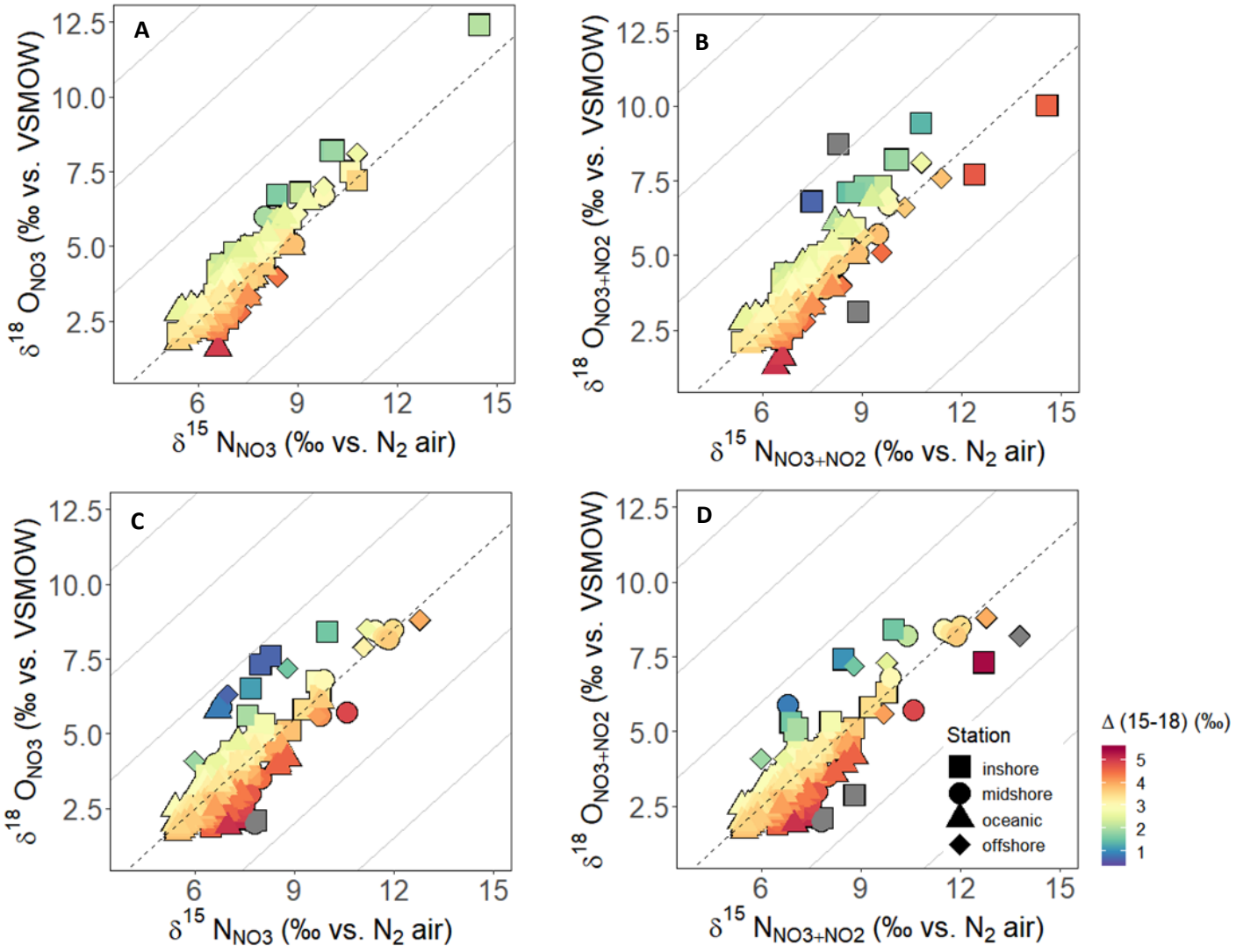

**Figure D1.** $\delta^{18}O$ versus $\delta^{15}N$ for A) nitrate-only samples in **summer**, B) nitrate+nitrite samples in **summer**, C) nitrate-only samples in **winter**, and D) nitrate+nitrite samples in **winter**. The colour bar indicates the $\Delta$(15-18) for each sample, calculated as $\delta^{15}N$ - $\delta^{18}O$. The grey lines have a slope of 1:1. The dashed black line also has a slope of 1:1, but passes through the source waters (SAMW) that have a $\Delta$(15-18) of ~3.5‰. Grey symbols show samples with a $\Delta$(15-18) >5.5‰ or <0.5‰.

***Subduction of surface waters below the fronts***

The rise in nitrate $\delta^{15}N$ and $\delta^{18}O$ extends down to 200 m in some regions, well below the mixed layer depth (Figures 3.11, 3.12 and 3.14). This was observed to the west of all the fronts and was likely due to surface waters being subducted below the fronts. The upwelling fronts are associated with strong, north-flowing jet currents that extend down to 200 m (Bang and Andrews 1974). Although the fronts are regarded as areas of uplift during upwelling (Shannon 1966), Andrews and Hutchings (1980) observed maximum chlorophyll concentrations at the base of the frontal thermoclines. They attributed this to the subduction of coastal waters down the fronts and beneath the surface waters. The subduction of coastal surface waters below the fronts is to be expected for an upwelling system. The westward movement (i.e., offshore transport) of the coastal surface waters is induced by the Coriolis force. This transport tends to follow isopycnals, flowing along the thermocline where water is likely to be mixed into the jet currents (Andrews and Hutchings 1980). The subduction of surface waters below the fronts explains both the rise in the chlorophyll concentrations in the subphotic layer observed by Andrews and Hutching (1980) and the rise in nitrate $\delta^{15}N$ and $\delta^{18}O$ below the mixed layer depth, particularly at the stations immediately west of the fronts.

## Appendix E: Water mass properties

The $\delta^{15}N$ and $\delta^{18}O$ of the mode and deep water masses present in the SBUS remain unchanged at all offshore stations in both seasons (Figures 3.11 and 3.12). Temperature and salinity (TS) plots for both seasons show the proportion of each water mass in the region and are overlaid with the $\delta^{15}N$ and $\delta^{18}O$ of nitrate in the mode and deep water masses (Figure 3.3). The average $\delta^{15}N$ and $\delta^{18}O$ of nitrate in SAMW was 6.6‰ and 3.1‰, respectively (Table 3.1). SAMW nitrate $\delta^{15}N$ in the SBUS is slightly higher than that reported by Tuerena et al. (2015) at 40ºS

in the South Atlantic (6.2‰), while the average $\delta^{18}O$ was slightly lower than the Tuerena et al. (2015) value (3.4‰). The change in the nitrate isotopes of SAMW in the SBUS compared to the South Atlantic may be due to modification by remineralization (see sections 4.3 and 4.4). SASTMW, the water mass overlaying SAMW, had an average $\delta^{15}N$ of 7.7‰ and $\delta^{18}O$ of 4.4‰ (only values reported to date). The average nitrate $\delta^{15}N$ and $\delta^{18}O$ in AAIW was 6.2‰ and 2.8‰, respectively, while the average $\delta^{15}N$ and $\delta^{18}O$ for UCDW was 5.7‰ and 2.2‰, respectively (Figure 3.3; Table 3.1). The ranges reported here for both AAIW and UCDW in the SBUS are similar to those estimated by Tuerena et al. (2015) and Campbell (2016), the latter at 34.5ºS, for the South Atlantic. These studies reported a $\delta^{15}N$ and $\delta^{18}O$ for AAIW of 5.9‰ and 3‰ (Tuerena et al. 2015) and 5.9‰ and 2.7‰ (Campbell 2016), respectively, and a $\delta^{15}N$ and $\delta^{18}O$ for UCDW of 5.4‰ and 2.4‰ (Tuerena et al. 2015) and 5.4‰ and 2.3‰ (Campbell 2016), respectively. The decrease in the $\delta^{18}O$ of nitrate in this study and Campbell (2016) compared to Tuerena et al. (2015) is likely due to the modification of the deep water masses by remineralization as they move north in the South Atlantic gyre.

The nitrate concentrations for the source and deep water masses are consistent with those given by Tuerena et al. (2015) and Campbell (2016). SAMW had an average nitrate concentration of 21.3 $\pm$ 5.4 µM in the SBUS (Figure 3.3; Table 4.1), with Tuerena et al. (2015) reporting the nitrate concentration at 40 °S to be ~23 µM (Tuerena et al. 2015). AAIW and UCDW have higher nitrate concentrations than the source water. The nitrate concentration of AAIW was 27 $\pm$ 3.5 µM, consistent with Tuerena et al. (2015) estimate of ~26 µM and Campbell (2016) estimate of (30.2 µM). The nitrate concentration of UCDW was 33 $\pm$ 1.3 µM, which is also consistent with the values of ~33 µM and 33.7 µM reported by Tuerena et al. (2015) and Campbell (2016), respectively.

## 7. References


Altabet MA and McCarthy JJ. 1986. Vertical patterns in 15N natural abundance in PON from the surface waters of warm-core rings. *Journal of Marine Research*. 44: 185-201

Andrews WRH and Hutchings L. 1980. Upwelling in the Southern Benguela Current. *Progress in Oceanography*. 9(1): 1-8

Baertschi P. 1976. Absolute 18O content of standard mean ocean water. *Earth and Planetary Science Letters*. 21(3): 341-344

Bailey GW and Chapman P. 1985. 'The nutrient status of the St Helena Bay region in February 1979' in Shannon LV (ed.) *South African Ocean Colour and Upwelling Experiment*. Cape Town, Sea Fisheries Research Institute. pp. 125-145.

Bailey GW. 1987. 'Distribution and cycling of nutrients at four sites in the Benguela system' in Bas C, Margalef R and Rubles P (ed.) *International Symposium on Most Important Upwelling Areas Off Wester Africa (Cape Blanco and Benguela), Barcelona. Instituto de Investigaciones Pesqueras*. 1: 305-317

Bailey GW. 1991. 'Organic carbon flux and development of oxygen deficiency on the modern Benguela continental shelf south of 22S: spatial and temporal variability' in Tyson RV and Pearson TH (ed) *Modern and Ancient Continental Shelf Anoxia. Geological Society Special Publication No. 58*. pp. 171-183

Bakun A. 1990. Global climate change and intensification of coastal ocean upwelling. *Nature.* 247: 198-201

Bang ND and Andrews WRD. 1974. Direct current measurement of an oceanic frontal jet in the upwell regime west of Cape Town. *Journal of Marine Research*. 32:405-417.

Barange M and Pillar SC. 1992. Cross-shelf circulation, zonation and maintenance mechanisms of Nyctiphanes capensis and Euphausia hanseni (Euphausiacea) in the northern Benguela upwelling system. *Continental Shelf Research*. 12(9): 1027-1042

Barange M, Pillar SC and Hutchings L. 1992. Major pelagic borders of the Benguela upwelling system according to euphausiid species distributions. *African Journal of Marine Science*. 12:3-17

Barber RT and Smith RL. 1981. 'Coastal upwelling ecosystems' in Longhurts AR (ed.) *Analysis of Marine Ecosystems*. London, Academic Press. pp. 31-68.

Barlow RG, Lamont T, Mitchell-Innes B, Lucas M and Thomalla S. 2009. Primary production in the Benguela ecosystem, 1999-2002. *African Journal of Marine Science.* 31(1): 97-101.

Bendschneider K and Robinson RJ. 1952. A new spectrophotometric method for the determination of nitrite in sea water. *Technical Report No. 8. University of Washington*

Bigg GR and Rohling EJ. 2000. An oxygen isotope data set for marine waters. *Journal of Geophys. Re*s.105: 8527-8535

Bograd SJ, Gastro CG, Di Lorenzo E, Palacios DM, Bailey H, Gilly W and Chavez FP. 2008. Oxygen declines and the shoaling of the hypoxic boundary in the California Current. *Geophysical Research Letters*. 35(12): L12607

Böhlke JK, Mroczkowski SJ and Coplen TB. 2003. Oxygen isotopes in nitrate: a new reference materials for 18O:17O:16O measurements and observations on nitrate-water equilibration. *Rapid communications in mass spectrometry*. 17: 1835-1846

Boyd AJ and Nelson G. 1998. Variability of the Benguela Current off the Cape Peninsula, South Africa. *African Journal of Marine Science.* 19(1):27-39

Boyd AJ and Shillington F. 1994. Physical forcing and circulation patterns on the Agulhas Bank. *South African Journal of Science*. 90: 114-122

Boyd AJ, Taunton-Clark J and Oberholster GPJ. 1992. Spatial features of the near-surface and midwater circulation patters off western and southern South Africa and their role in the life histories of various commercially fishes species. *South African Journal of Marine Science.* 12:189-206

Brandes JA and Devol AH. 1997. Isotopic fractionaion of oxygen and nitrogen in coastal marine sediments. *Geochimica et Cosmochimica Acta*. 61(9): 1793:1801

Bronk DA, Glibert PM, and Ward BB. 1994. Nitrogen uptake, dissolved organic nitrogen release, and new production. *Science* 265: 1843–1843.

Bronk DA. 2002. 'Dynamics of DON' in Hansell DA and Carlson CA (ed.) *Biogeochemistry of marine dissolved organic matter*. Academic Press. pp. 153-247

Brown PC and Field JG. Factors limiting phytoplankton production in a nearshore upwelling area. *Journal of Plankton Research*. 8(1): 55-68

Brown PC, Painting SJ and Cochrane KL. 1991. Estimates of phytoplankton and bacterial biomass and production in the northern and southern Benguela ecosystems. *South African Journal of Marine Science.* 11: 537–564. doi: 10.2989/025776191784287673.

Brown PC. 1984. Primary production at two contrasting nearshore sites in the southern Benguela upwelling region, 1977 — 1979. *African Journal of Marine Science.*

Brown ZW, Casciotti KL, Pickart RS, Swift JH and Arrigo KR. 2015. Aspects of the marine nitrogen cycle of the Chukchi Sea shelf and Canada Basin. *Deep Sea Research Part II: Topical Studies in Oceanography.* 118(Part A): 73-87

Buchwald C and Casciotti KL. 2012. Oxygen isotopic fractionation and exchange during baterial nitrite oxidation. *Limnol Oceanogr*. 55: 1064-1074

Calvert SE and Price NB. 1971. Upwelling and nutrient regeneration in the Benguela Current. *Deep Sea Research.* 18: 505-523

Carpenter EJ, Harvey HR, Fry B and Capone DG. 1997. Biogeochemical tracers of the marine cyanobacterium Trichodesmium. *Deep Sea Research I.* 44(1): 27–38.

Carpenter JH. 1965. The Chesapeake Bay Institute technique for the Winkler dissolved oxygen method. *Limnol. Oceanogr.* 10: 141–143. doi:10.4319/lo.1965.10.1.0141.

Carr ME and Kearns EJ. 2003. Production regimes in the four Eastern Boundary Current systems. *Deep Sea Research II*. 50: 3199-3221

Carr ME. 2001. Estimation of potential productivity in the Eastern Boundary Currents using remote sensing. *Deep Sea Research II*. 49(1-3): 59-80

Casciotti KL, Sigman DM, and Ward BB. 2003. Linking Diversity and Stable Isotope Fractionation in Ammonia-Oxidizing Bacteria. *Geomicrobiology Journal*. 20: 335–353.

Casciotti KL, Sigman DM, Hastings MG, Böhlke JK, and Hilkert A. 2002. Measurement of the oxygen isotopic composition of nitrate in seawater and freshwater using the denitrifier method. *Anal. Chem*. 74: 4905–4912. doi:10.1021/ac020113w.

Casciotti KL. 2009. Inverse kinetic isotope fractionation during bacterial nitrite oxidation. *Geochimica et Cosmochimica Acta.* 73: 2061–2076.

Casciotti KL. 2016. Nitrogen and Oxygen isotopic studies of the marine nitrogen cycle. *Annual Review of Marine Science.* 8:379-407.

Chapman P and Bailey GW. 1991. Short-term variability during an anchor station study in the southern Benguela upwelling system: Introduction. *Prog. Oceaonog*. 28: 1-7

Chapman P and Shannon L. 1985. The Benguela Ecosystem Part II. Chemistry and Related Processes. *Oceanography Marine Biology Annual Review*. 23: 183–251.

Checkley DM and Miller CA. 1989. Nitrogen isotope fractionation by oceanic zooplankton. *Deep Sea Research Part A. Oceanographic Research Papers*. 36(10): 1449-1456

Christensen JP, Smethie WM, and Devol AH. 1987. Benthic nutrient regeneration and denitrification on the Washington continental shelf. *Deep Sea Res. Part A.* 34: 1027–1047

Cockcroft AC. 2001. Jasus Ialandii 'walkouts' or mass strandings in South Africa during the 1990s: an overview. *Marine Freshwater Research*. 52(8): 1085-1093

Conley DJ, Carstensen J, Vaquer-Sunyer R and Duarte CM. 2007. 'Ecosystem thresholds with hypoxia' in Andersen JH and Conley DJ (ed.). *Eutrophication in coastal ecosystems*. Nybord, Denmark. pp. 21-29

De Decker AHB. 1970. Notes on an oxygen-depleted subsurface current off the west coast of South Africa. *Investigational Report, Devision of Fisheries, South Africa*. 84: 1-24

Defant A. 1936. Das Kaltwasserauftriebsgebiet vor der Küste Südwestafrikas. *Landerkundliche Forschung, Festschrift, Norbet Krebs, Stuttgart*: 52-66

Deutsch C, Sarmiento JL, Sigman DM, Gruber N and Dunner JP. 2007. Spatial coupling of nitrogen inputs and losses in the ocean. *Nature*. 445: 163-167

Devol AH and Christensen JP. 1993. Benthic fluxes and nitrogen cycling in sediments of the continental margin of the eastern North Pacific. *J. Mar. Res.* 51: 345–372, doi:10.1357/0022240933223765.

Devol AH. 1991. Direct measurement of nitrogen gas fluxes from continental?shelf sediments. *Nature.* 349: 319–321, doi:10.1038/349319a0.

Diamond D. 1994. QuikChem Method 10-114-21-1-B: Silicate by flow injection analysis. *Lachat Instruments*

Diaz F and Raimbault P. 2000. Nitrogen regeneration and dissolved organic nitrogen release during spring in a NW Mediterranean coastal zone (Gulf of Lions): Implication for the estimation of new production. *Marine Ecology Progress Series.* 197: 51–65.

Dittmar T and Birkicht M. 2001. Regeneration of nutrients in the northern Benguela upwelling and the Angola-Benguela Front areas. *South African journal of science.* 97:239-246

Donners J, Drijfhout SS and Hazeleger W. 2005. Water Mass Transformation and Subduction in the South Atlantic. *Journal of Physical Oceanography*.

Dore JE and Karl DM. 1996. Nitrification in the euphotic zone as a source for nitrite, nitrate and nitrous oxide at Station ALOHA. *Limnology and Oceanography.* 41(8): 1619–1628.

Dugdale RC, and Goering JJ. 1967. Uptake of new and regenerated forms of nitrogen in primary productivity. *Limnology and Oceanography.* 12(2): 196–206.

Duncombe Rae C. 2005. A demonstration of the hydrographic partition of the Benguela upwelling ecosystem at 26°40'S. *African Journal of Marine Science.* 27(3): 617–628

Emeis K, Eggert A, Flohr A, Lahajnar N, Nausch G, Neumann A, Rixen T, Schmidt M, Van der Plas A and Wasmund N. 2017. Biogeochemical processes and turnover rates in the Northern Benguela Upwelling System. *Journal of Marine Science.*

Emeis KC, Struck U, Leipe T and Ferdelman TG. 2009. Variability in upwelling intensity and nutrient regime in the coastal upwelling system offshore Namibia: Results from sediment archives. *Int. J. Earth Sci*. 98:309-326

Eppley RW and Peterson BJ. 1979. Particulate organic matter flux and planktonic new production in the deep ocean. *Nature,* 282: 677–680.

Evans W, Hales B, Strutton PG, Shearman RK and Barth JA. 2015. Failure to bloom: intense upwelling results in negligible phytoplankton response and prolonged CO2 outgassing over the Orgeon shelf. *JGR Oceans*. 120(3): 1445-1461

Falkowski PG, Barber RT, and Smetacek V. 1998. Biogeochemical controls and feedbacks on ocean primary production. *Science*. 281(5374): 200–206.

Fawcett SE, Ward BB, Lomas MW and Sigman DM. 2015. Vertical decoupling of nitrate assimilation and nitrification in the Sargasso Sea. *Deep-Sea Research I*. 103: 64-72

Field JG, Crawford RJM, Wickens PA, Moloney CL, Cochrane KL and Villacastin-Herrero CA. 1991. Network analysis of Benguela pelagic foodwebs.

Flynn RF, Burger JM, Pillay K and Fawcett SE. 2018. Wintertime rates of net primary production and nitrate and ammonium uptake in the southern Benguela upwelling system. *African Journal of Marine Science.* 40: 253-266.

Garzoli SL and Gordon AL. 1996. Origins and variability of the Benguela Current. *Journal of Geophysical Research: Oceans*. 101: 897-906

Gibbons M and Hutchings L. 1996. Zooplankton diversity and community structure around southern Africa, with special attention to the Benguela upwelling system. *Journal of African Science.* 92:63-76

Gonfiantini R, Stichler W and Rozanski K. 1995. Standards and intercomparison material distributed by the International Atomic Energy Agency for stable isotope measurements. *Proceedings of a consultants meeting held in Vienna, 1-3 December 1993*

Graham WM and Largier JL. 1997. Upwelling shadows as nearshore retention sites: the examples of northern Monterey Bay. *Continental Shelf Research.* 17(5): 509-532

Granger J and Sigman DM. 2009. Removal of nitrite with sulfamic acid for nitrate N and O isotope analysis with the denitrifier method. *Rapid communication in mass spectrometry.* 23: 3753-3762

Granger J, Sigman DM, Lehmann MF, and Tortell PD. 2008. Nitrogen and oxygen isotope fractionation during dissimilatory nitrate reduction by denitrifying bacteria. *Limnol. Oceanogr.* 53: 2533–2545. doi:10.4319/lo.2008.53.6.2533.

Granger J, Prokopenko MG, Sigman DM, Mordy CW, Morse ZM, Morales LV, Sambrotto RN and Plessen B. 2011. Coupled nitrification-denitrification in sediment of the eastern Bering Sea shelf leads to 15N enrichment of fixed N in shelf waters. *JGR Oceans*. 116: C11006

Granger J, Sigman DM, Needoba JA, and Harrison PJ. 2004. Coupled Nitrogen and Oxygen Isotope Fractionation of Nitrate during Assimilation by Cultures of Marine Phytoplankton. *Limnology and Oceanography*. 49(5): 1763–1773.

Granger J, Sigman DM, Prokopenko MG, Lehmann MF and Tortell PD. 2006. A method of nitrite removal in nitrate N and O isotope analyses. *Limnology and Oceanography*. 4(7): 205- 212

Granger J, Sigman DM, Rohde MM, Maldonado MT, and Tortell PD. 2010. N and O isotope effects during nitrate assimilation by unicellular prokaryotic and eukaryotic plankton cultures. *Geochimica et Cosmochimica Acta.* 74: 1030–1040.

Grasshoff K, Kremling K and Ehrhardt M. 1983. Methods of Seawater Analysis. Verlag Chemia, Florida

Grasshoff K. 1976. Methods of seawater analysis. Verlag Chemie, Weinheim and New York

Gruber N and Sarmiento JL 1997. Global patterns of marine nitrogen fixation and denitrification. *Global Biogeochemical Cycles*. 11(2): 235-266

Hardman-Mountford NJ, Richardson AJ, Agenbag JJ, Hagen E, Nykjaer L, Shillington FA and Villacastin C. 2003. Ocean climate of the South East Atlantic observed from satellite data and wind models. *Progress in Oceanography*. 59:181-221

Harris TFW and Shannon LV. 1979. Satellite-tracked drifter in the Benguela Current system. *South African Journal of Science*. 75(7): 316-317

Hart TJ and Currie RI. 1960. The Benguela Current. *Discovery Reports*. 31:123-298

Hayes JM. 2002. Practice and Principles of Isotopic Measurements in Organic Geochemistry (Revision 2). Woods Hole Oceanographic Institution, Woods Hole, MA 02543.

Hensen SA, Sanders R, Madsen E, Morris PJ, Le Moigne F, and Quartly GD. 2011. A reduced estimate of the strength of the ocean's biological carbon pump. *Geophysical Research Letters.* 38(4).

Holden CJ. 1987. Observations of low frequency currents and continental shelf waves along the west coast of South Africa. *South African Journal of Marine Science*. 5: 197-208

Hutchings L, Jarre A, Lamont T, van den Berg M and Kirkman SP. 2012. St Helena Bay (southern Benguela) then and now: muted climate signals, large human impact. *African Journal of Marine Science*. 34(4): 559-583

Hutchings L, Van Der Lingen CD, Shannon LJ, Crawford RJM, Verheye HMS, Bartholomae CH, Van Der Plas AK, Louw D, Kreiner A, Ostrowski M, Fidel Q, Barlow RG, Lamont T, Coetzee J, Shillington F, Veitch J, Currie JC and Monteiro PMS. 2009a. The Benguela Current: An ecosystem of four components. *Progress in Oceanography*. 83(1–4):. 15–32.

Jahnke RA and Jahnke DB. 2000. Rates of C, N, P and Si recycling and denitrification at the US Mid-Atlantic continental slope depocenter. *Deep Sea Research: Part I*. 47: 1405-1428

Jarre A, Hutchings L, Crichton M, Wieland K, Lamont T, Blamey LK, Illert C, Hill E and van den Berg M. 2015. Oxygen-depleted bottom waters along the west coast of South Africa, 1950-2011. *Fisheries Oceanography.* 24: 56-73

Jones PGW. 1971. The southern Benguela Current region in February, 1966: I. Chemical observations with particular reference to upwelling. *Deep Sea Research*. 18(2): 193-208

Jury MR. 1985. 'Case studies of alongshore variations in wind-driven upwelling in the southern Benguela region' in Shannon LV (ed.) *South African Ocean Colour and Upwelling Experiment*. Cape Town, Sea Fisheries Research Institute. pp. 29-46

Kampf J and Chpman P. 2016. Upwelling Systems of the World. Springer International Publishing Switzerland.

Kamstra F. 1985. 'Environmental features of the southern Benguela with special reference to the wind stress' region' in Shannon LV (ed.) *South African Ocean Colour and Upwelling Experiment*. Cape Town, Sea Fisheries Research Institute. pp. 13-27

Karsh KL, Granger J, Kritee K and Sigman DM. 2012. Eukaryotic assimilatory nitrate reductase fractionates N and O isotopes with a ratio near unity. *Environ. Sci. Technol*. 46(11): 5727- 5735

Kemp WM, Boynton WR, Adolf JE, Boesch DF, Boicourt WC, Bruch G, Cornwell JC, Fisher TR, Glibert PM, Hagy JD, Harding LW, Houde ED, Kimmel DG, Miller WD, Newell RIE, Roman MR, Smith EM and Stevenson JB. 2005. Eutrophication of Chesapeake Bay: historical trends and ecological interactions. *Marine Ecology Progress Series*. 303: 1-29

Kuypers M.M., Lavik G, Woebken D, Schmid M, Fuchs BM, Amann R, Jorgensen BB and Jetten MSM. 2005. Massive nitrogen loss from the Benguela upwelling system through anaerobic ammonium oxidation. *Proceedings of the National Academy of Sciences of the United States of America.* 102(18) pp.6478–6483.

Lachkar Z and Gruber N. 2011. What controls biological production in coastal upwelling systems? Insights from a comparative modelling study. *Biogeosciences.* 8: 2961-2976.

Lachkar Z and Gruber N. 2012. A comparative study of biological production in eastern boundary upwelling systems using an artificial neural network. *Biogeosciences.* 9: 293-308

Lamont T, Barlow RG and Kyewalyanga MS. 2014. Physical drivers of phytoplankton production in the southern Benguela upwelling system. *Deep Sea Research Part I:* Oceanographic Research Papers 90: 1-16

Lamont T, Hutchings L, van den Berg MA, Goschen WS and Barlow RG. 2015. Hydrographic variability in the St. Helena Bay region of the southern Benguela ecosystem. *Journal of Geophysical Research: Oceans*. 120(4): 2920–2944. doi: 10.1002/2014JC010619.

Largier JL, Chapman P, Peterson WT and Swart VP. 1992. The western Agulhas Bank: circulation stratification and ecology. *South African Journal of Marine Science*. 12:319-339

Laws EA, Falkowski PG, Smith WO, Ducklow H and McCarthy JJ. 2000.Temperature effects on export production in the open ocean. *Global Biogeochem. Cycles*. 14(4): 1231–1246. doi:10.1029/1999GB001229.

Legendre L. 1981. 'Hydrodynamic control of marine phytoplankton production: the paradox of stability' in Nihoul JCJ (ed.) *Ecohydrodynamic*s. Elsevier, Amsterdam. pp. 191-207

Lett C, Veitch J, Van Der Lingen CD and Hutchings L. 2007. Assessment of an environmental barrier to transport of ichthyoplankton from the southern to the northern Benguela ecosystems. *Marine Ecology Progress Series*. 347: 247–259. doi: 10.3354/meps06982

Levin LA, Whitcraft CR, Mendoza GF, Gonzalez JP and Cowie G. 2009. Oxygen and organic matter thresholds for benthic faunal activity on the Pakistan margin oxygen minimum zone (700–1100 m). *Deep-Sea Res II*

Lleonart J and Roel BA. 1984. Analisis de las comunidades de peces y crustaceos demersales de la costa de Namibia (Atlantic Sudoriental). *Investigation pesq. Barcelona*. 48(2): 187-206

Louw D, van der Plas A, Mohrholz V, Wasmund N, Junker T and Eggert A. 2016. Seasonal and interannual phytoplankton dynamics and forcing mechanisms in the northern Benguela upwelling system. *J. Mar. Syst*. 157: 124–134. http://dx.doi. org/10.1016/j.jmarsys.2016.01.009.

Lutjeharms JRE, Meyer AA, Ansorge IJ, Eagle GA and Orren MJ. The nutrient characteristics of the Agulhas Bank. *African Journal of Marine Science*. 171(1): 253-274

Macko SA, Estep MF, Engel MH and Hare PE. 1986. Kinetic fractionation of stable nitrogen isotopes during amino acid transaminations *Geochim, Cosmochim. Acts*. 50: 2143-2146

Margeson JH, Suggs JC and Midgett MR. 1980. Reduction of nitrate to nitrite with cadmium. *Anal. Chem.* 52: 1955-1957

Mariotti A, Germon JC, Hubert P, Kaiser P, Letolle R, Tardieux A, and Tardieux P. 1981. Experimental determination of nitrogen kinetic isotope fractionation: Some principles; illustration for the denitrification and nitrification processes. *Plant and Soil.* 62: 413–430.

Mas-Riera J, Lombarte A, Gordoa A and Macpherson E. 1990. nfludence of Benguela upwelling on the structure of demersal fish populations off Namibia. *Mar. Biol*.104: 175-182

McCarthy MJ, McNeal KS, Morse JW and Gardner WS. 2008. Bottom-water hypoxia effects on sediment-water interface nitrogen transformations in a seasonally hypoxic, shallow bay (Corpus Christi Bay, TX, USA). *Estuaries and Coasts*. 21(3): 521-531

McIlvin MR and Casciotti KL. 2011. Technical Updates to the Bacterial Method for Nitrate Isotopic Analyses. *Analytical Chemistry*, 83: 1850–1856.

Meisel S, Struck U and Emeis KC. 2011. Nutrient dynamics and oceanographic features in the central Namibian upwelling region as reflected in d15N-signals of suspended matter and surface sediments. *Fossil Record*. 14(2): 153-169

Meredith MP, Grose KE, McDonagh EL, Heywood KJ, Frew RD and Dennis PF. 1999. Distribution of oxygen isotopes in the water masses of Drake Passage and the South Atlantic. *JGR Oceans.* 104(C9): 20949-20962

Minagawa M and Wada E. 1986. Nitrogen isotope ratios of red tide organisms in the East China Sea: a characterization of biological nitrogen fixation. *Marine Chemistry*. 19(3): 245-259

Mitchell-Innes BA and Walker DR. 1991. Short-term variability during an anchor station study in the southern Benguela upwelling system: Phytoplankton production and biomass in relation to specie changes. *Progress in Oceanography*. 28(1-2): 65-89

Mobius J. 2013. Isotope fractionation during nitrogen remineralization (ammonification): Implications for nitrogen isotope biogeochemistry. *Geochimica et Cosmochimica Acts*. 105: 422-432

Monteiro PMS and van der Plas AK. 2006. 'Low oxygen water (LOW) variability in the Benguela System: Key processes and forcing scales relevant to forecasting.' in Shannon V, Hempel G, Malanotte-Rizzoli, Moloney C and Woods J (ed.) *Large Marine Ecosystems.* Elsevier, Amsterdam. pp. 71-90

Monteiro PMS, Dewitte B, Scranton MI, Paulmier A and van der Plas AK. 2011. The role of open ocean boundary forcing on seasonal to decadal-scale variability and long-term change of natural shelf hypoxia. *Environmental Research Letters*. 6(2): 025002

Monteiro PMS, van der Plas AK, Mélice JL and Florenchie P. 2008. Dynamical characteristics of interannual hypoxia variability in a coastal upwelling system: climate and ecosystem state implications, *Deep Sea Research I*, 55:435-450.

Nagel B, Emeis KC, Flohr A, Rixen T, Schlarbaum T, Mohrholz V and van der Plas A. 2013. N-cycling and balancing of the N-deficit generated in the oxygen minimum zone over the Namibian shelf- An isotope-based approach. *Journal of Geophysical Research*: *Biogeosciences*. 118(1): 361-371

Nagel B, Gaye B, Lahajnar N, Struck U and Emeis KC. 2016. Effects of current regimes and oxygenation on particulate matter preservation on the Namibian shelf: Insights from amino acid biogeochemistry. *Marine Chemistry.* 186: 121-132

Nakajima M, Hayamizu T and Nishiura H. 1984. Effect of oxygen concentration on the rates of denitrification and denitrification in the sediments of an eutrophic lake. *Water Research.* 18(3): 335-338

National Ocims 2018, accessed 12 July 2018, < https://www.ocims.gov.za/dataset>

Nelson G and Hutchings L. 1983. The Benguela upwelling area. *Progress in Oceanography* 12(3): 333–356.

Nelson G and Polito A. 1987. Information on currents in the Cape Peninsula Area. African *Journal of Marine Science*. 1:199-299

Nelson G. 1989. 'Poleward motion in the Benguela Area' in Neshyba SJ, Mooers CNK, Smith RL and Barber RT (ed.) *Poleward Flows Along Eastern Ocean Boundaries, Vol. 34.* Sprinter-Verlag, New York. Chapter 10

Olivar MP. 1987. Ichthyoplankton assemblages off northern Namibia. In The Benguela and Comparale Ecosystems. *S. Afr. J. Mar. Sci.* 5: 627-643

Olivar MP. 1988. Plantonic stagers of lanterfishes (Osteichthyes, Myctophidae) in the Benguela upwelling region. *Investigacionpesq., Barcelona*. 52: 387-420

Parada C, van der Lingen C, Mullon C and Penven P. 2003. Modelling the effect of buoyancy on the transport of anchovy (Engraulis capensis) eggs from spawning to nursery

grounds in the southern Benguela: An IBM approach. *Fisheries Oceanography*.

Parsons TR, Maita Y and Lalli CM. 1984. A Manual of Chemical and Biological Methods for Seawater Analysis.

Patti B, Guisande C, Vergara AR, Riveiro I, Maneiro I, Barreiro A, Conanno A, Buscaino G, Cuttitta A and Basilone G. Factors responsible for the differences in satellite based chlorophyll-a concentration between the major global upwelling ares. *Estuarine, Coast, Shelf Sci.* 76(4): 775-786

Pauly D and Christensen V. 1995. Primary production required to sustain global fisheries. *Nature*. 374(6519), pp.255–257.

Peterson R and Stramme L. 1991. Upper-level circulation in the South Atlantic. *Prog. Oceanogr*. 26:1-73

Pitcher GC and Calder D. 2000. Harmful algal blooms of the southern Benguela Current: a review and appraisal of monitoring from 1989 to 1997. *South African Journal of Marine Science.* 22(1): 255-271

Pitcher GC and Nelson G. 2006. Characteristics of the surface boundary layer important to the development of red tide on the southern Namaqua shelf of the Benguela upwelling system. *Limnology and Oceanography*. 51(6): 2660-2674

Pitcher GC and Weeks SJ. 2006. 'The variability and potential for prediction of harmful algal blooms in the southern Benguela ecosystems' in Shannon V, Hempel G, Malanotte-Rizzoli P, Moloney C and Woods J (ed.) *Benguela: predicting a large marine ecosystem.* Elsevier, Amsterdam. pp. 125-146

Pitcher GC, Brown PC and Mitchell-Innes BA. 1992. Spatio-temporal variability of phytoplankton in the southern Benguela upwelling system. *South African Journal of Marine Science*. 12: 439-456

Pitcher GC, Probyn TA, du Randt A, Lucas AJ, Bernard S, Evers-King H, Lamont T and Hutchings L. 2014. Dynamics of oxygen depletion in the nearshore of a coastal embayment of the southern Benguela upwelling system. *Journal of Geophysical Research: Oceans.* 119(4): 2183-2200

Pitcher GC, Walker DR and Mitchell-Innes BA. 1989. Phytoplankton sinking rate dynamics in the southern Benguela upwelling system. *Marine Ecology Progress Series*. 55: 261-269

Pitcher GC, Walker DR, Mitchell-Innes BA and Moloney CL. 1991. Short-term variability during an anchor station study in the southern Benguela upwelling system: Phytoplankton dynamics. *Progress in Oceanography*. 28: 39-64

Probyn TA. 1987. The inorganic nitrogen nutrition of phytoplankton in the southern Benguela: new production, phytoplankton size and implications for pelagic foodwebs. *South African Journal of Marine Science*. 21(1): 411-420

Prokopenko MG et al. 2006. Nitrogen cycling in the sediments of Santa Barbara basin and eastern subtropical North Pacific: Nitrogen isotopes, diagenesis and possible chemosymbiosis between two lithotrophs (Thioploca and Anamox) - Riding on a glider. *Earth Planet. Sci. Lett*. 242: 186-204

Rafter PA, DiFiore PJ, and Sigman DM. 2013. Coupled nitrate nitrogen and oxygen isotopes and organic matter remineralization in the Southern and Pacific Oceans. *Journal of Geophysical Research.* 118: 4781–4794.

Ragueneau O. et al. 2000. A review of the Si cycle in the modern ocean: Recent progress and missing gaps in the application of biogenic opal as a paleoproductivity proxy. *Glob. Planet. Change.* 26: 317–365

Raimbault P, Slawyk G, Boudjellal B, Coatanoan C, Conan P, Coste B, Garcia N, Moutin T, and Pujo-Pay M. 1999. Carbon and nitrogen uptake and export in the equatorial Pacific at 150°W: Evidence of an efficient regenerated production cycle. *J. Geophys. Res.* 104: 3341–3356.

Redfield AC, Ketchum BH and Richards FA. 1963. 'The influence of organisms on the composition of sea water' in Hill MN (ed.) *The Sea, Vol. 2*. Interscience Publishers, New York. pp. 26-77

Redfield AC. 1934. The haemocyanins. Biological Reviews*: Cambridge Philosophical Society.* 9(2): 175-212

Redfield AC. 1942. The processes determining the concentration of oxygen, phosphate and other organic derivatives within the depths of the Atlantic Ocean. *Contribution No. 308 from the Woods Hole Oceanographic Institution.*

Redfield AC. 1958. The biological control of chemical factors in the environment. *American Scientist*. 46: 205-221.

Rosenberg R, Arntz WE, de Flores EC, Flores LA, Carbajal G, Finger I and Tarazona Juan. 1983. Benthos biomass and oxygen deficiency in the upwelling system off Peru. *Journal of Marine Research*. 42(2): 263-279

Rossi V, Lopez C, Hernandez-Garcia E, Sudre J and Morel Y. 2008. Surface mixing and biological activity in the four Eastern Boundary Upwelling Systems. *Nonlin. Processes Geophys.* 16: 557-568

Rowe GT, Clifford CH, Smith KL and Hamilton PL. 1975. Benthic nutrient regeneration and

its coupling to primary production in coastal waters. *Nature*. 255:215-217

Rozan T, Taillefert M, Trouwborst RE, Glazer BT and Ma S. Iron-sulfur-phosphorus cycling in the sediments of a shallow coastal bay: Implications for sediment nutrient release and benthic macroalgal blooms. *Limnol. Oceanogra*. 45(5): 1346-1354

Ryther JH. 1969. Photosynthesis and fish production in the sea. *Science*. 166: 72-76

Saino T and Hattori A. 1980 15N natural abundance in oceanic suspended particulate matter. *Nature*. 283: 752-754

Santoro AE and Casciotti KL. 2011. Enrichment and characterization of ammonia-oxidizing archaea from the open ocean: phylogeny, physiology and stable isotope fractionation. *Geomicrobiology and Microbial Contributions to Geochemical Cycles*. 5: 1796-1808

Sarmiento JL, Gruber N, Brzezinksi MA and Dunne JP. 2004. High-latitude controls of the thermocline nutrients and low latitude biological productivity. *Nature*. 427(6969): 56-60

Schulz HN and Schulz HD. 2005. Large sulfur bacteria and the formation of phosphorite. *Science*. 207: 416-418

Seitzinger SP. 1988. Denitrification in fresh water and coastal marine ecosystems—Ecological and geochemical significance, *Limnol. Oceanogr*. 33

Shannon L and Pillar S. 1986. 'The Benguela Ecosystem. Part 3. Plankton' in Barnes H and Barnes M (ed.*) Oceanography and Marine Biology*. Aberdeen University Press, pp. 65–171

Shannon LV and Nelson G. 1996. 'The Benguela: Large Scale Features and Processes and System Variability' in Shannon LV and Nelson G (eds) *The South Atlantic: Present and Past Circulation*. Berlin, Heidelberg: Springer Berlin Heidelberg. pp. 163–210. doi: 10.1007/978-3-642-80353-6_9

Shannon LV and O'Toole MJ. 2003. 'Sustainability of the Benguela: ex Africa semper aliquid novi' in Sherman K and Hempel G (ed.) *Large marine ecosystems of the world - trends in exploitation, protection and research*. Elsevier BV. 227-253

Shannon LV, Hutchings L, Bailey GW and Shelton PA. 1984. Spatial and temporal distribution of chlorophyll in southern African waters as deduced from ship and satellite measurements and their implications for pelagic fisheries. *South African Journal of Marine Science*. 7615 doi: 10.2989/02577618409504363

Shannon LV, Stander GH and Campbell JA. 1973. Oceanic circulation deduced from plastic drift cards. *Investigational Report, Sea Fisheries, South Africa, 108.* pp. 31

Shannon LV. 1966. Hydrology of the south and west coasts of South Africa. *Investigational Report, Sea Fisheries, South Africa, 58.* pp. 52

Shannon LV. 1985. The Benguela Ecosystem, I., *Evolution of the Benguela, physical features and processes in Oceanography and Marine Biology*. 23: 105-182

Sharp Z. 2007. Principles of stable isotope geochemistry. The University of Michigan, Pearson/Prentice Hall.

Shelton PA and Hutchings L. 1982. Transport of anchovy, Engraulis capensis Gilchrist, eggs and early larvae by a frontal jet current. J. *Cons. Perm. Int. Explo. Mer*. 40(2): 185-198

Shillington FA. 1998. 'The Benguela upwelling system off southwestern Africa' in Robinson AR and Brink KH (eds) *The Sea Vol. 11, The Global Coastal Ocean, Regional Studies and Syntheses*. Wiley, New York. pp. 583-604

Sigman D, Altabet M, McCorkle D, Francois R and Fischer G. 2000. The d15N of nitrate in the Southern Ocean: Nitrogen cycling and circulation in the ocean interior. J. *Geophys. Res*. 105(C8), 19: 599–19,614.

Sigman D, Casciotti KL, Andreani M, Barford C, Galanter M and Böhlke JK. 2001. A Bacterial Method for the Nitrogen Isotopic Analysis of Nitrate in Seawater and Freshwater. *Analytical Chemistry.* 73: 4145–4153.

Sigman DM and Hain MP. 2012. The biological productivity of the ocean. *Nature education*. 3(6):1-16

Sigman DM, Altabet MA, Francois R, McCorkle DC and Gaillard JF. 1999b. The isotopic composition of diatom-bound nitrogen in the Southern Ocean sediments. *Paleoceanography.* 14:118-134.

Sigman DM, Altabet MA, Michener R, McCorkle DC, Fry B and Holmes RM. 1997. Natural abundance-level measurement of the nitrogen isotopic composition of oceanic nitrate: an adaptation of the ammonia diffusion method. *Marine chemistry*. 57(3-4): 227-242

Sigman DM, Casciotti KL, Andreani M, Barford C, Galanter M and Böhlke JK. 2001. A bacterial method for the nitrogen isotopic analysis of nitrate in seawater and freshwater. *Anal. Chem.* 73: 4145–4153. doi:10.1021/ac010088e.

Sigman DM, DiFiore PJ, Hain MP, Deutsch C, Wang Y, Karl DM, Knapp AN, Lehmann MF and Pantoja S. 2009a. The dual isotopes of deep nitrate as a constraint on the cycle and budget of oceanic fixed nitrogen. *Deep-Sea Research I.* 56: 1419–1439.

Sigman DM, DiFiore PJ, Hain MP, Deutsch C and Karl DM. 2009c. Sinking organic matter spreads the nitrogen isotope signal of pelagic denitrification in the North Pacific. *Geophysical Research Letters.* 36(L08605), 1–5.

Sigman DM, Granger J, DiFiore PJ, Lehmann MM, Ho R, Cane G and van Green A. 2005. Coupled nitrogen and oxygen isotope measurements of nitrate along the eastern North Pacific margin. *Global Biogeo Cycles*. 19: GB4022

Sigman DM, Karsh KL and Casciotti KL. 2009b. Ocean process tracers: nitrogen isotopes in the ocean in *Encyclopaedia of ocean science. 2nd edition*. Elsevier, Amsterdam. Chap. pp. 4138–4152.

Sigman DM., Altabet MA, McCorkle DC, Francois R and Fischer G. 1999a. The 15N of nitrate in the Southern Ocean: Consumption of nitrate in surface waters. *Global Biogeochemical Cycles*. 13(4): 1149–1166.

Silfer JA, Engel MH and Macko SA. 1992. Kinetic fractionation of stable carbon and nitrogen isotopes during peptide bond hydrolysis: Experimental evidence and geochemical implication. *Chemical Geology: Isotope Geoscience section*. 101(3-4): 211-221

Sohm JA, Hilton JA, Noble AE, Zehr JP, Saito MA and Webb EA. 2011. Nitrogen fixation in the South Atlantic Gyre and the Benguela Upwelling System. *Geophysical Research Letters*. 38: 1–6.

Stander GH and De Decker AHB. 1969. Some physical and biological aspects of an oceanographic anomaly off South West Africa in 1963. *Invest Rep. Div. Sea. Fish. S. Afr*. 81: 46

Stander GH. 1964. The Benguela Current off South West Africa. *Investi. Rep. mar. Res. Lab. S.W. Afr*. 12:43

Strickland JD and Parsons TR. 1968. A practical handbook of seawater analysis. *Bull. Fish. Res. Bd. Can*. 167.

Sydeman W, Garcia-Reyes M, Schoeman D, Rykaczewski R, Thompson S, Black B and Bograd S. 2014. Climate change and wind intensification in coastal upwelling ecosystems. *Science*. 345(6192): 77–80. doi: 10.1126/science.1250830

Treibergs LA, and Granger J. (201). Enzyme level N and O isotope effects of assimilatory and dissimilatory nitrate reduction. *Limnology and Oceanography.* 62(1): 272-288.

Tuerena RE, Ganeshram RS, Geibert W, Fallick AE, Dougans J, Tait A, Henly SF and Woodward EMS. 2015. Nutrient cycling in the Atlantic basin: The evolution of nitrate isotope signature in water masses. *Global Biogeochemical Cycles.* 29.

Tyrrell T and Lucas MI. 2002. Geochemical evidence of denitrification in the Benguela upwelling system. *Continental Shelf Research.* 22: 2497–2511

van der Lingen CD, Shannon LJ, Curry P, Kreiner A, Moloney CL, Roux J-P and Vaz-Vehlo

F. 2006. ‘Resource and ecosystem variability, including regime shifts in the Benguela Current System’ in Shannon V, Hempel G, Malanotte-Rizzoli P, Moloney CL and Woods J (ed.) *Benguela: Predicting a Large Marine Ecosystem, Large Marine Ecosystem 14.* Elsevier, Amsterdam. pp. 147-185.

Veitch J, Penven P and Shillington F. 2010. Modelling Equilibrium Dynamics of the Benguela Current System. *Journal of Physical Oceanography*. 40: 1942-1964

Veitch J, Penven P and Shillington F. 2009. The Benguela: A laboratory for comparative modelling studies. *Prog. Oceanogr*. 83: 296-302

Velinsky DJ, Fogel ML, Todd JF and Tebo BM. 1991. Isotopic fractionation of dissolved ammonium at the oxygen-hydrogen sulfide interface in anoxic wates. *Geophy. Res. Lett.* 16: 649-652

Volk T and Hoffert MI. 1985. Ocean carbon pumps: Analysis of relative strengths and efficiencies in ocean driven atmospheric CO2 changes. *The carbon cycle and atmospheric CO2: natural variations Archean to present.* 32: 99-110

Waldron HN, Probyn TA, Lutjeharms JRE & Shillington FA. 1992. Carbon export associated with the Benguela upwelling system. *South African Journal of Marine Science*. 12(1): 369-374.

Wankel SD, Kendall C, Pennington JT, Chavez FP and Paytan A. 2007. Nitrification in the euphotic zone as evidenced by nitrate dual isotopic composition: Observations from Monterey Bay, *California. Global Biogeochemical Cycles.* 21(2): 1–13. doi: 10.1029/2006GB002723

Wasmund N, Struck U, Hansen A, Flohr A, Nausch G, Grüttmüller A and Voss M. 2015. Missing nitrogen fixation in the Benguela region. *Deep-Sea Research I.* 106: 30–41.

Wedepohl PM, Lurjeharms JRE and Meeuwis JM. 2000. Surface drift in the south-east Atlantic Ocean. South *African Journal of Marine Science*. 22:71-79

Weigand MA, Foriel J, Barnett B, Oleynik S and Sigman DM. 2016. Updates to instrumentation and protocols for isotopic analysis of nitrate by the denitrifier method. *Rapid Communications in Mass Spectrometry.* 30: 1365-1383

Yool A, Martin AP, Fernandez C and Clark DR. 2007. The significance of nitrification for oceanic new production. *Nature.* 447: 999–1002. doi: 10.1038/nature05885.

Yoshida H, Hirooka T, Oyamada A, Okabe Y, Takahashi T, Sasaki T, Ochiai A, Suzuki T, Mascarenhas AH, Pankove JI, Ciszek TF, Deb SK, Goldfarb RB and Li Y. 1988. Oxygen isotope effect in the superconducting Bi:Sr:Ca:Cu:O system. *Physica C: Superconductivity.* 156(3): 481-484.